Neutron Reflection Study on Surfactant Systems at Different Interfaces



Kun Ma

Wolfson College, University of Oxford

D.Phil. Thesis

Hilary Term, 2016

Contents

1 Surfactants and Mixed Surfactant Systems **8**

1.1 Introduction 8

1.2 Zwitterionic Surfactants 12

1.3 Mixed Surfactant Systems 14

1.3.1 Introduction 14

1.3.2 The Chemical Potential 16

1.3.3 Thermodynamics of the Ideal Solution 17

1.3.4 Regular Solutions 19

1.3.5 Surfactant Mixtures 21

2 Surface Tension and Neutron Reflectivity **30**

2.1 Surface Tension 30

2.1.1 Introduction 30

2.1.2 Instrumentation 32

2.1.3 Experimental Procedure 32

2.1.4 Interpretation of Surface Tension and Gibbs Adsorption Isotherm 32

2.2 Neutron Reflectivity 35

2.2.1 Introduction 35

2.2.2 Instrumentation 37
2.2.3 Sample Environment 38
2.2.4 Sample Preparation 39
2.2.5 Experimental Procedure 40
2.2.6 Neutron Reflection at a Planar Boundary 41
2.2.7 Neutron Reflection from a single homogeneous layer . . . 46
2.2.8 Neutron Reflection from Multilayers 48
2.2.9 The Kinematic Approximation 53

3 Synthesis of Surfactants 66

3.1 Materials 66
3.2 Synthesis of Alkyl Chain Quaternary Ammonium Surfactants . . . 67
3.2.1 Synthesis of N,N-Dimethyldodecylamine 67
3.2.2 N-Dodecyl-N,N-dimethyl-3-ammonio-1-propanesulfonate 68
3.2.3 N-Dodecyl-N,N-Dimethylamino Betaine 69
3.3 Synthesis of Carboxybetaine Surfactants with Different Size Methylene Groups 70
3.3.1 $C_{12}H_{25}N^{+}(CH_3)_2(CH_2)_4COO^{-}$ 70
3.3.2 $C_{12}H_{25}N^{+}(CH_3)_2(CH_2)_8COO^{-}$ 75
3.4 Purification of Ionic Surfactants 77

4 Adsorption of Mixtures at the Air/liquid Interface 81

4.1 Introduction 81
4.2 Adsorption of DSB Surfactant 84
4.3 Adsorption of Surfactant Mixtures at Air-liquid Interface 89
4.3.1 Mixtures at CMC 89

4.3.2 Mixtures: Surface Tension and Composition at and below the CMC 97
4.4 Conclusions 113

5 Mixtures of Anionic/Zwitterionic surfactants at the Solid-liquid Interface 118

5.1 Introduction 118
5.2 Experimental Details 122
5.3 Results and Discussion 125
5.3.1 Characterization of the Oxide layer 125
5.3.2 Surfactant Adsorption at the Interface 126
5.3.3 Adsorption of SDS/Zwitterionic Mixtures 132
5.4 Conclusion 145

6 Mixtures of Cationic/Zwitterionic Surfactants at the Solid-liquid Interface 153

6.1 Introduction 153
6.2 Experimental Details 154
6.3 Adsorption of DTAB/Zwitterionic Mixtures 154
6.4 Conclusion 164

7 Air/liquid Interface Experiments on Carboxybetaine with Different Inter-charge Spacer 168

7.1 Introduction 168
7.2 Experiment details 172
7.3 Discussion and Conclusion 175
7.3.1 Surface tension 175

7.3.2 Neutron Reflection Experiments 179
7.4 Conclusion 192

8 Concluding Remarks **199**

Appendices **203**

A Neutron reflection fitting profiles at air–liquid interface **204**

B Neutron reflection fitting profiles at solid–aqueous interface **210**

Abstract

The interfacial behaviour of several surfactant mixtures containing zwitterionic surfactants has been studied employing surface tension measurements and neutron reflection experiments. The mixing of surfactants at air–liquid interface could not be well understood using the pesudophase approximation and the regular solution model. By introducing the expansion of excess free energy to analysis the surface tension and neutron reflection data simultaneously, it is found that the mixing deviates strongly from ideal and the excess free energy is asymmetric.

It is observed that the presence of ionic surfactant at solid–liquid interface enhanced the adsorption of zwitterionic surfactants. The configuration of the surfactant molecule in the inner layer adjacent to the surface is invoked to explain the underlying mechanism. Maxima in the adsorption just above the CMC occurred at all three compositions studied for the mixed system SDS with dodecyl dimethylammonium propanesulfonate (DSB). The neutron reflection experiments suggest that the phenomenon may result in part from the mixture and in part from ion segregation in the micelles.

Structural studies on a series of dodecyl dimethylammonium acetate with different inter–charge spacer revealed that the configuration of the surfactants changes

dramatically as the headgroup gets larger. Combined with the higher pK_a value, it is highly possible that the carboxybetaine with longer spacer is adsorbed in its undissociated form, and the headgroup is oriented towards the air. This configuration might explain why the saturated monolayer structure is favoured over the micellization.

Acknowledgement

First and foremost I would like to express my deep and sincere gratitude to my supervisors Dr. Robert K Thomas and Prof. Jeff Penfold. Many thanks for their help, guidance and advise at varies stage of my Dphil study, all of which have helped me to a very great extent to accomplish this thesis.

I would also like to send my gratitudes to the people of Thomas group, whose assistance during this project has been invaluable. Many thanks to Peixun Li, Ian Tucker for the guidance, discussion and data analysis through the neutron experiments. Thanks to Chuchuan Dong for the help on organic synthesis works. I also take this as an opportunity to thanks all my friends in Oxford, thanks for making my life here fruitful and happy.

Finally, I would like to thank my parents and my wife Ting Chu for their supporting and confidence in me, and without whose influence I certainly would not have got this far. You have been a huge source of encouragements.

Chapter 1

Surfactants and Mixed Surfactant Systems

1.1 Introduction

Surfactants are compounds which consist of both hydrophobic groups (tails) and hydrophilic groups (headgroups). They form a unique class of chemical components which have the ability to change surface and interfacial properties radically and to self-associate and solubilize themselves in micelles. These properties provide the means to apply surfactants in detergency, lubrication, mineral and petroleum processing, biological systems, health and personal care products, foods and pharmaceutical sciences.

Since the surfactant has a molecular structure consisting of two very different parts, the non-polar hydrophobic tail and the polar hydrophilic head–group, when the surfactant dissolves in water, the hydrophobic tail may alter the structure of the water, increasing the free energy of the system, and the system responds in

a way to minimize contact between the hydrophobic tail and the water. In the case of a surfactant dissolved in an aqueous medium, the result is that some of the molecules are repelled to the interface of the system, with the hydrophobic tails oriented toward the air [1]. This tendency of non-polar substances to aggregate in aqueous solution and exclude water molecules is termed the hydrophobic effect.

Under the driving force of the hydrophobic effect, the surface becomes covered by a single layer of surfactant molecules with the hydrophobic tails are oriented towards the air. If we compare the molecules at the interface with those in the bulk solution, the latter have higher potential energy because they experience equal attractive forces in all directions. However, the molecules at the surface interact more strongly with the molecules in the interior of the substance than they do with the widely separated gas molecules above. This results in a net inward pull which causes foam bubbles and water drops to tend to be spherical in shape. The surface tension is a measure of this change in surface energy and is defined as the work required to increase the area of a surface isothermally and reversibly by unit amount [2].

As the hydrophobic parts of the surfactants have a lower surface energy than water, the aggregation of the surfactants at the surface lowers the surface tension of the solution. With an increase of the bulk concentration, the amount of surfactant adsorbed at the interface increases and the surface tension decreases. Surfactants can also reduce the interfacial tension between water and oil at the liquid-liquid interface. Many surfactants also assemble in the bulk solution into aggregates and examples of such aggregates are vesicles and micelles. The concentration at

which surfactants begin to form micelles is known as the critical micelle concentration (CMC). When micelles form in water, their tails form a core and their polar head–groups form an outer shell that maintains favourable contact with water, as shown in Figure (1.1).

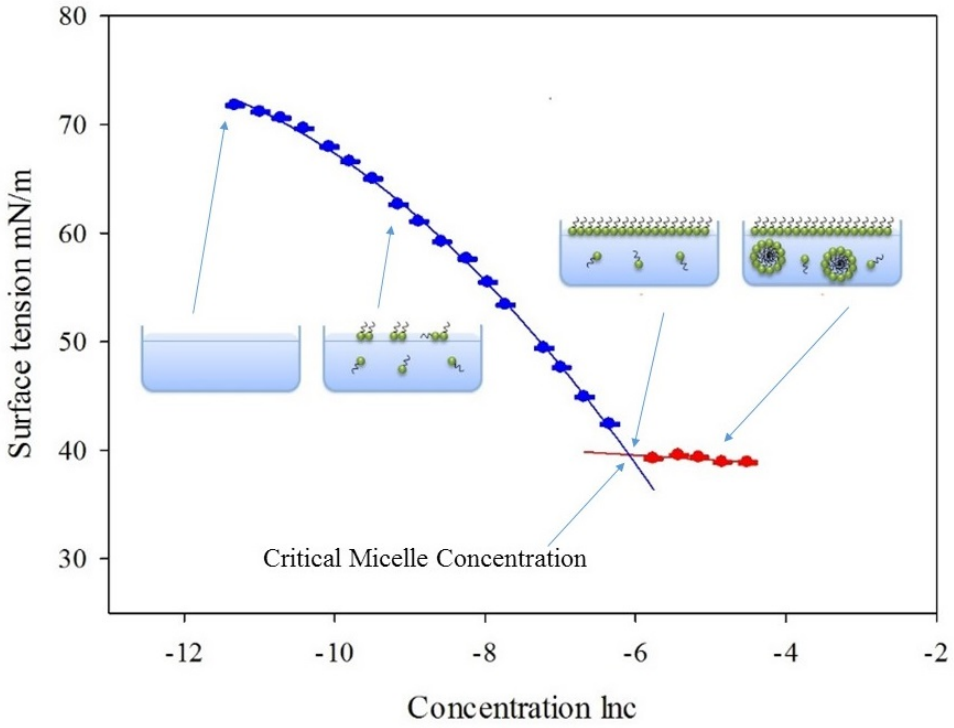


Figure 1.1: Surface tension of a surfactant solution with increasing concentration, formation of micelles.

The critical micelle concentration causes a sharp turning point in many physical properties of the solution, such as surface tension, electrical conductivity and osmotic pressure with respect to surfactant concentration, as shown in Figure (1.2) [1], in which the surface tension measurements on SDS were made using a Du Noüy ring tensiometer at air–liquid interface, the interfacial tension against xylene was measured by the drop weight method [3], the electrical conductivity

of SDS is from Howell et. al [4], and the detergency data is from the research of Presto [5]. The minimum in the plot of surface tension may be attributed to the impurity of the sample. The concentration band highlighted in the figure implies that the determination of the exact value of CMC depends on the choice of method for examining the behaviour of the bulk solution property.

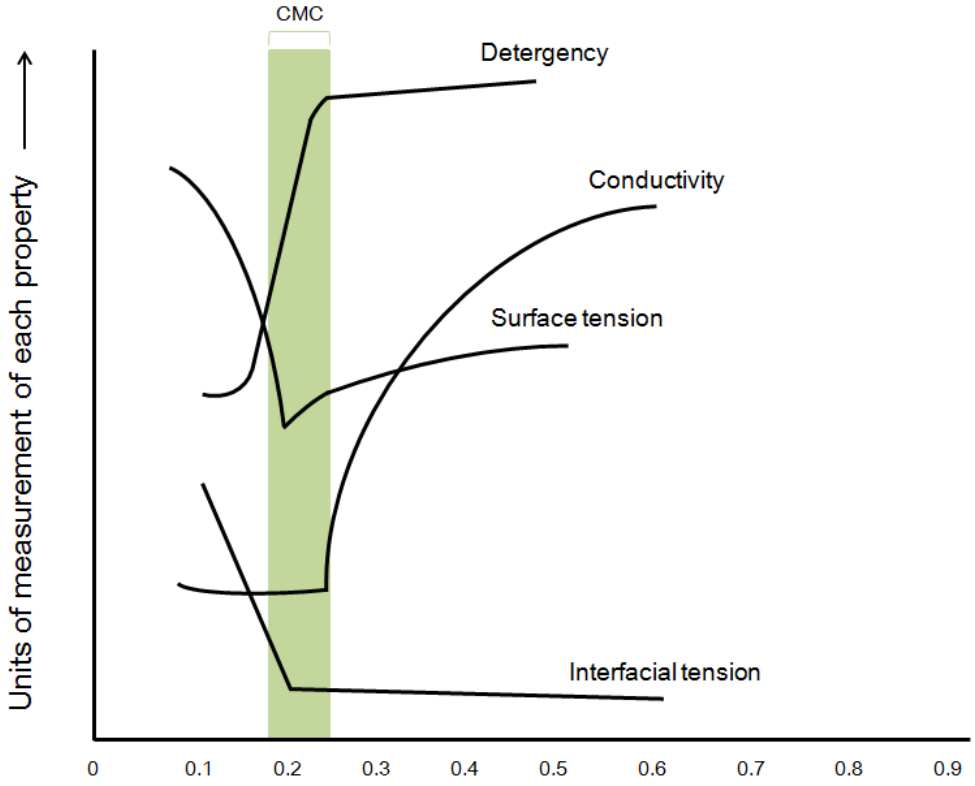


Figure 1.2: Changes in the physical properties of an aqueous solution of surfactant sodium dodecyl sulfate as a function of surfactant concentration, the figure is adapted from [5].

The classification of surfactants is based on the nature of the hydrophilic head–groups. A non-ionic surfactant has no charge group in its headgroup but derives its water solubility from highly polar groups [1]. The headgroup of an ionic sur-

factant carries a net charge. If the charge is negative, the surfactant is more specifically called anionic. If the charge is positive, it is named cationic. If a surfactant contains a head with two oppositely charged groups, it is termed zwitterionic. This thesis is mainly concerned with zwitterionic surfactants.

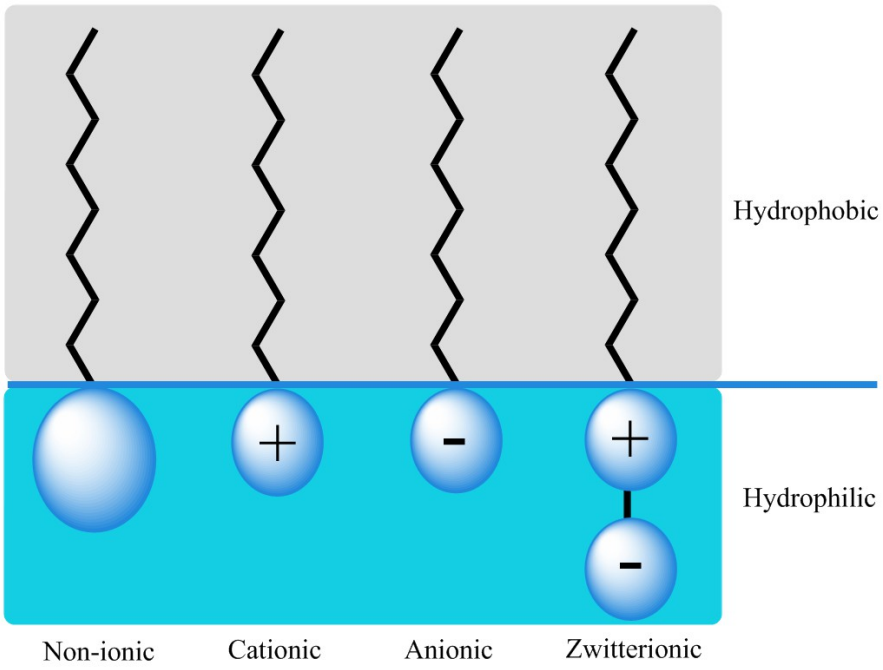


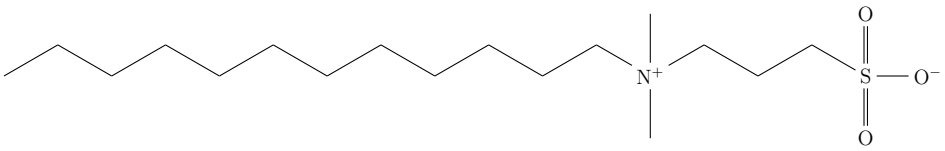
Figure 1.3: The classification of surfactants based on the nature of the headgroups

1.2 Zwitterionic Surfactants

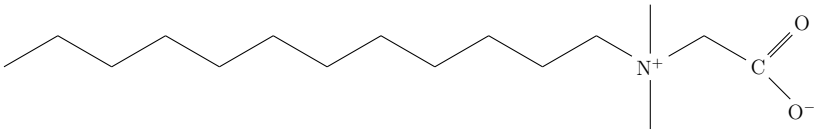
A zwitterionic surfactant has both a positive and a negative charge in the head–group. This separation of charged groups creates a dipole moment in the head–group and therefore makes it polar and soluble in water. Zwitterionic surfactants are of great interest in both scientific research and commercial applications.

The head–group structure makes a zwitterionic surfactant tolerant to strong electrolytes, hard water, oxidizing and reducing agents and gives it low toxicity and compatibility with all other types of surfactants. [6–8].

A betaine is an overall neutral chemical compound with a positively charged cationic functional group such as quaternary ammonium which bears no hydrogen atom and with a negatively charged functional group such as a carboxylate group or a sulfonic acid group which may not be adjacent to the cationic site. A betaine thus may be a specific type of zwitterionic surfactant. Betaines are widely used in commercial hair conditioners or shampoos as foam boosters because they stabilize foam against the anti-foaming action of the oil droplets [9]. Furthermore, these surfactants cause less irritation than ionic ones on the eye and skin [10]. In this thesis, the research is mainly focused on the following two betaines, N-Dodecyl-N,N-dimethyl-3-ammonio-1-propanesulfonate (C_{12} sulfobetaine, abbreviated as DSB), N-Dodecyl-N,N-dimethylglycine (C_{12}carboxybetaine, abbreviated as DCB) and their mixed systems with ionic surfactants.



N-Dodecyl-N,N-dimethyl-3-ammonio-1-propanesulfonate(C_{12} sulfobetaine)



N-Dodecyl-N,N-dimethylglycine (C_{12}carboxybetaine)

It has been reported that the pK_a of carboxybetaine is around 2 when the carboxyl group is separated from quaternary ammonium by only one methylene group [11, 12] and can only show characteristics of a cationic at low pH. Therefore it is necessary to take into account of the propensity of the carboxybetaine to become protonated. Hines et al. investigated the pH of solution containing SDS and carboxybetaine and found that some protonation occurs. However, the magnitude of the effect is very small so that even if one makes the assumption that all additional OH^- generated is due to protonation, then at concentrations over 50 times the CMC, less than 1 in 20 000 carboxybetaine molecules can be protonated. Therefore the interaction can be described as anionic–zwitterionic, not anionic–cationic [13]. Although the relatively high pK_a of the -COOH group in betaines makes them sensitive to changes in pH, changes in their environment, e.g. in a micelle, and changes in structure, the sulfobetaines are insensitive to such changes because the pK_a of alkyl sulfonic acid is around -2 [14]. It is therefore expected to behave similar to non–ionic surfactant [1, 12].

1.3 Mixed Surfactant Systems

1.3.1 Introduction

The study of surfactant mixtures is of considerable interest, from both practical and theoretical viewpoints. Mixed surfactant systems are involved in most domestic, industrial and technological applications of surfactants [15]. The mixing behaviour can be divided into two categories.

In the first category, a level of mixing occurs in all formulations of commercial surfactants due to the impurity of samples, which may include not only unreacted

material and by–products that arise from the manufacturing process, but also a nominally pure surfactant will show a distribution of hydrophobic chain lengths. Since the driving force of micellization is the hydrophobic effect and a random arrangement of monomer units in aggregates is favoured, this type of mixing is usually straightforward to predict [16–18] .

Many commercial products, however, consist of deliberately mixed systems in order to enhance various important properties. It has been shown that the properties of surfactant mixtures can be superior to those of any of the individual components, for example, the addition of non–ionic surfactant can reduce the tendency of anionic surfactant to precipitate at equilibrium by synergizing micelle formation, reducing the concentration of anionic surfactant monomer, which is the driving force for precipitation. Thus the non–ionic surfactant cause a synergistic interaction in the micellization by screening the electrostatic repulsion between the anionic surfactants [1, 19, 20]. The thermodynamic treatment of this important type of mixing is complicated by the fact that the interaction which produces enhanced behaviour also results in strong deviations from ideality.

In order to predict the behaviour of mixed surfactant systems, it is necessary to develop a model that describes observed behaviour. It is common to approximate the mixture system's behaviour by using the pseudophase approximation, in which the micelles are treated as a separate thermodynamic phase in equilibrium with the monomer solution. This equilibrium is then assumed to be similar to a vapour-liquid equilibrium as in both cases the dilute phase with little intermolecular interaction is in equilibrium with a concentrated phase in which intermolecular

forces can not be ignored, Thermodynamic methods from liquid mixing can then be applied to the mixed micelles.

1.3.2 The Chemical Potential

It is convenient to describe the total value of the thermodynamic functions of state associated with the system as a whole in terms of the contributions made to them by each species. These individual contributions are defined partial molar quantities. In the case of surfactant mixing, the most important one would be partial molar Gibbs function, or the chemical potential , μ, which can be written for any species of a multi–component system as

$$\mu_i = \left(\frac{\partial G}{\partial n_i}\right)_{p,T,n_{j,j\neq i}} \tag{1.1}$$

The total Gibbs function of the system can thus be given as

$$G = n_1\mu_1 + n_2\mu_2 + ... + n_i\mu_i \tag{1.2}$$

where μ_1, μ_2 and μ_i are the chemical potentials of each species present in the mixture and the n is the molar amounts of each. In general, it can be written as

$$G = \sum_i n_i\mu_i \tag{1.3}$$

It can also be shown that for small changes in the value of G, at constant pressure and temperature [21],

$$\sum_i n_i d\mu_i = 0 \tag{1.4}$$

which is the general form of the Gibbs–Duhem equation. It describes the independence of the chemical potentials. Combined with the fact that the chemical potentials at equilibrium of a given species in a mixture must be everywhere identical, this quantity becomes useful in formulating expressions describing the

thermodynamic state of mixtures.

In the case of mixture of liquids, each component will be in thermodynamic equilibrium with its vapour, which can be expressed as

$$\mu_i = \mu_i^{\Theta} + RT \ln \frac{p_i}{p_i^{\Theta}} \tag{1.5}$$

where μ_i^{Θ} is the standard chemical potential of species i, which is defined as a hypothetical 1 mol kg^{-1} solution of species i in which interactions are the same as they would be at infinite dilution, at constant T and P, p_i is the partial pressure of i in the vapour above the mixture, and p_i^{Θ} is the vapour pressure of i over its pure liquid. Raoult discovered experimentally that in mixtures of very similar liquids, the ratio of vapour pressure is proportional to the mole fraction of the component i in the liquid, x_i. This relationship is the basis of Raoult's Law and written as

$$p_i = x_i p_i^{\Theta} \tag{1.6}$$

This leads directly to the definition of an ideal solution, which obeys Raoult's Law for all compositions. A more general form of the chemical potential equation, which implies Raoult's Law is given as

$$\mu_i = \mu_i^{\Theta} + RT \ln x_i \tag{1.7}$$

1.3.3 Thermodynamics of the Ideal Solution

The entropy of mixing of two ideal gases is identical to the formula assumed for the ideal mixing of liquids. The entropy of expansion of an ideal gas is first derived. From the first and second laws

$$dU = TdS - PdV \tag{1.8}$$

which can be rearranged to give

$$dS = \frac{dU}{T} + \frac{P}{T}dV \tag{1.9}$$

For an ideal gas, $PV = nRT$ and U does not change during a change in volume of the gas. Hence, for one mole of gas,

$$\int_{S_2}^{S_1} dS = R \int_{V_2}^{V_1} \frac{dV}{V} \tag{1.10}$$

and

$$\Delta S = R \ln \left(\frac{V_1}{V_2} \right) \tag{1.11}$$

If two pure gases i and j occupying volumes V_i and V_j are allowed to mix the new volume becomes $V_i + V_j$ and each gas has increased its entropy by expanding into the space occupied by the other,

$$\Delta S = R \ln \frac{V_i + V_j}{V_i} \tag{1.12}$$

and the total entropy change is

$$\Delta S = R \left[x_i \ln \frac{V_i + V_j}{V_i} + x_j \ln \frac{V_i + V_j}{V_j} \right] = -R(x_i \ln x_i + x_j \ln x_j) \tag{1.13}$$

The difference for liquids is that the volume available for each to expand into is only a proportion of the actual volume because the molecules themselves occupy a significant fraction of the volume. Thus the entropy of the mixing of two liquids might be written as

$$\Delta S = R \left[x_i \ln \frac{V_{i,f} + V_{j,f}}{V_{i,f}} + x_j \ln \frac{V_{i,f} + V_{j,f}}{V_{j,f}} \right] \tag{1.14}$$

where $V_{i,f}$, etc. denotes the available free volume. Assuming that the fraction, f, of the molar volume that is free is the same for i as for j, then

$$\Delta S = R \left[x_i \ln \frac{fV_i + fV_j}{fV_i} + x_j \ln \frac{fV_i + fV_j}{fV_j} \right] = -R[x_i \ln \phi_i + x_j \ln \phi_j] \tag{1.15}$$

where ϕ_i and ϕ_j are the volume fractions. The second assumption if that $V_i = V_j$. Then ϕ_i is

$$\phi_i = \frac{x_i V_i}{x_i V_i + x_j V_j} = x_i \tag{1.16}$$

and

$$\Delta S_{mix} = -R\left(x_i \ln x_i + x_j \ln x_j\right) \tag{1.17}$$

and the enthalpy of mixing is zero for ideal solution

$$\Delta H_{mix} = 0 \tag{1.18}$$

The Gibbs free energy of mixing is therefore

$$\Delta G_{mix} = \Delta H_{mix} - T\Delta S_{mix} = RT(x_i \ln x_i + x_j \ln x_j) \tag{1.19}$$

Since mole fractions are always less than unity, the $\ln$ terms are always negative, and the entropy of mixing is always positive. The Gibbs free energy is always negative and becomes more negative as the temperature is increased.

1.3.4 Regular Solutions

Non–ideal Behaviour: Activity Coefficient

A solution may be non–ideal because ΔH_{mix} is not zero or because ΔS_{mix} does not have its ideal value. If there is a deviation from ideal behaviour the equation for the chemical potential must be modified to

$$\mu_i = \mu_i^{\Theta} + RT \ln x_i + F(x) \tag{1.20}$$

where F is the difference between the real and ideal chemical potentials. Usually F depends on concentration and then it is convenient to express it in the form

$$\mu_i = \mu_i^{\Theta} + RT \ln x_i + RT \ln f_i = \mu_i = \mu_i^{\Theta} + RT \ln a_i \tag{1.21}$$

where f_i is called the activity coefficient and a_i is called the activity. The activity coefficient is a quantity that is determined by experiment.

Regular Solution

The regular solution model is a quantitative explanation of non–ideal behaviour. The model assumes that the entropy of mixing is the same as ideal mixing but the enthalpy of mixing is not zero. Consider a mixture of i and j where i and j are randomly mixed and the average coordination number is z. If there are n_j molecules of j in the mixture these will be in contact with a total of zn_j molecules, of which $x_i z n_j$ contacts are with molecules of i. This is the total number of ij contacts. Before mixing, these contacts would have been jj contacts in pure j and so the change in energy of mixing is, for the j molecules,

$$x_i z n_j(\epsilon_{ij} - \epsilon_{jj})$$

By the analogous argument the change in energy on mixing of the i molecule is

$$x_j z n_i(\epsilon_{ij} - \epsilon_{ii})$$

and the total energy change on mixing is

$$E = \frac{1}{2}\frac{z n_i n_j}{n_i + n_j}(2\epsilon_{ij} - \epsilon_{ij} - \epsilon_{jj}) = \beta\frac{n_i n_j}{n_i + n_j} \tag{1.22}$$

The β used to replace $z(2\epsilon_{ij} - \epsilon_{ij} - \epsilon_{jj})/2$ is called interaction parameter. By assuming that the enthalpy of mixing is the same as the energy of mixing, the non–zero enthalpy (energy) of mixing leads to an additional term in the chemical potential, $\mu_{regular}$, which can be obtained b differentiating the enthalpy of mixing.

$$\mu_{regular} = \left(\frac{\partial E}{\partial n_i}\right)_{T,P,n_j} = \beta x_j^2 \tag{1.23}$$

Hence the chemical potential of a regular solution is

$$\mu_{i,regular} = \mu_i^{\Theta} + RT \ln x_i + \beta x_j^2 = \mu_i^{\Theta} + RT \ln x_i + RT \ln f_i \tag{1.24}$$

where a new quantity is defined, the activity coefficient, given by

$$\ln f_i = \frac{\beta}{RT} x_j^2 = B x_j^2 \tag{1.25}$$

A similar result is obtained for the activity coefficient of i, and the β is most usually divided by RT and written as B, the non–ideality parameter. For a regular solution, the free energy of mixing is

$$\Delta G_{mix,regular} = n_i \Delta \mu_{i,regular} + n_j \Delta \mu_{j,regular} \tag{1.26}$$

which has the final form

$$\Delta G_{mix,regular} = RT(x_i \ln x_i + x_j \ln x_j) + RT(x_i \ln f_i + x_j \ln f_j) \tag{1.27}$$

The physical significance of the second is the free energy in excess of that found upon ideal mixing, due to non–ideality. Thus the excess free energy, G_E, can be written

$$G_E = \Delta G_{mix,regular} - \Delta G_{mix,ideal} \tag{1.28}$$

and

$$G_E = RT(x_i \ln f_i + x_j \ln f_j) = RTBx_i x_j \tag{1.29}$$

1.3.5 Surfactant Mixtures

The chemical potential of the component i as monomer in solution, μ_i, and its activity, a_i, which can be equated to its concentration as monomer, c_i, provided that its activity coefficient is assumed to be unity, is given as

$$\mu_i = \mu_i^{\Theta} + RT \ln c_i \tag{1.30}$$

When the only species in solution is i, equation (1.30) can be modified to give the chemical potential of the species in aggregation, $\mu_{i,modified}$

$$\mu_{i,modified} = \mu_i^{\Theta} + RT \ln CMC_i \tag{1.31}$$

where CMC_i is the CMC of solution only containing species i. The chemical potential of i in the mixed micelle, $\mu_{i,micelle}$, can be written as

$$\mu_{i,micelle} = \mu_{i,modified} + RT \ln x_i f_i \tag{1.32}$$

where the activity of i is presented as the product of f_i and the mole fraction of i in the mixed micelle, x_i

The definition of the chemical potential requires that at equilibrium values are identical for each component in a system. Hence, equations (1.30) and (1.32) may be combined to give an expression for the relationship between the monomer concentration of i, the CMC of i and the composition of the mixed micelle.

$$c_i = x_i f_i CMC_i \tag{1.33}$$

The CMC of the mixture at any composition, CMC_{mix}, can be found since at this point the monomer concentration of component i, c_i, will equal its mole fraction of total surfactant in the system, a_i, multiplied by the total surfactant concentration. The sum of all mole fraction of surfactant must equal unity, giving

$$\frac{1}{CMC_{mix}} = \sum_{i=1}^{n} \frac{a_i}{f_i CMC_i} \tag{1.34}$$

If the mixing is ideal, equation (1.34) is straightforward to be solved since all activity coefficients take on a value of unity. In the case of a binary mixture system following regular solution theory, the relation in equation (1.25), gives

$$ln\left(\frac{f_1}{f_2}\right) = B(x_1 - x_2) = ln\left[\frac{x_1 a_2 CMC_1}{x_2 a_1 CMC_2}\right] \tag{1.35}$$

Iteration of

$$B(x_1 - x_2) - ln\left[\frac{x_1 a_2 CMC_1}{x_2 a_1 CMC_2}\right] = 0 \tag{1.36}$$

can be done using the simplest iteration method, the sector method [22], given that

$$a_1 + a_2 = 1 \tag{1.37}$$

$$x_1 + x_2 = 1 \tag{1.38}$$

Mulqueen et al. presented a theoretical framework to predict the surface tension and monolayer composition at the air–liquid interface containing mixtures of ionic, nonionic and zwitterionic surfactants, which treat the electrostatic effects associated with the adsorption of zwitterionic surfactants at the interface rigorously [23]. Good agreement was found between the theoretical prediction and experimental observation for not only binary systems, but also ternary mixtures containing zwitterionic betaine surfactant. McLachlan et al. have studied the interaction between zwitterionic and ionic surfactant mixtures employing surface tension, conductivity measurements and nuclear magnetic resonance (NMR) spectroscopy [24], in which the nonideal parameter of micelles are calculated according to Rubingh's nonideal solution theory [25]. Evidence of strong interaction for the anionic/zwitterionic mixture was found for three systems studied and a nearly ideal mixing behaviour was observed for the cationic/zwitterionic mixtures. Diaz et al. conducted a investigation on the synergism in mixtures of zwitterionic and ionic surfactants using conductivity and fluorescence probing [26]. Similar behaviour was found for anionic/zwitterionic and cationic/zwitterionic mixtures. The addition of inert electrolytes was found to favour the interactions between the ionic and the zwitterionic surfactants. Li et al. also studied the synergism in mixed zwitterionic/anionic surfactant solutions with surface tension measurements and

fluorescence studies [27], and found that the synergism is greatest when the mixture is rich in anionic surfactant, i.e. a large molar ratio of anionic in mixed solutions of SDS and cocoamidopropyl betaine, measured by means of the Wilhelmy plate method [28]. Several properties of surfactant adsorption were calculated for SDS, Betaine and salt, such as adsorption of the two surfactants and the total adsorption, the surface dilatational (Gibbs) elasticity, the occupancy of the Stern layer by bound counterions, and the surface electric potential. Misselyn-Bauduin has analysed anionic/zwitterionic mixtures by using pulsed field gradient NMR [29], and compared the experimental data to theoretical predictions based on the regular solution theory. Some discrepancy between theory and experimental data was observed for the system, especially at a high mole fraction of anionic SDS. Hines et al. investigated the strongly interacting anionic/zwitterionic and nonionic/zwitterionic mixtures by means of surface tension and neutron reflection [30, 31]. Both surface composition and layer structure information were obtained for the anionic/zwitterionic mixture, and the surface layer was found to be significantly dehydrated in comparison with layers of the single surfactants, which might also explain the deviations from the first-order model observed for both micellization and surface interaction. In the case of nonionic/zwitterionic mixtures, the surface behaviour was closer to being ideal, and direct measurements from neutron reflection were consistent with the surface tension results using the integrated form of the Gibbs equation.

Bibliography

[1] M. J. Rosen and J. T. Kunjappu. *Surfactants and interfacial phenomena*. John Wiley & Sons, 2012.

[2] D. J. Shaw. *Introduction to colloid and surface chemistry*. Colloid and Surface Engineering Series. Butterworth-Heinemann, 1992.

[3] J. Powney and C. C. Addison. The properties of detergent solutions. *Transactions of the Faraday Society*, 33:1243–1260, 1937.

[4] O. R. Howell and H. G. B. Robinson. The electrical conductivities of aqueous solutions of sodium dodecyl sulphate and sodium hexadecyl sulphate at different temperatures. *Proceedings of the Royal Society of London. Series A, Mathematical and Physical Sciences*, 155(885):386–406, 1936.

[5] W. C. Presto. Some correlating principles of detergent action. *The Journal of Physical and Colloid Chemistry*, 1948.

[6] I. Harwigsson, F. Tiberg, and Y. Chevalier. Nature of the adsorption of zwitterionic surfactants at hydrophilic surfaces. *Journal of Colloid and Interface Science*, 183(2):380 – 387, 1996.

[7] J. D. Hines, R. K. Thomas, P. R. Garrett, G. K. Rennie, and J. Penfold. Investigation of mixing in binary surfactant solutions by surface tension and neutron reflection: anionic/nonionic and zwitterionic/nonionic mixtures. *The Journal of Physical Chemistry B*, 101(45):9215–9223, 1997.

[8] V. Seredyuk, E. Alami, M. Nydén, K. Holmberg, A. V. Peresypkin, and F. M. Menger. Micellization and adsorption properties of novel zwitterionic surfactants. *Langmuir*, 17(17):5160–5165, 2001.

[9] E. S. Basheva, S. Stoyanov, N. D. Denkov, K. Kasuga, N. Satoh, and K. Tsujii. Foam boosting by amphiphilic molecules in the presence of silicone oil. *Langmuir*, 2001.

[10] G. Broze. *Handbook of Detergents: Properties*. CRC Press, 1999.

[11] J. G. Weers, J. F. Rathman, F. U. Axe, C. A. Crichlow, L. D. Foland, D. R. Scheuing, R. J. Wiersema, and A. G. Zielske. Effect of the intramolecular charge separation distance on the solution properties of betaines and sulfobetaines. *Langmuir*, 7(5):854–867, 1991.

[12] R. G. Laughlin. Fundamentals of the zwitterionic hydrophilic group. *Langmuir*, 7(5):842–847, 1991.

[13] J. D. Hines. *Investigation of Surfactants and Surfactant Mixtures*. PhD thesis, University of Oxford, 1996.

[14] Naomichi Furukawa and Hisashi Fujihara. Acidity, hydrogen bonding and metal complexation of sulfonic acids and derivatives. *Sulphonic Acids, Esters and their Derivatives (1991)*, pages 261–281, 1991.

[15] M. Abe. *Mixed surfactant systems*. CRC Press, 2010.

[16] C. Tanford. The hydrophobic effect and the organization of living matter. *Science*, 200(4345):1012–1018, 1978.

[17] M. J. Vold. Colloidal surfactants. some physicochemical properties. *Journal of the American Chemical Society*, 86(7):1461–1461, 1964.

[18] J. H. Clint and T. Walker. Thermodynamics of micellization of homologous series of n-alkyl methyl sulphoxides and n-alkyl(dimethyl)phosphine oxides. *J. Chem. Soc., Faraday Trans. 1*, 71:946–954, 1975.

[19] J. F. Scamehorn and J. H. Harwell. Precipitation of surfactant mixtures. *Mixed Surfactant Systems*, page 283, 1993.

[20] S. Soontravanich and J. F. Scamehorn. Use of a nonionic surfactant to inhibit precipitation of anionic surfactants by calcium. *Journal of surfactants and detergents*, 13(1):13–18, 2010.

[21] I. Prigogine, R. Defay, and D. H. Everett. *Chemical thermodynamics*. Longmans New York, 1962.

[22] J. D. Hoffman and S. Frankel. *Numerical methods for engineers and scientists*. CRC press, 2001.

[23] M. Mulqueen and D. Blankschtein. Prediction of equilibrium surface tension and surface adsorption of aqueous surfactant mixtures containing zwitterionic surfactants. *Langmuir*, 16(20):7640–7654, 2000.

[24] A. A. McLachlan and D. G. Marangoni. Interactions between zwitterionic and conventional anionic and cationic surfactants. *Journal of colloid and interface science*, 295(1):243–248, 2006.

[25] D. N. Rubingh. Mixed micelle solutions. In *Solution chemistry of surfactants*, pages 337–354. Springer, 1979.

[26] D. Lopez-Diaz, I. Garcia-Mateos, and M. M. Velázquez. Synergism in mixtures of zwitterionic and ionic surfactants. *Colloids and Surfaces A: Physicochemical and Engineering Aspects*, 270:153–162, 2005.

[27] F. Li, G. Z. Li, and J. B. Chen. Synergism in mixed zwitterionic–anionic surfactant solutions and the aggregation numbers of the mixed micelles. *Colloids and Surfaces A: Physicochemical and Engineering Aspects*, 145(1):167–174, 1998.

[28] K. D. Danov, S. D. Kralchevska, P. A. Kralchevsky, Ananthapadmanabhan K. P., and A. Lips. Mixed solutions of anionic and zwitterionic surfactant (Betaine): Surface-Tension isotherms, adsorption, and relaxation kinetics. *Langmuir*, 2004.

[29] A. M. Misselyn-Bauduin, A. Thibaut, J. Grandjean, G. Broze, and R. Jérôme. Mixed micelles of anionic-nonionic and anionic-zwitterionic surfactants analyzed by pulsed field gradient nmr. *Langmuir*, 16(10):4430–4435, 2000.

[30] J. D. Hines, R. K. Thomas, P. R. Garrett, G. K. Rennie, and J. Penfold. Investigation of mixing in binary surfactant solutions by surface tension and neutron reflection: strongly interacting Anionic/Zwitterionic mixtures. *The Journal of Physical Chemistry B*, 1998.

[31] J. D. Hines, R. K. Thomas, P. R. Garrett, G. K. Rennie, and J. Penfold. Investigation of mixing in binary surfactant solutions by surface tension and

neutron reflection: Anionic/Nonionic and Zwitterionic/Nonionic mixtures. *The Journal of Physical Chemistry B*, 1997.

Chapter 2

Surface Tension and Neutron Reflectivity

2.1 Surface Tension

2.1.1 Introduction

Many commonly occurring phenomena observed in systems containing an interface in which one of the phases is liquid can be understood through the concept of surface tension. The study of surface tension not only provides a sensitive measure of the surfactant impurity, but is also used to determine the CMC of the surfactants and mixed systems. In addition, it gives quantitative information about the interfacial behaviour, such as surface excess and area per molecule.

It is well known that insoluble and partially soluble substances in solution segregate to the interface [1], and the process of creating the interface requires energy from the system. The term “interfacial tension“ or “surface tension“ is a measure of work done on the system during this process.

The surface tension measurements in this thesis were conducted using the instrument Krüss K10T. The instrument uses a force balance to measure the maximum pulling force, F_p as the ring or plate is dragged out of the liquid. For the Du Noüy ring method [2], the surface tension was originally thought to be equal to the maximum pulling force per centimetre giving,

$$\gamma = F_p / L_r \tag{2.1}$$

where R is the radius of of the ring, and L_r is the length of the ring. However, it was then found that this method gave values which were often in error by as much as 30%. The error lies in the fact that account must be taken of the volume of liquid raised up under the ring. The problem was first addressed by Harkins and an empirical correction factor was introduced, β [3],

$$\gamma = \frac{F_p \beta}{L_r} \tag{2.2}$$

and values tabulated for a range of raised volumes, for which Freud established the theoretical basis [4]. Later Zuidema & Waters [5] analysed and developed an equation that allows calculation of the correction factor,

$$(\beta - a)^2 = \frac{4b}{\pi^2 R^2} \left(\frac{F}{\rho_{upper} - \rho_{lower}} \right) + C \tag{2.3}$$

where F is the measured surface tension, a and b are universal constants for all rings and with the values 0.725 and 9.075×10^{-4} respectively, ρ_{upper} and ρ_{lower} are the densities of the upper and lower phases of the ring respectively and C is a constant given by,

$$C = 0.04534 - 0.84 \frac{d}{R} \tag{2.4}$$

where d is the cross sectional dimension of the ring.

2.1.2 Instrumentation

Surface tension measurements were performed using Krüss K10T Digital Tensiometer, which has a water bath to control the temperature of the sample and a motor drive to draw the sample down away from the ring for tension measurement. There is also a digital display of the surface tension and an analogue panel meter to determine the point of maximum force on the instrument. The rings used are made of Pt-Ir alloy and have dimensions R=9.545mm and r=0.185mm.

2.1.3 Experimental Procedure

It is difficult to measure the surface tension accurately and one of the problems is to prevent contamination from the samples. In order to address this issue, two precautions are taken. Firstly, the glass sample containers were prepared by soaking in 5% solution of a commercial alkaline detergent (Decon 90) solution and rinsed with UHQ water until no bubbles persisted,indicating that the rinsing water was free from surface active impurities. Secondly, before every measurement the ring was rinsed in UHQ water and flamed to red heat. In addition, at each sample concentration the measurement was repeated until there were three measurements in agreement to within the accuracy of the instruments, ± 0.2 mN/m.

2.1.4 Interpretation of Surface Tension and Gibbs Adsorption Isotherm

The interfacial region is not a simple boundary between two homogeneous and immiscible phases as it appears on macroscopic level, but an inhomogeneous layer with non-zero thickness. To describe the adsorption of surfactant at interfaces, the interface is represented mathematically by a dividing plane known as Gibbs dividing plane [6].

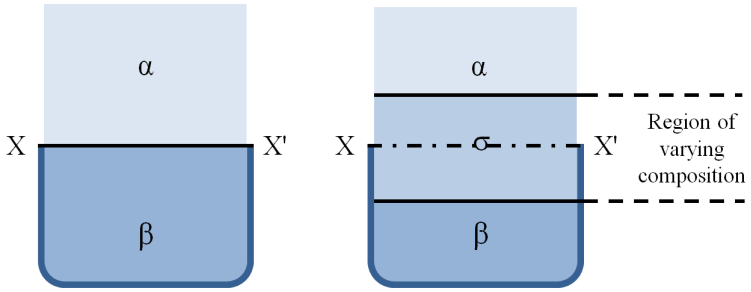


Figure 2.1: The Gibbs dividing model

Total adsorption at this interface is usually described in terms of the surface excess concentration, Γ. At a dividing plane where the solvent surface excess is zero, the total adsorption is the sum of the individual components adsorbed at the interface,

$$\Gamma_i = \frac{n_i^\sigma}{A} \tag{2.5}$$

where n_i^σ is the number of moles of component i adsorbed at the interface, and A is the interfacial area. The value of Γ_i and n_i^σ depends on the location of the mathematically divided surface, Γ_i may be positive, indicating an accumulation of component i at the interface, or negative, indicating a deficiency of i in the interface region.

The total adsorption for a surface phase σ, can be described thermodynamically by considering the total internal energy, U^σ, involved in the process,

$$U^\sigma = TS^\sigma - pV^\sigma + \sum_i \mu_i n_i^\sigma + \gamma A \tag{2.6}$$

where T is the temperature in K, S^σ is the entropy, p is the pressure and V^σ is the volume. The parameters μ_i and n_i^σ are the chemical potential and number of molecule of component i in the interfacial phase, and γ is the surface tension.

Differentiation of equation (2.6) gives,

$$dU^{\sigma} = TdS^{\sigma} + S^{\sigma}dT - pdV^{\sigma} - V^{\sigma}p + \gamma dA + Ad\gamma + \sum_i \mu dn_i^{\sigma} + \sum_i n_i^{\sigma} d\mu_i \quad (2.7)$$

For the bulk phase, by following the first and second laws of thermodynamics,

$$dU = TdS - pdV + \sum_i \mu_i n_i \quad (2.8)$$

so for the surface phase,

$$dU^{\sigma} = TdS^{\sigma} - pdV^{\sigma} + \sum_i \mu_i n_i^{\sigma} + \gamma dA \quad (2.9)$$

Subtracting equation (2.9) from equation (2.7), gives,

$$S^{\sigma}dT - V^{\sigma}dp + Ad\gamma + \sum_i n_i^{\sigma} d\mu_i = 0 \quad (2.10)$$

which under isobaric and isothermal conditions may be reduced to,

$$d\gamma = \text{-} \sum_i \frac{n_i^{\sigma}}{A} d\mu_i = \text{-} \sum_i \Gamma_i d\mu_i \quad (2.11)$$

the equation (2.11) relates the change in surface tension with the change in chemical potential of species i. For a simple binary system containing a surfactant, denoted by suffix 1, and a solvent, denoted by suffix sol, equation(2.11) may be written as

$$d\gamma = \text{-}\Gamma_1 d\mu_1 - \Gamma_{sol} d\mu_{sol} \quad (2.12)$$

Since the surface excesses are defined relative to the arbitrarily chosen dividing surface, a convenient choice of location is for the surface is where the excess of solvent, $\Gamma_{sol} = 0$, equation (2.12) then becomes,

$$d\gamma = \text{-}\Gamma_1 d\mu_1 \quad (2.13)$$

and since the chemical potential and activity, a, is related as

$$\mu_1 = \mu_1^0 + RT \ln a_1 \tag{2.14}$$

and hence

$$d\mu_1 = RT d \ln a_1 \tag{2.15}$$

the surface excess can be expressed as follows,

$$\Gamma_1 = -\frac{1}{nRT} \frac{d\gamma}{d \ln a_1} \tag{2.16}$$

which is the Gibbs equation. The addition of the multiplier, n, is to account for the different number of kinetic objects associated with charged surfactants where both surfactant and counterion are dissociated, and in this case $n = 2$. For uncharged surfactants, $n = 1$. If the solution is sufficiently dilute and activity approximates to concentration, the surface excess becomes,

$$\Gamma_1 = -\frac{C_1}{nRT} \frac{d\gamma}{dC_1} \tag{2.17}$$

From the slop of a plot of surface tension versus concentration, the surface excess and hence the area per molecule, can be calculated.

2.2 Neutron Reflectivity

2.2.1 Introduction

Since the first investigation of neutron optical phenomenon was made by Fermi and Zinn in 1944 [7], neutron reflectivity is now applied in a wide range of studies on surface and interfacial phenomena [8–13] and is one of the most powerful techniques for studying surfactant layers at an interface [14].

The wave-length of the neutron is given by the equation:

$$\lambda = \frac{h}{(mkT)^{\frac{1}{2}}} \tag{2.18}$$

where h is Planck's constant, m is the mass of the neutron, k is Boltzmann's constant and T is the temperature. For thermal neutrons (226 pm at 100°C), the wave-lengths are about two orders of magnitude shorter than visible light and therefore comparable to dimensions of many molecules and sensitive to structure distributions at the molecular level. Another important characteristic is the large difference between the neutron scattering lengths of hydrogen and deuterium. Isotopic substitution of hydrogenous systems can be exploited extensively in the study of different interfaces to allow greater resolution of composition and structure. The technique now has been well established in the study of single surfactants [13, 15, 16], polymers [17, 18],mixtures of surfactants [19–21], mixtures of surfactant and polymer [22–25], and the structure of membrane or protein layers [26, 27] adsorbed at different interfaces.

There are two main methods for analysing the neutron reflectometry data, the optical matrix method [28] and the kinematic approximation [29]. In the first approach, the neutron reflection is treated as the mathematical equivalent of light reflection with the plane of polarisation perpendicular to the reflection plane. These two types of reflection have been demonstrated to be completely equivalent [30]. The experimental data can then be analysed by applying the standard theory of optics [31, 32]. A model is used where the interface is divided into a set of uniform layers, leading to a set of parameters (layer thickness, scattering length density) of the interface which is fitted to the experimental data until good agreement is

observed. The problem of this approach is that although the data may be fitted perfectly, the fit is not necessarily unique. Other variations may also give rise to an equally good fit. For this reason the kinematic approximation, which relates the reflectivity to the interfacial scattering length density profile by a Fourier transform has proved a complementary method of data analysis [33], because the approximation gives a more direct description of the structure of soluble surfactant monolayers [34].

2.2.2 Instrumentation

The neutron experiments discussed in this thesis were measured on the reflectometers SURF and INTER at the Rutherford-Appleton Laboratory, Chilton, Oxon, UK [35, 36]. For both instruments the neutrons are produced by a pulsed source, using a pulsed beam of electrons or protons hits a heavy nucleus e.g. tantalum. Following the production os high-energy neutrons, moderation is required before they are fed to the instruments. This is accomplished by passing the neutrons through a moderator of cold (20-25K) hydrogen or deuterium rich environment where multiple inelastic scattering events thermalize the neutrons to lower temperatures and longer wavelengths

The measurable parameter in neutron reflection experiments is the variation of reflectivity, $R = I/I_0$, where I and I_0 are the intensities of the reflected and incident beams respectively, with q_z, the wave vector transfer perpendicular to the interface which is given by

$$q_z = \frac{4\pi \sin\theta}{\lambda} \tag{2.19}$$

According to this expression, the variation of q can be achieved either by using a monochromatic beam of neutrons and variation in the angle of incidence, or using a fixed angle of incidence and varying wavelength. Both reflectometer used in this work are of the time-of-flight type in which the angle is kept constant and a range of wavelengths is incident on the sample.

2.2.3 Sample Environment

The sample environment for air-liquid studies using INTER consists of seven Teflon troughs mounted in a moveable sample changer. The troughs each measure 235mm long, 50mm wide and 2mm deep with a 5mm groove around the edge to catch spilled solution and will hold approximately 20-25 ml of solution. The temperature of each housing can be thermostatically controlled. Each trough is covered by an air-tight lid to reduce problems caused by evaporation and contamination.

The cell designed for solid-liquid neutron experiments reported in this thesis consist of a PTFE trough, which is clamped to a polished single crystal silicon block which has dimensions 50mm$\times$50mm$\times$10mm.

The experimental solution was held in a Teflon container with a volume of approximately 25ml, which was clamped against the silicon block between temperature-controlled aluminium blocks. The cells can be mounted on a base plate, which is attached to a translation table. Sample changes were made through inlet and outlet ports located on opposite sides of the container, which could be connected to plastic tubes for injection. Both the SURF and INTER reflectometers have horizontal alignment with the silicon crystal sitting on top of the liquid. A computer

controlled water bath allows temperature to be varied remotely.

2.2.4 Sample Preparation

Due to the nature of the air-liquid experiment and the fact that surfactant systems are being studied there is a high sensitivity to surface-active impurities. Therefore all the glassware used was soaked in 20% hot Decon 90 solution, then rinsed and soaked in UHQ water until no bubbles persisted. The glassware was then dried in a vacuum oven at $60^{\circ}C$ to avoid isotopic contamination of D_2O solutions by H_2O. The troughs were cleaned with all parts being scrubbed with neat Decon 90 then rinsed with UHQ water and dried with tissues.

The solid-liquid interface experiments used single crystal silicon blocks with dimensions of $50\times50\times10$ mm^3 that were polished on the (111) face. The blocks were supplied and polished by Crystan Ltd. In order to produce the hydrophilic interface for the neutron measurements, the silicon blocks were cleaned by immersion in piranha solution (a 5:4:1 mixture of $H_2O/H_2SO_4/H_2O_2$) at 75 °C and by UV/ozone treatment, then rinsing and soaking in clean UHQ water(Elgastat Ultrapure). Great care at this stage was taken to remove all air bubbles as this reduces the reflected intensity greatly and results in a poorly defined critical edge on the reflectivity profile. Following this treatment, the silicon (111)surface typically has a layer of oxide of about 15 Å in depth. The neutron beam is incident at glancing angles at the solid-liquid interface by transmission through the crystalline silicon upper phase.

2.2.5 Experimental Procedure

For the air-liquid experiments, the samples were poured into the Teflon troughs set in the sample position of the reflectometer. Alignment was accomplished by using a visible laser beam that follows the same path as the neutrons, and the height of sample was adjusted until the laser beam was central in the detector silt. Pasteur pipettes were used to remove any bubbles on the sample. Up to seven troughs can be seated in the sample changer which was used for all measurements.

For the solid-liquid experiments, once the cells were seated on the translation table, the first stage is to align the oxide surface such that the maxima of the specular ridge is being recorded. An approximate position was found using a visible laser beam. The alignment was then refined using the neutron beam follows a series of height and angle scans by doing iterative scans over range of height and rocking angle parallel to the direction of neutron beam. It is also necessary to scale the magnitude of reflectivity to an absolute scale by a run with D_2O.

The sample changer was linked to the computer and could be operated either directly via the software or by using command files to automate its movement and data collection. Before any measurements, all the samples are aligned as above. During each measurements, sample changer and data collection were controlled by command files so each sample was moved into the beam and a reflectivity file recorded and stored.

2.2.6 Neutron Reflection at a Planar Boundary

When an incident beam arrives at a smooth surface at an angle not normal to the interface, it is both reflected and refracted. The ratio of neutron specular reflection, transmission and scattering depends on the neutron interaction potential of the medium and nature of the surface. The surface structure can be derived through this relation.

The Schrödinger equation for the neutron can be written as:

$$-\frac{\hbar^2}{2m} \bigtriangledown^2 \psi(r) + V\psi(r) = E\psi(r) \tag{2.20}$$

where m is the mass of the neutron, V is the potential to which it is subject, E its energy, $\psi(r)$ is the neutron wave function and $\hbar = \frac{h}{2\pi}$ where h is Planck's constant. The potential, V, which describes the interaction of a neutron at R with a single nucleus at r_j. The average potential experienced by the neutron over all interactions is given by:

$$V(r) = \frac{2\pi\hbar^2}{m} \left\langle \sum_j b_j \delta\left(R - r_j\right) \right\rangle \tag{2.21}$$

where b_j is a constant for nucleus j and is known as the coherent scattering length. The Kronecker delta function is defined as:

$$\delta(R - r_j) = \begin{cases} 1, & \text{if } R = r_j, \\ 0, & \text{if } R \neq r_j. \end{cases} \tag{2.22}$$

The sum of the coherent scattering length b_j over all the nuclei in the material can be termed scattering length density, ρ, defined as:

$$\rho = \sum_j n_j b_j \tag{2.23}$$

where n_j is the number density of species j with a coherent scattering length b_j. By following the equations (2.20) and (2.23), the neutron experiences a mean potential that therefore can be described as:

$$V = \frac{2\pi\hbar^2}{m}\rho \tag{2.24}$$

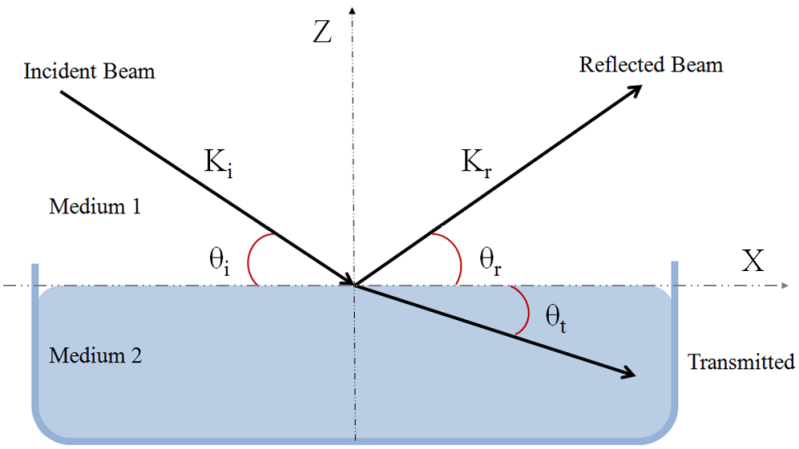


Figure 2.2: Neutron reflection at a planar boundary

Figure 2.2 shows the neutron beam incident on a plane boundary of two medium 1 and 2 represented as a planar wave. The neutron motion through the interface depends only on the potential along the z direction which is normal to the interface. The variables of $\psi(z,x)$ can then be separated

$$\psi(z,x) = e^{ik_x}\psi(z) \tag{2.25}$$

where k_x is the x component of the wave vector, parallels to the surface. It then follows that,

$$\frac{d^2\psi(z,x)}{dx^2} = \text{-}\psi(z,x)k_x^2 \tag{2.26}$$

Substituting equation (2.26) into equation(2.20) gives,

$$\frac{d^2\psi}{dz^2} + q^2\psi = 0 \tag{2.27}$$

where q is the wave vector normal to the interface,

$$q^2 = \left\{ \frac{2m}{\hbar^2}[E - V] - k_x^2 \right\} \tag{2.28}$$

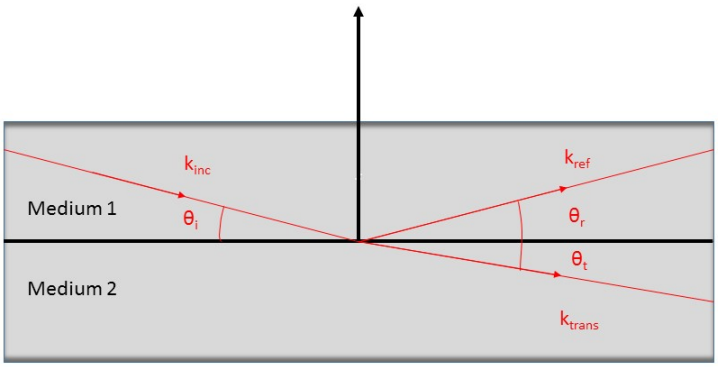


Figure 2.3: A schematic for neutron reflection obeying Snells Law

As shown in Figure (2.3), the wave vector for the incident, reflected and transmitted waves are denoted as k_{inc}, k_{ref} and k_{trans} respectively and θ_i, θ_r and θ_t as the angles of incidence, reflection and refraction. Thus Snell's law can be written as

$$k_{inc}\cos\theta_i = k_{ref}\cos\theta_r = k_{trans}\cos\theta_t \tag{2.29}$$

For a homogeneous medium, the neutron refractive index can be written as:

$$n_i = \frac{|k_i|}{|k_0|} \tag{2.30}$$

where k_i and k_0 are the neutron wave vectors in medium i and vacuum respectively.

Combination of equations (2.29) and (2.30) gives a more common expression of Snell's law:

$$n_1 \cos\theta_i = n_2 \cos\theta_t \tag{2.31}$$

where n_1 and n_2 are the neutron refractive indices of medium 1 and 2 respectively, by using the equation:

$$\frac{n_1}{n_2} = \frac{k_{inc}}{k_{trans}} \tag{2.32}$$

and follows the equation (2.28) gives

$$\frac{n_1^2}{n_2^2} = \frac{(E - V_1)}{(E - V_2)} \tag{2.33}$$

Consider a case of vacuum with $V_1 = 0$ and $n_1 = 1$, and a medium with potential V_2 follows equation (2.24), then insert the de Broglie relation into equation (2.33) gives the refractive index as

$$n^2 = 1 - \frac{\lambda^2}{\pi}\rho \tag{2.34}$$

where λ is the wave-length and ρ is the scattering length density. This expression describes the neutron refractive index in terms of its chemical composition and the neutron wave-length. For values of ρ less than about 10^{-5} Å^{-2}, equation (2.34) may be written,

$$n_i \approx 1 - \frac{\lambda^2}{2\pi}\rho_i \tag{2.35}$$

From Snell's law in the form of equation (2.30), the relative refractive index across a plane boundary is given by

$$n_{12} = \frac{n_2}{n_1} = \frac{\cos\theta_i}{\cos\theta_t} \tag{2.36}$$

Combination of (2.35) and (2.36) gives

$$n_{12} = 1 - \frac{\lambda^2}{2\pi}(\rho_2 - \rho_1) \tag{2.37}$$

On the base of equation (2.36), if $\theta_2 = 0$, then total reflection of the neutron beam occurs and equation (2.37) becomes,

$$n_{12} = \cos\theta_c = 1 - \frac{\lambda^2}{2\pi}(\rho_2 - \rho_1) \tag{2.38}$$

where θ_c is the critical angle of reflection and for all the angles below θ_c total reflection occurs. From this expression, the value of θ_c depends only on the neutron wave-length and the relative scattering length density of the media which the beam is passing through. In neutron experiments it is convenient to express the reflectivity as a function of the total momentum transfer perpendicular to the interface Q. As $k = 2\pi/\lambda$, the total momentum transfer, Q, is given by,

$$Q = \frac{4\pi \sin\theta}{\lambda} = 2q_0 \tag{2.39}$$

The condition for total reflection can then be expressed in terms of momentum transfer:

$$Q_c = \frac{2\pi \sin\theta_c}{\lambda} \tag{2.40}$$

In this thesis the reflection studies at interfaces are concerned with conditions above the critical angle, where the reflectivity is less than one and decreases with increasing momentum transfer [37].

2.2.7 Neutron Reflection from a single homogeneous layer

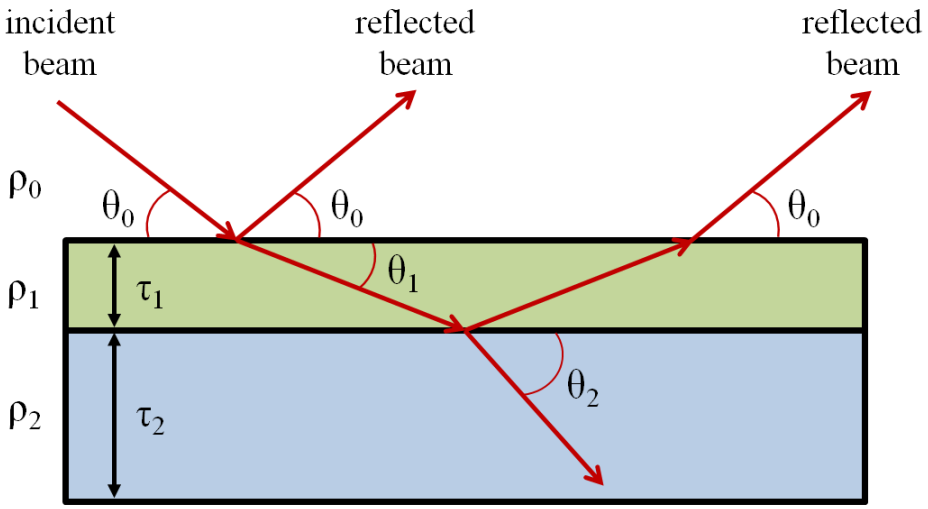


Figure 2.4: Neutron reflection from a monolayer interface

Goldberger and Seitz first showed that the Schrödinger equation may be solved in the form of Fresnel reflection and transmission coefficients [38, 39]. Hence for a monolayer adsorbed at an interface as shown in Figure (2.4), the amplitude of the reflected neutron wave is the sum of all reflected waves. This amplitude, $\mathfrak{R}$, may be written in terms of Fresnel reflection and transmission coefficients r_{ij} and t_{ij} of the geometric series,

$$\mathfrak{R} = r_{01} + t_{01}r_{12}t_{10}e^{2i\beta} + t_{01}r_{12}r_{10}r_{12}t_{10}e^{4i\beta} + ... \tag{2.41}$$

where β is the optical path length of the waves reflected from two consecutive boundaries of a layer i with a thickness of τ_i, q_i is the neutron wave vector in the layer and normal to the interface, and traversing the layer once gives,

$$\beta_1 = q_1\tau_1 \sin\theta_{01} \tag{2.42}$$

where θ_{01} is the angle of the beam refracted at the interface between layers 0 and 1 in the case where layer 0 has a zero neutron scattering cross section (i.e. is air). Applying conservation of energy:

$$t_{01}t_{10} = 1 - (r_{01})^2 \tag{2.43}$$

substitution of this relation into the equation (2.40) gives

$$\mathfrak{R} = \frac{r_{01} + r_{12}e^{2i\beta}}{1 + r_{01}r_{12}e^{2i\beta}} \tag{2.44}$$

In the case of a monolayer of uniform composition and density at the interface between two bulk media (air and a substrate), the neutron reflection, R, can be derived as,

$$R = |\mathfrak{R}^2| = \frac{(r_{01}^2) + (r_{12})^2 + 2r_{01}r_{12}\cos 2\beta}{1 + (r_{01}r_{12})^2 + 2r_{01}r_{12}\cos 2\beta} \tag{2.45}$$

where r_{ij} refers to the reflection amplitude per plane and the subscripts 1, 2, 3 denote the air phase, the monolayer, and the substrate. Under conditions where the solvent is null–reflecting, the reflectivity arises only from the adsorbed layer at the interface. It can be seen that the denominator of equation (2.44) is always close to unity and the numerator is the dominant factor in the relation. When $\cos 2\beta = \pm 1$, the maximum and minimum values of R occurs respectively.

Above the critical angle, the Fresnel reflection coefficient can be related to q, the wave vector transfer normal to the interface,

$$r_{ij} = \frac{(q_i - q_j)}{(q_i + q_j)} \tag{2.46}$$

For a smooth surface, an approximate result can be obtained when q is much larger than the critical angle,

$$R \approx \frac{16\pi^2 \triangle\rho}{q^4} \tag{2.47}$$

And for a monolayer,

$$R \approx \frac{16\pi^2}{q^4}\left[(\rho_1-\rho_0)^2+(\rho_2-\rho_1)^2+2(\rho_1-\rho_0)(\rho_2-\rho_1)\cos(q\tau)\right] \quad (2.48)$$

where τ is the thickness of the layer. Equation (2.48) is very useful for discussing the main characteristics of neutron reflection from a surfactant monolayer.

2.2.8 Neutron Reflection from Multilayers

The calculation of Fresnel reflection coefficients forms the basis of the optical matrix method. The model proposed by Born separated the interface into a series of parallel, homogeneous layers to describe the refractive index profile normal to the interface with sufficient resolution [39]. Chemically adsorbed layers can therefore be approximated by as many uniform layer as necessary with appropriate chemical composition, denoted by the scattering length density, ρ. Figure (2.5) provides a schematic example of the treatment of an interface.

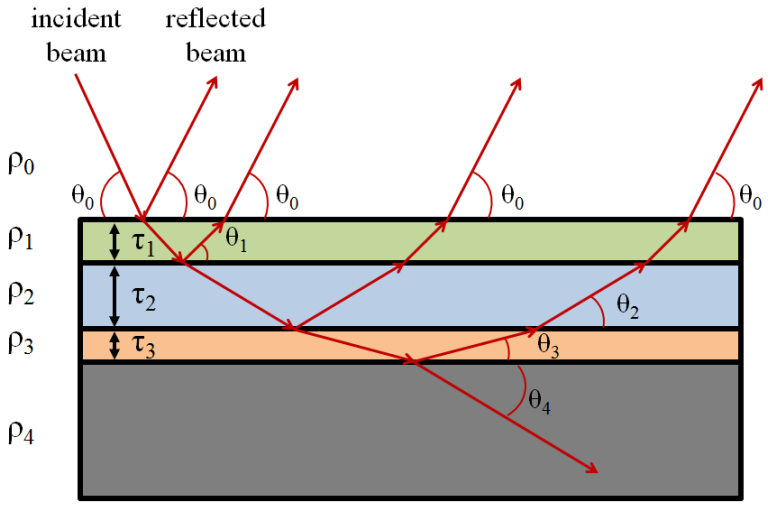


Figure 2.5: Neutron reflection from multilayer

Application of Maxwell's equations at each successive boundary gives a characteristic 2×2 matrix for each layer,

$$[M_j] = \begin{pmatrix} \cos\beta_j & -\frac{i}{q_j}\sin\beta_j \\ iq_j \sin\beta_j & \cos\beta_j \end{pmatrix} \tag{2.49}$$

and the overall reflectivity can be obtained by multiplying the characteristic matrices of successive layers,

$$[M] = [M_1] \times [M_2] \times [M_3] \times ... \times [M_n] \tag{2.50}$$

The reflectivity is given by,

$$R = |\mathfrak{R}|^2 = \left| \frac{(m_{11} + m_{12}q_{(n+1)})q_0 - (m_{21} + m_{22}q_{(n+1)})}{(m_{11} + m_{12}q_{(n+1)})q_0 + (m_{21} + m_{22}q_{(n+1)})} \right|^2 \tag{2.51}$$

where m_{ij} are the elements of $[M_{ij}]$, q_0 and $q_{(n+1)}$ refer to the initial and bulk phases. For the real interface, it may require many layers to describe it with sufficient accuracy. The problem may be approached by using a matrix with linear gradations in scattering length density between successive layers [32], or by the introduction of interfacial roughness [40].

There are two main sources of interfacial roughness. Residual surface roughness at the solid-liquid interface is inevitable even with extremely careful polishing and this can generates off-specular scattering, which leads to the reduction of the measured specular reflectivity. Another source that can affect the measured reflectivity is interfacial diffuseness, which results from the interface itself being a distribution of solute and solvent, and is of very short wave-length. In order to modify the measured specular reflectivity, the model based on a Debye-Waller factor is introduced [41], which takes the form:

$$I^+ = Ie^{-q^2\sigma^2} \tag{2.52}$$

where σ is the mean square roughness, I^+ and I are the reflected intersities with and without surface roughness respectively. Incorporation of this factor permits an alternative characteristic matrix for each layer to be defined as [42]:

$$[M_j] = \begin{bmatrix} e^{i\beta_{j-1}} & r_j^+ e^{i\beta_{j-1}} \\ r_j^+ e^{i\beta_{j-1}} & e^{-i\beta_{j-1}} \end{bmatrix} \tag{2.53}$$

where β_j is the phase shift given by equation (2.42) and r_j^+ is the modified reflection coefficient given by

$$r_j^+ = r_j e^{\frac{q^2\sigma^2}{2}} \tag{2.54}$$

The reflectivity can then be written in terms of m_{ij} and m_{ij}^*,

$$R = \frac{m_{21}m_{21}^*}{m_{11}m_{11}^*} \tag{2.55}$$

In practical, the measured reflectivity is compared with profiles generated by a computer program based on the theory discussed above. In this work the program used for the analysis of the data was Motofit [43], which works within the analysis package Igro Pro. This program implements the optical matrix method for reflectivity calculations and allows variation of layer thickness, scattering length density and roughness independently of one another for each layer in a multilayer model. By changing these parameters the shape of the calculated profile changes accordingly and can be compared with the experimental recorded profile. The best fit can be archived by least squares or by eye. By developing a base of knowledge of simple systems, such as the Si/SiO_2/H_2O interface and Si/SiO_2/OTS/H_2O, it becomes possible to fit the experimental observations from increasingly complex system.

It is necessary to measure a number of contrasts in order to ensure the model is exclusive. For systems with the same structure but different deuteration characteristics(contrast), once the satisfactory fit has been obtained, the values of thickness, scattering length density and roughness used to produce the fit can then be used to calculate the amount of the component of interest that presents at the interface. Thus yields the volume fraction of solvent, the area per molecule, the number of associated water molecules per molecule, and the surface excess.

For a layer is made up of two components, species s and water, the scattering length density of the layer, ρ_{layer} is

$$\rho_{layer} = \phi\rho_{water} + (1 - \phi)\rho_s \tag{2.56}$$

where ϕ is the volume fraction of water in the layer and ρ_{water} and ρ_s are the scattering length densities of the two components. The use of different water contrasts, which have known scattering length density (see Table 2.1), leads to a set of simultaneous equations from which the volume fraction of water and scattering length density of species s can be calculated.

Materials	Volume ($Å^3$)	Scattering length ($b/10^{-4}Å$)	Scattering length density ($\rho/10^{-6}Å^{-2}$)
H_2O	30	-0.168	-0.56
D_2O	30	1.915	6.35
$Water_{2.07}$	30	0.621	2.07
$Water_{4.00}$	30	1.200	4.00
Si	20	0.415	2.07
SiO_2	47	1.585	3.41

Table 2.1: Physical parameters for the calculation of the properties of the interface

To calculate the hydration number, it is necessary to define a fragment of the monolayer with volume V_a, containing one adsorbed molecule and n water molecules where

$$(1-\phi)V_a = V_s \tag{2.57}$$

Using equation (2.70) and since

$$\rho_i = \frac{\sum_i b_i}{V_i} \tag{2.58}$$

where b_i is the scattering length of species i, and

$$\phi V_a = nV_w \tag{2.59}$$

the hydration number, n, is given by:

$$n = \frac{\phi \sum b_s}{(V_w \rho_{layer} - \phi b_w)} \tag{2.60}$$

the relationship between volume, V_i, thickness, τ, and area per molecule, A, is given by

$$V_a = A\tau = V_s + nV_w \tag{2.61}$$

The area per molecule can be calculated using equation (2.57) as

$$A = \frac{nV_w}{\tau\phi} \tag{2.62}$$

and surface excess,

$$\Gamma = \frac{1}{AN_A} \tag{2.63}$$

where N_A is Avogadro's number.

2.2.9 The Kinematic Approximation

The neutron reflectivity from a planar surface can be written in the kinematic approximation as [44]:

$$R = \frac{16\pi^2}{Q^2} |\rho(Q)|^2 \tag{2.64}$$

where Q is the momentum transfer and $\rho(Q)$ is the one dimensional Fourier transform of the mean scattering length density profile perpendicular to the surface, $\rho(z)$.Since

$$\rho(Q) = \int_{-\infty}^{\infty} \rho(z) e^{-iQz} dz = \frac{1}{iQ} \int_{-\infty}^{\infty} e^{iQz} \frac{d\rho(z)}{dz} dz = \frac{1}{iQ} \int_{-\infty}^{\infty} e^{iQz} \hat{\rho}(z) dz \tag{2.65}$$

where $\hat{\rho}(z)$ is the scattering length density gradient, equation (2.56) can be written as

$$R = \frac{16\pi^2}{Q^4} |\hat{\rho}(Q)|^2 \tag{2.66}$$

No matter which form of the equation is chosen, the next step is to describe the scattering length density profile. In the kinematic approximation method, the model chosen is more clearly related with the interfacial structure than a series of uniform layers used in the optical method. For a simple molecular system consisting of a hydrophobic chain, C, a hydrophilic head-group, H, and a solvent, S, the scattering length density profile can be described as,

$$\rho(z) = \rho_C(z) + \rho_H(z) + \rho_S(z) \tag{2.67}$$

where each of the $\rho_i(z)$ are given by

$$\rho_i(z) = b_i n_i(z) \tag{2.68}$$

and b_i is the scattering length and n_i denotes the number density of the related fragment. Substituting equation (2.67) into the equation (2.64) gives

$$R = \frac{16\pi^2}{Q^2}\left[b_C^2 H_{CC} + b_H^2 H_{HH} + b_S^2 H_{SS} + 2b_C b_H H_{CH} + 2b_C b_S H_{CS} + 2b_H b_S H_{HS}\right] \tag{2.69}$$

the H_{ii} and H_{ij} are partial structure factors.

For surfactant adsorbed at the air–liquid interface, it is assumed to have a number density profile described by a Gaussian function,

$$n_i(z) = n_i^0 \exp(\text{-}4z^2/\sigma_i^2) \tag{2.70}$$

where n_i^0 is the number density at the peak of the Gasussion distribution at $1/e$ of its maximum height. The surface excess of i is given by

$$\Gamma_i = 1/A_i = \sigma_i n_i^0 \pi^{\frac{1}{2}}/2 \tag{2.71}$$

where Γ_i is the coverage and A_i is the area per molecule. The resulting self partial structure factor is

$$H_{ii} = Re\left[(\hat{n}_i(z)\hat{n}_i^*(z)\right] = |\hat{n}_i(z)|^2 = (1/A_i^2)\exp(Q^2\sigma^2/8) \tag{2.72}$$

Application of the shift theorem of Fourier transforms, result in the following expression for the cross partial structure factor H_{ij}

$$H_{ij} = Re\left[\hat{n}_i(z)\hat{n}_j(z)\right] \tag{2.73}$$

where $\hat{n}_i$ is the one dimensional Fourier transform of the number density and Re is the real part of R. If the distribution of $n_i(z)$ and $n_j(z)$ are both symmetrical about their centre,

$$H_{ij} = \hat{n}_i \hat{n}_j \cos\left(iQ\delta_{ij}\right) = \pm\sqrt{H_{ii}H_{jj}}\cos\left(Q\delta_{ij}\right) \tag{2.74}$$

if one of $n_i(z)$ and $n_j(z)$ is even and another is odd,

$$H_{ij} = \hat{n}_i \hat{n}_j \cos\left(iQ\delta_{ij}\right) = \pm\sqrt{H_{ii}H_{jj}}\sin\left(Q\delta_{ij}\right) \tag{2.75}$$

where δ_{ij} is the distance between the centres of the two distribution, the $\pm$ arises from the uncertainty in the phase. Many fragment distributions across interfaces approximate closely to these two limits and these two equations above offer a means of determining the separation between pairs of distributions without either Fourier transformation or any other specific assumptions about the type of distribution apart from it being odd or even [45]. This method has the advantage that the interface is modelled in a realistic way and less cumbersome to apply comparing to the optical matrix method. However, in many systems of interest a full set of partial structure factors or partial structure factors involving components of interest can not be extracted due to the lack of suitable contrasts. Even when they can be reliably extracted, fitting of these parameters is not ideal. They are strongly sensitive to imperfections in the data and physical constrains are difficult to apply. Therefore it is often necessary to adapt the method to a limited set of reflectivity profiles but using the partial structure factor to provide an analytical model [45].

When the number density distributions of the various components can be described by functions whose Fourier transform are also analytical functions, equations of the form of (2.69) give an analytical expression for the reflectivity in terms

of the momentum transfer, the scattering lengths of the components and the parameters describing their distributions. By a least–squares procedure the best fit parameters may be obtained.

For a system comprising two adsorbed fragments at the air–liquid interface, equation (2.69) may be written explicitly:

$$\begin{aligned} R =& (16\pi^2/Q^2)\{(b_c^2/A_c^2)\exp(-Q^2\sigma_1^2/8) \\ &+ (b_h^2/A_h^2)\exp(-Q^2\sigma_2^2/8) \\ &+ (b_s^2 n_s^2/Q^2)(\zeta\pi Q/2)^2 cosech^2(\zeta\pi Q/2) \\ &\pm 2b_c b_h\{(1/A_c A_h)\exp[-Q^2(\sigma_c^2+\sigma_2^2)/8]\}^{\frac{1}{2}} \\ &\pm 2b_c b_s[(n_s^2/Q^2 A_c)\exp(-Q^2\sigma_c^2/8)(\zeta\pi Q/2)^2 \times cosech^2(\zeta\pi Q/2)]^{\frac{1}{2}} sinq\delta_{cs} \\ &\pm 2b_h b_s[(n_s^2/Q^2 A_h)\exp(-Q^2\sigma_h^2/8)(\zeta\pi Q/2)^2 \times cosech^2(\zeta\pi Q/2)]^{\frac{1}{2}} sinQ\delta_{hs}\} \end{aligned} \tag{2.76}$$

The parameters describing the number density distributions of the two adsorbed fragments are A_c and A_h, the areas per molecule, σ_c and σ_h the full width at $1/e$ of the maximum height of the two Gaussian number density distributions, and σ_{ch} the centre–to–centre separation of the two distributions. The water distribution is described as a tanh function and its only adjustable parameter is ζ, a width parameter defined as

$$n_s = (n_{bulk}/2)[1+\tanh(z/\zeta)] \tag{2.77}$$

where n_{bulk} is the number density of the bulk solution, n_s the number density of the solvent at a depth z. The offsets of the centres of the two Gaussian distributions from the centre of the solvent distribution are given by δ_{cs} and δ_{hs}.

It can be seen that only the magnitudes and not the signs of the distributions offsets, δ_{ij}, can be determined without recourse to independent information. Even if no assumptions are made concerning the relative positions of the components in the interface, only certain sets are physically consistent. The relative positions of components within the interface are often known, in the case of a charged surfactant, the distribution of hydrocarbon chain is further from the bulk solution phase than the charged head–group. Application of this assumption leads to the general statement of the relation between δ_{ij} in equation (2.76)

$$\sigma_{ch} = \sigma_{cs} - \sigma_{hs} \tag{2.78}$$

where the positive direction is defined as away from the bulk solution in the direction of the vapour. Thus, σ_{ch} may be eliminated from the fitting procedure.

Stoichiometry or the requirement for charge neutrality may provide relationships between the coverages of the adsorbed species that may lead to the removal of one or more area terms from the fitting procedure. In some instances, the coverage of a component may already be known from some independent experiments, i.e. surface tension or pressure isotherm measurements. Other constraints including space–filling and geometry. It is crucial that the volume fraction profile resulting from the number density distribution parameters are physically reasonable.

Unlike the basic kinematic approximation model, the reflectivity profiles themselves are directly fitted by applying the method discussed above, rather than extract the partial structure factors from the data. The direct fitting method is considered more realistic because the partial structure factors are extremely sensitivity to the imperfection in the data, especially for the cross terms. Also, the

improved method is readily to incorporate physical constraints and other experiments measurements in order to aid the determination of the structure.

Bibliography

[1] D. J. Shaw. *Introduction to colloid and surface chemistry*. Colloid and Surface Engineering Series. Butterworth-Heinemann, 1992.

[2] P. L. Du Noúy. A new apparatus for measuring surface tension. *The Journal of general physiology*, 1(5):521, 1919.

[3] W. D. Harkins and H. F. Jordan. A method for the determination of surface and interfacial tension from the maximum pull on a ring. *Journal of the American Chemical Society*, 52(5):1751–1772, 1930.

[4] B.B. Freud and H.Z. Freud. A theory of the ring method for the determination of surface tension. *Journal of the American Chemical Society*, 52(5):1772–1782, 1930.

[5] H. Zuidema and G. Waters. Ring method for determination of intrfacial tension. *Industrial & Engineering Chemistry Analytical Edition*, 13(5):312–313, 1941.

[6] J. W. Gibbs. *The collected works of J. Willard Gibbs*, volume 1. Yale University Press, 1948.

[7] E. Fermi and W.H. Zinn. *Reflection of neutrons on mirrors*. Manhattan District, 1946.

[8] J. Penfold and R. K. Thomas. The application of the specular reflection of neutrons to the study of surfaces and interfaces. *Journal of Physics: Condensed Matter*, 2(6):1369, 1990.

[9] R. K. Thomas and J. Penfold. Neutron and x-ray reflectometry of interfacial systems in colloid and polymer chemistry. *Current Opinion in Colloid & Interface Science*, 1(1):23–33, 1996.

[10] R. K. Thomas. Neutron reflection from surfactants adsorbed at the solid/liquid interface. In *Amphiphiles at Interfaces*, pages 216–225. Springer, 1997.

[11] J. Penfold, R. M. Richardson, J. R. P. Zarbakhsh, A .and Webster, D. G. Bucknall, A. R. Rennie, R. A. L. Jones, T. Cosgrove, R. K. Thomas, and J. S. Higgins. Recent advances in the study of chemical surfaces and interfaces by specular neutron reflection. *Journal of the Chemical Society, Faraday Transactions*, 93(22):3899–3917, 1997.

[12] J. R. Lu and R. K. Thomas. Neutron reflection from wet interfaces. *J. Chem. Soc., Faraday Trans.*, 94(8):995–1018, 1998.

[13] J. R. Lu, R. K. Thomas, and J. Penfold. Surfactant layers at the air/water interface: structure and composition. *Advances in colloid and interface science*, 84(1-3):143–304, 2000.

[14] R. K. Thomas. Neutron reflection from liquid interfaces. *Annu. Rev. Phys. Chem.*, 55:391–426, 2004.

[15] M. Yaseen, Y. Wang, T. J. Su, and J. R. Lu. Surface adsorption of zwitterionic surfactants:¡ i¿ n¡/i¿-alkyl phosphocholines characterised by surface tensiometry and neutron reflection. *Journal of colloid and interface science*, 288(2):361–370, 2005.

[16] A. Zarbakhsh, A. Querol, J. Bowers, M. Yaseen, J. R. Lu, and J. R. P. Webster. Neutron reflection from the liquid-liquid interface: Adsorption of hexadecylphosphorylcholine to the hexadecane-aqueous solution interface. *Langmuir*, 21(25):11704–11709, 2005.

[17] T. P. Russell. X-ray and neutron reflectivity for the investigation of polymers. *Materials Science Reports*, 5(4):171–271, 1990.

[18] Q. S. Mu, J. R. Lu, Y. H. Ma, M. V. Paz de Banez, K. L. Robinson, S. P. Armes, A. L. Lewis, and R. K. Thomas. Neutron reflection study of a water-soluble biocompatible diblock copolymer adsorbed at the air/water interface: The effects of ph and polymer concentration. *Langmuir*, 22(14):6153–6160, 2006.

[19] J. Penfold, E. Staples, I. Tucker, R. K. Thomas, R. Woodling, and C. C. Dong. The structure of mixed nonionic surfactant monolayers at the air–water interface: the effects of different alkyl chain lengths. *Journal of colloid and interface science*, 262(1):235–242, 2003.

[20] P. X. Li, C. C. Dong, R. K. Thomas, J. Penfold, and Y. Wang. Neutron reflectometry of quaternary gemini surfactants as a function of alkyl chain length: anomalies arising from ion association and premicellar aggregation. *Langmuir*, 27(6):2575–2586, 2011.

[21] J. D. Hines, R. K. Thomas, P. R. Garrett, G. K. Rennie, and J. Penfold. Investigation of mixing in binary surfactant solutions by surface tension and neutron reflection: Anionic/Nonionic and Zwitterionic/Nonionic mixtures. *The Journal of Physical Chemistry B*, 1997.

[22] E. Staples, I. Tucker, J. Penfold, N. Warren, R. K. Thomas, and D. J. F. Taylor. Organization of polymer-surfactant mixtures at the air-water interface: Sodium dodecyl sulfate and poly (dimethyldiallylammonium chloride). *Langmuir*, 18(13):5147–5153, 2002.

[23] D. J. F. Taylor, R. K. Thomas, and J. Penfold. The adsorption of oppositely charged polyelectrolyte/surfactant mixtures: neutron reflection from dodecyl trimethylammonium bromide and sodium poly (styrene sulfonate) at the air/water interface. *Langmuir*, 18(12):4748–4757, 2002.

[24] J. H. Clint and T. Walker. Thermodynamics of micellization of homologous series of n-alkyl methyl sulphoxides and n-alkyl(dimethyl)phosphine oxides. *J. Chem. Soc., Faraday Trans. 1*, 71:946–954, 1975.

[25] J. Penfold, I. Tucker, R. K. Thomas, and J. Zhang. Adsorption of polyelectrolyte/surfactant mixtures at the air-solution interface: Poly (ethyleneimine)/sodium dodecyl sulfate. *Langmuir*, 21(22):10061–10073, 2005.

[26] G. Fragneto, T. J. Su, J. R. Lu, R. K. Thomas, and A. R. Rennie. Adsorption of proteins from aqueous solutions on hydrophobic surfaces studied by neutron reflection. *Physical Chemistry Chemical Physics*, 2(22):5214–5221, 2000.

[27] J. R. Lu, X. Zhao, and M. Yaseen. Protein adsorption studied by neutron reflection. *Current Opinion in Colloid & Interface Science*, 12(1):9–16, 2007.

[28] J. R. Lu, E. M. Lee, and R. K. Thomas. The analysis and interpretation of neutron and x-ray specular reflection. *Acta Crystallographica Section A: Foundations of Crystallography*, 52(1):11–41, 1996.

[29] T. L. Crowley. A uniform kinematic approximation for specular reflectivity. *Physica A: Statistical Mechanics and its Applications*, 195(3):354–374, 1993.

[30] H. L. Anderson, E. Fermi, A. Wattenberg, G. L. Weil, and W. H. Zinn. Method for measuring neutron-absorption cross sections by the effect on the reactivity of a chain-reacting pile. *Physical Review*, 72:16–23, 1947.

[31] D. E. Aspnes. Optical properties of thin films. *Thin solid films*, 89(3):249–262, 1982.

[32] J. Lekner. *Theory of Reflection of Electromagnetic and Particle Waves: Of Electromagnetic and Particle Waves*, volume 3. Springer, 1987.

[33] T. I. Rhodes. *Neutron Reflection Used to Investigate Polymers and Surfactants at the Solid-liquid Interface*. PhD thesis, University of Oxford, 2003.

[34] E. A. Simister, R. K. Thomas, J. Penfold, R. Aveyard, B. P. Binks, P. Cooper, P. D. I. Fletcher, J. R. Lu, and A. Sokolowski. Comparison of neutron reflection and surface tension measurements of the surface excess of tetradecyltrimethylammonium bromide layers at the air/water interface. *The Journal of Physical Chemistry*, 96(3):1383–1388, 1992.

[35] D. G. Bucknall, J. Penfold, J. R. P. Webster, A. Zarbakhsh, R. M. Richardson, A. Rennie, J. S. Higgins, R. A. L. Jones, R. K. Thomas, S. Roser, et al. Surf-a second generation neutron reflectometer. *Proceedings of the meetings ICANS-XIII and ESS-PM4. Volume I*, 1995.

[36] J. Webster, S. Holt, and R. Dalgliesh. Inter the chemical interfaces reflectometer on target station 2 at isis. *Physica B: Condensed Matter*, 385:1164–1166, 2006.

[37] J. Lekner. Reflection and refraction by uniaxial crystals. *Journal of Physics: Condensed Matter*, 3(32):6121, 1991.

[38] M. L. Goldberger and F. Seitz. Theory of the refraction and the diffraction of neutrons by crystals. *Physical Review*, 71(5):294–310, 1947.

[39] M. Born and E. Wolf. *Principles of optics: electromagnetic theory of propagation, interference and diffraction of light*. CUP Archive, 1999.

[40] R. A. Cowley and T. W. Ryan. X-ray scattering studies of thin films and surfaces: thermal oxides on silicon. *Journal of Physics D: Applied Physics*, 20(1):61, 1987.

[41] L. Nevot and P. Croce. Caractérisation des surfaces par réflexion rasante de rayons x. application à l'étude du polissage de quelques verres silicates. *Revue de Physique appliquée*, 15(3):761–779, 1980.

[42] O. S. Heavens. *Optical properties of thin solid films*. Courier Dover Publications, 1991.

[43] A. Nelson. Co-refinement of multiple-contrast neutron/x-ray reflectivity data using motofit. *Journal of Applied Crystallography*, 39(2):273–276, 2006.

[44] J. A. Henderson, R. W. Richards, J. Penfold, and R. K. Thomas. Partial structure factor analysis of neutron reflectometry from spread monolayers of isotactic polymethyl methacrylate. *Acta polymerica*, 44(4):184–191, 1993.

[45] E. M. Lee and J. E. Milnes. Direct fitting of grazing-incidence neutron and x-ray reflectivity profiles using the kinematic approximation. *Journal of applied crystallography*, 28(5):518–526, 1995.

Chapter 3

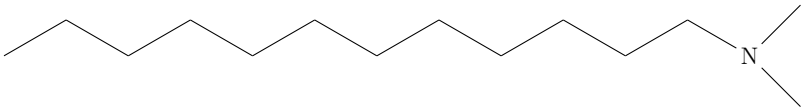
Synthesis of Surfactants

3.1 Materials

1-Bromododecane, dimethylamine, 1,3-propane sultone, ethyl 5-bromovalerate, ethanol, chloroacetic acid sodium salt and Dowex monosphere 550A UPW ion-exchage resin were purchased from Sigma-Aldrich at the highest available purity and used without any further purification. Hydrochloric acid, diethyl ether, petroleum ether, acetone, ethyl acetate, magnesium sulfate, sodium carbonate were purchased from Fisher. Deuterated 1-bromododecane, deuterated THF, sodium dodecyl sulphate and dodecyl trimethylammonium bromide were obtained from Dr. R.K.Thomas and Dr. C.C.Dong at Oxford. All water used for experiments was ultra-purified from either an Elga or Millipure filtration apparatus.

3.2 Synthesis of Alkyl Chain Quaternary Ammonium Surfactants

3.2.1 Synthesis of N,N-Dimethyldodecylamine



N,N-Dimethyldodecylamine

Both protonated and deuterated N,N-Dimethyldodecylamine were synthesised as the starting compounds for the synthesis of zwitterionic surfactants. The materials were synthesised by using an method first reported by Epshtein and later adopted by Menger [1, 2]. The reaction was conducted in a 250ml round-bottomed flask. To a solution of 1–bromododecane (26.88ml, 0.11mol), 70ml dimethylamine (0.1mol) was added slowly, the mixture was heated at 40°C under stirring and refluxed overnight. After the solution became clear, 0.1M/L NaOH was used to adjust the pH value to 10–11, then the solution was extracted three times with petroleum ether, dried by Na_2SO_4 and the crude product obtained after rotary evaporation of the petroleum ether solution. The structure of the final product was confirmed by using ^{1}H-NMR, obtained with a Bruker DPX200 instrument. The yields of final products were 85% for the protonated and 82% for the deuterated product.

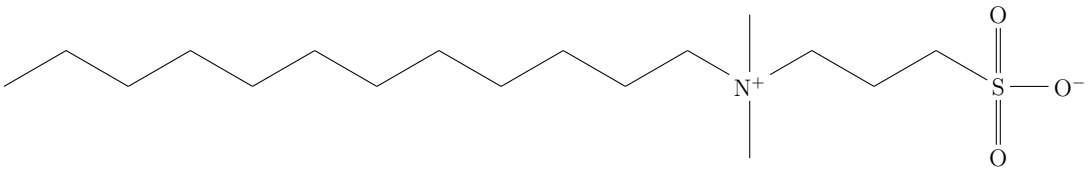
Dodecyl dimethylamine ^{1}H-NMR [200 MHz, ($CDCl_3$)] δ= 0.865-0.890 (t, 3H, -CH3), δ = 1.277-1.424 (m, 22H, -$(CH2)_{11}$-), δ = 2.264-2.267 (t, 2H, -CH2-N^+), δ = 2.317-2.654 (s, 6H, $N^+(CH3)_2$),

Deuterated 1-bromododecane was prepared by reduction of the corresponding fat-

ty acid with $LiAlD_4$ to give the alcohols followed by bromination of the alcohol using HBr (48% wt aq.) and tetrabutylamonium bromide under reflux for 6 hours (prepared by Dr. C.C.Dong), followed by extraction with diethyl ether , drying by Na_2SO_4. The bromododecane was purified by preparative medium pressure liquid chromatography with a petroleum ether and diethyl ether mixture.

3.2.2 N-Dodecyl-N,N-dimethyl-3-ammonio-1-propanesulfonate

One of the zwitterionic surfactants investigated in this thesis is N-Dodecyl-N,N-dimethyl-3-ammonio-1-propanesulfonate (C_{12}sulfobetaine, abbreviated to DSB). The DSB was prepared by following the procedure reported by Qu [3].



N-Dodecyl-N,N-dimethyl-3-ammonio-1-propanesulfonate(DSB)

1,3-propane sultone (0.25ml) was dissolved in 50ml acetone and added to a stirred solution of dimethyldodecylamine(0.05mol) in 50ml acetone over a period of 15 minutes. The mixture was then refluxed at 60°C overnight to give the end product of DSB as a white solid. The solids were filtered and washed with acetone. Recrystallization from mixtures of acetone and methanol was repeated at least three times until sufficient purity was attained as assessed by surface tension, i.e., no surface tension minimum. The yield of final product of DSB was 86%. The structure of the final product was confirmed by using ^{1}H-NMR, obtained with a Bruker DPX200 instrument.

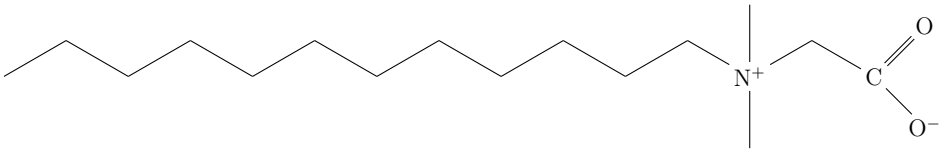
DSB ^{1}H-NMR [200 MHz, ($CDCl_3$)] δ= 0.745-0.851 (t, 3H, -CH3), δ = 1.035-

1.260 (m, 18H, -(CH2)9-), δ = 1.610-1.733 (m, 2H, -CH2CH2-N^+), δ = 2.010-2.046(m, 2H, N^+-CH2CH2CH2-), δ = 2.842-2.935 (t, 2H, -CH2CH2-N^+), δ = 2.991-3.182 (s, 6H, $N^+(CH3)_2$), δ = 3.310-3.374 (t, 2H, N^+-CH2–CH2CH2-), δ = 3.452-3.531 (t, 2H, N^+-CH2CH2–CH2-).

The deuterated DSB was synthesised and purified following the procedure above by using chain deuterated dimethyldodecylamine. The yield of deuterated final product was 80%.

3.2.3 N-Dodecyl-N,N-Dimethylamino Betaine

Another zwitterionic surfactant used in the solid–liquid neutron experiments is N-Dodecyl-N,N-dimethylamino betaine. This surfactant consists of an identical hydrocarbon chain but a smaller head-group than DSB. The method used here was first reported by Laughlin and a similar method was adopted by Hines [4, 5].



N-Dodecyl-N,N-dimethylamino betaine(DB)

Chloroacetic acid sodium salt (13g, 0.11mol) dissolved in EtOH (0.8g/ml) was added to a 150ml three-neck round bottomed flask, to which a condenser and stirrer had been fitted and dodecyldimethylamine(21.34g 0.1mol) dissolved in E-tOH(0.8g/ml) was added to the stirred solution to give a 1.1:1 molar ratio, and the reaction was heated under reflux for more than 18 hours (80-90°C). After cooling, the reaction mixture was dried by rotary evaporation and the resultant solid dissolved in ethanol. The solution was then filtered in order to remove inorganic

solids before drying by rotary evaporation. The resultant sticky solid was dissolved in the minimum amount of hot acetone, and allowed to recrystallise in an ice bath and the white solid was filtered and dried under vacuum. Recrystallization was repeated three times until sufficient purity was attained as assessed by surface tension, i.e., no surface tension minimum. The deuterated DB was synthesised following the same procedure above with deuterated dodecyldimethylamine.

3.3 Synthesis of Carboxybetaine Surfactants with Different Size Methylene Groups

Apart from the DB surfactant mentioned above, two similar surfactants of the betaine family, $C_{12}H_{25}N^{+}(CH_3)_2(CH_2)_nCOO^{-}$, with n=4 and 8 were synthesised via a two-step procedure [6]. In the first step of this method a tertiary amine and an alkyl bromide mono ester were combined to form the corresponding quaternary ammonium salt. This was performed in a variety of organic solvents, including ethyl acetate, 2-propanol and ethanol. The resulting crude ammonium salt was then dissolved in UHQ water and treated with anion exchange resin. The hydrogen ion that is associated with the cationic resin promotes a base-catalysed ester hydrolysis of the ester which results in the liberation of the betaine. The final compounds were recrystallized from acetone-methanol mixtures and obtained as white crystals which were freeze-dried.

3.3.1 $C_{12}H_{25}N^{+}(CH_3)_2(CH_2)_4COO^{-}$

The zwitterionic surfactant $C_{12}H_{25}N^{+}(CH_3)_2(CH_2)_nCOO^{-}$ with n=4, was synthesised using the following procedure. In a 150ml round bottom flask, 23.8g dodecyl dimethylamine (30ml, 0.1mol) was dissolved in 50ml ethanol and 20g ethyl

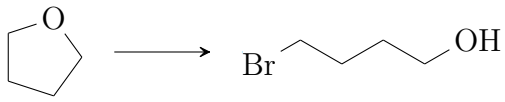
5-bromovalerate was slowly added into the solution. The mixture was stirred and refluxed at 80 °C for 18 hours. The solvent was then evaporated and the crude product extracted with ether.

A 50% excess of Dowex 550A anion exchange resin (exchange capacity 1.1 meq ml^{-1}, OH^- counter-ion), which had been thoroughly rinsed in UHQ water, was mixed with an aqueous solution of surfactant containing bromide counter-ion. The mixture was stirred at room temperature for at least 8 hours and filtered. The ion-exchange procedure was repeated three times. The surfactant was recovered from the aqueous solution by freeze-drying and finally purified by recrystallization from acetone-methanol mixture. The purity was tested by surface tension measurement and no minimum was observed in the plot of surface tension against lnC.

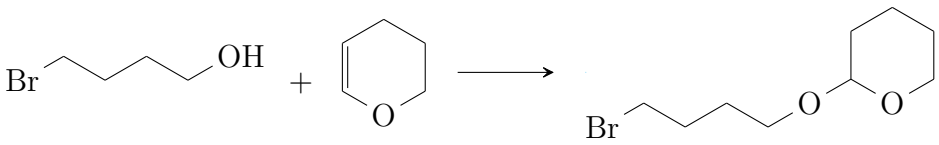
The chain deuterated surfactant was synthesised in the same way as protonated one by using deuterated dodecyldimethylamine.

Ethyl 5-bromovalerate

In order to highlight the neutron reflectivity signal from the head-group, betaines with polymethylene units were synthesised with their head-group deuterated. For the deuterated 5-bromovalerate used in the procedure above, deuterated THF was used as a starting compound [7, 8]. Since the structure of deuterated substances is difficult to confirm by NMR, the protonated 5-bromovalerate was first synthesised and then the deuterated one was obtained using same procedure.

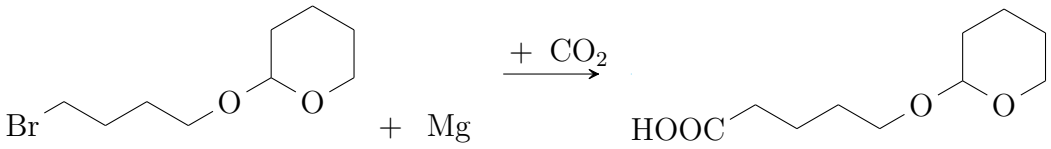


In a 250ml round bottom flask, concentrated H_2SO_4 (3ml) and then 48ml HBr (48% w/v 0.42mol) were added dropwise to 30g deuterated THF (0.4mol) at 0 °C. The mixture was then stirred and refluxed for 90 minutes. After cooling down to 0°C the mixture was neutralized with $NaHCO_3$, and 50ml of UHQ water was added. The alcohol product was extracted with 180ml diethyl ether for three times (3 $\times$ 60ml), washed with brine, and the organic fraction was dried with magnesium sulfate, Removal of the solvent in vacuo afforded 4-bromo-1-butanol. The final product obtained had a yield of 86% (55g)

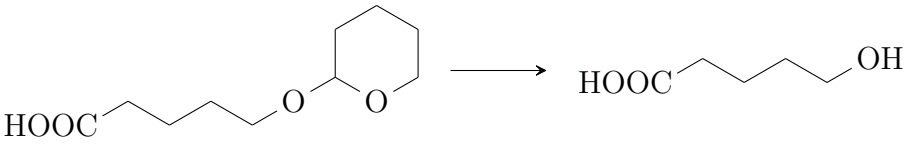


The 2-tetrahydropyranyl group was first introduced as a protecting group for alcohol [9]. In a 250ml round bottom flask, 30ml dihydropyran (0.34mol) was added via syringe to a cooled solution (0°C) of 4-bromo-1-butanol (40g, 0.26mol) in 100 ml anhydrous ether containing 100mg of p-toluenesulfonic acid. After 1 hour at ambient temperature, the reaction mixture was washed with 200ml saturated sodium bicarbonate solution twice and 100ml brine once. The organic layer was dried over anhydrous potassium carbonate. The solution was then filtered, and the solvent was removed in vacuo, providing 64.4g of 4-bromobutyl tetrahydropyranyl ether as a colourless oil. The crude product was purified by liquid chromatography with a petroleum ether/ether mixture and final product was confirmed by using ^{1}H-NMR.

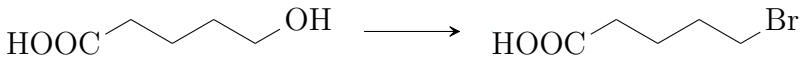
^{1}H-NMR [200 MHz, ($CDCl_3$)] δ = 4.63 (m, 1H), δ = 3.83–3.98 (m, 2H), δ = 3.50–3.70 (m, 2H), δ = 1.90-2.20 (m, 2H), δ = 1.70–1.90 (m, 4H), δ = 1.45-1.60 (m, 4H),



Magnesium turnings and anhydrous THF were placed in a dried 250ml three-neck round-bottom flask which contained a stirring bar. In an addition funnel, 4.18 mL (20g) of 4-bromobutyl tetrahydropyranyl ether and 50 mL of anhydrous THF from a freshly opened bottle were added. The magnesium and anhydrous THF mixture was stirred. Addition of approximately 1 mL of the 4-bromo-1-butanol to 4-bromobutyl tetrahydropyranyl ether/THF solution to the round-bottom flask,caused cloudiness and bubbles at the surface of the metal and indicated that the reaction had begun. Once the reaction was started, the remainder of the mixed solution was added dropwise to maintain a steady reflux. The freshly made Grignard reagent was poured into excess carbon dioxide (dry ice) for carboxylation of the THP-protected compound. The reaction mixture was then warmed up to ambient temperature over a period of 1 hour and then extracted with water(100 ml). The aqueous solution was washed with diethyl ether (2 $\times$ 50ml), the extracts were dried and concentrated under reduced pressure. The residue was used without further purification [10].

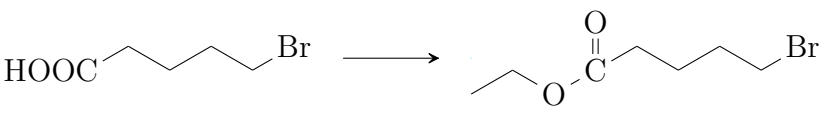


The THP ether was selectively deprotected by following a mild and effective method [11]. In a 250 mL round bottom flask, a magnetically stirred mixture of 20g THP ether (0.1mol), 20g LiCl (0.5 mol), and 18 mL H_2O (1 mol) in DMSO (100 mL) was heated at 90°C for 6 hours under N_2 protection. The reaction mixture was allowed to cool to room temperature, diluted with H_2O (100 mL), and extracted with ether (100 mL×3). The crude product was dried over anhydrous sodium sulfate. Evaporation of the solvent followed by purification of the residue on a silica gel column using a combination of ethyl acetate and light petroleum (boiling range 60°C to 80°C). The final product was obtained with a yield of 81%(9.2g).



The bromination of the ester was conducted following the method reported by Buchi [12]. In a 150 mL round bottom flask, 9.2g of the above ester were added to an ice cold mixture of 40ml of 40% HBr and 10 mL of H_2SO_4. Stirred at room temperature overnight, then steam bathed for 5 hours. The crude product was extracted with ether (100 mL×3) and purified through silica gel column using petroleum ether. the final product was obtained with a yield of 49% (9g) and confirmed by using ^{1}H-NMR

^{1}H-NMR [200 MHz, ($CDCl_3$)] δ = 1.78–1.84 (s, 4H, $(CH_2)_2$), δ = 2.32–2.37 (t, 2H, $CH_2C(O)$), δ = 3.28–3.31 (t, 2H, $BrCH_2$),



Ethyl 5-bromovalerate was synthesised by using method reported by Kurata [13]. In a 150 ml round bottom flask which contained the mixture of 40ml EtOH (large excess) and 9g of 5-bromo-pentanoic acid (0.05mol), a catalysis amount of 4-methylbenzenesulfonic acid was added. The reaction mixture was then stirred and refluxed at 70-80°C overnight. The crude product was rotary evaporated and purified through silica gel column using petroleum ether. The final product was obtained with a yield of 73% (7.6g) and confirmed by using ^{1}H-NMR.

^{1}H-NMR [200 MHz, ($CDCl_3$)] δ = 1.11–1.18 (t, 3H, CH_3)), δ = 1.23–1.32 (m, 8H, C_4H_8), δ = 1.53–1.58 (m, 2H, CH_2), δ = 1.76–1.83 (m, 2H, CH_2), δ = 2.12–2.25 (t, 2H, $CH_2C{=}O$), δ = 3.27–3.32 (d, 2H, $BrCH_2$), δ = 4.08–4.13 (m, 2H, OCH_2)

3.3.2 $C_{12}H_{25}N^{+}(CH_3)_2(CH_2)_8COO^{-}$

The synthesis of dodecyl carboxy betaine with 8 methylene units was similar to the procedure described above. In a 150ml round bottom flask, 18.0g dodecyldimeylamine (25ml, 0.08mol)was dissolved in 50ml ethanol and 20g methyl 9-bromononanoate was slowly added into the solution. The mixture was stirred and refluxed under at 85 °C for 18 hours. The solvent was then evaporated and the crude product extracted with ether.

A 50% excess of Dowex 550A anion exchange resin (exchange capacity 1.1 meq ml^{-1}, OH^{-} counter-ion), which had been thoroughly rinsed in UHQ water, was mixed with an aqueous solution of surfactant containing bromide counter-ion. The mixture was stirred at room temperature for at least 8 hours and filtered. The ion-exchange procedure was repeated three times. The surfactant was recovered

from the aqueous solution by freeze-drying and finally purified by recrystallization from acetone-methanol mixture. The purity was tested by surface tension measurement and no minimum was observed in the plot of surface tension against lnC.

The protonated methyl 9-bromononanoate was synthesised with mono-methyl sebacate as the starting compound [14]. In a 500ml round bottom flask a mixture of 20.4g red HgO (0.1mol), 43.25g mono-methyl sebacate (0.2mol) and 200ml of CCl_4 was heated under a 50cm Vigreux column,with stirring, such that rate of distillation was about one drop per second. After 15 minutes of distillation in this manner, addition was begun of a solution of 30g of bromine in 60ml of CCl_4. Addition was completed during 70 minutes. During the last few minutes, the majority of the bromine distilled as added. After bromine addition had been completed, an addition of 60ml CCl_4 was made over 40 minutes,while distillation was continued as before.

Mercury salts were removed from the cooled reaction mixture by filtration with suction through a filter-aid mat. The clear filtrate was extracted with 50ml of 5% aqueous NaOH and the coagulated precipitate which formed was removed from the two phase solution by suction filtration. After the CCl_4 phase had been washed with UHQ water, the 1-Bromotridecane was recovered by fractional distillation. The final product was obtained by using liquid chromatography with petroleum ether and ethyl acetate mixture. The structure was confirmed by using ^{1}H-NMR.

^{1}H-NMR [200 MHz, ($CDCl_3$)] δ = 1.15–1.18 (t, 3H, CH_3)), δ = 1.51–1.59 (m,

2H, CH_2), δ = 1.70–1.78 (m, 2H, CH_2), δ = 2.23–2.31 (t, 2H, $CH_2C{=}O$), δ = 3.23–3.29 (d, 2H, $BrCH_2$), δ = 4.12–4.18 (m, 2H, OCH_2)

The deuterated methyl 9-bromononanoate used for synthesis of the headgroup deuterated surfactant was prepared by Dr. C.C. Dong.

3.4 Purification of Ionic Surfactants

The protonated SDS was purchased from Sigma-Aldrich at the highest available purity. The sample was then recrystallized in minimum amount of hot ethanol and cooled in an ice bath at least three times until sufficient purity was attained. The deuterated SDS was synthesised by Dr. R.K.Thomas at Oxford and purified in the same way as protonated SDS.

Both protonated and deuterated DTAB were synthesised by Dr. C.C. Dong and purified by recrystallization from an acetone/ethanol mixture for at least three times until sufficient purity was attained.

Bibliography

[1] A. E. Epshtein, V. E. Limanov, M. Y. Telegin, E. K. Skvortsova, and T. I. Maksimova. Bactericidal quaternary ammonium salts derived from monochloroacetate esters. *Pharmaceutical Chemistry Journal*, 14(5):292–295, 1980.

[2] F. M. Menger and C. A. Littau. Gemini-surfactants: synthesis and properties. *Journal of the American chemical society*, 113(4):1451–1452, 1991.

[3] G. Qu, J. Cheng, J. Wei, T. Yu, W. Ding, and H. Luan. Synthesis, characterization and surface properties of series sulfobetaine surfactants. *Journal of Surfactants and Detergents*, 14(1):31–35, 2011.

[4] R. G. Laughlin. Anti-ulcer composition, September 1 1981. US Patent 4,287,174.

[5] J. D. Hines. *Investigation of Surfactants and Surfactant Mixtures*. PhD thesis, University of Oxford, 1996.

[6] J. G. Weers, J. F. Rathman, F. U. Axe, C. A. Crichlow, L. D. Foland, D. R. Scheuing, R. J. Wiersema, and A. G. Zielske. Effect of the intramolecular charge separation distance on the solution properties of betaines and sulfobetaines. *Langmuir*, 7(5):854–867, 1991.

[7] S. Albu, E. Sverko, M. T. Arts, and A. Capretta. Synthesis of deuterated 5 (z), 11 (z)-eicosadienoic acid as a biomarker for trophic transfer. *Tetrahedron Letters*, 52(7):787–788, 2011.

[8] J. Nguyen, C. McEwen, and E. E. Knaus. Hantzsch 1, 4-dihydropyridines containing a nitrooxyalkyl ester moiety to study calcium channel antagonist structure–activity relationships and nitric oxide release. *Drug development research*, 51(4):233–243, 2000.

[9] S. W. Baldwin, J. D. Wilson, and J. Aube. Regiochemistry in the intramolecular cycloadditions of substituted 5-alkenyl and 6-alkenyl nitrones. *The Journal of Organic Chemistry*, 50(23):4432–4439, 1985.

[10] A. F. Khlebnikov, S. I. Kozhushkov, D. S. Yufit, H. Schill, M. Reggelin, V. Spohr, and A. de Meijere. A novel type of chiral triangulane-based diphosphane ligands for transition metals. *European Journal of Organic Chemistry*, 2012(8):1530–1545, 2012.

[11] G. Maiti and S. C. Roy. A mild and efficient method for selective deprotection of tetrahydropyranyl ethers to alcohols. *The Journal of Organic Chemistry*, 61(17):6038–6039, 1996.

[12] G. Bchi and O. Jeger. ber einige verbindungen mit dem kohlenstoffgerst des bicyclo-[0,5,5]-dodecans. *Helvetica Chimica Acta*, 32(2):538–544, 1949.

[13] T. Kurata and N. Kurita. Synthesis of 17 membered-ring oxalactones and its odor characteristics. *Fain Kemikaru*, 37(2):43–49, 2008.

[14] N. J. Bunce. Mercury salt pathway for the degradation of carboxylic acids to alkyl halides using halogen and mercuric oxide. *The Journal of Organic Chemistry*, 37(4):664–669, 1972.

Chapter 4

Adsorption of Mixtures at the Air/liquid Interface

4.1 Introduction

Surface tension (ST) and neutron reflection (NR) measurements have been made on a series of mixtures of two ionic surfactants, one anionic (sodium dodecyl sulfate, abbreviated to SDS) and one cationic (dodecyl trimethylammonium bromide, abbreviated to DTAB) with zwitterionic surfactant N-Dodecyl-N,N-dimethyl-3-ammonio-1-propanesulfonate (C_{12}sulfobetaine, abbreviated to DSB) following the procedures discussed in Chapter 2. Some previous results about mixtures contain another zwitterionic surfactant, namely dodecyl carboxybetaine (abbreviated to DB) from Hines et al. are also included for comparison [1]. This type of surfactant has been widely applied in both industry and scientific fields, especially in biochemistry where the non-denaturing character of sulfobetaine is useful for manipulating membrane proteins [2, 3]. The presence of charges within the overall neutral molecule gives them the two special properties of high water solubility,

even when the charges are well separated, and strong synergy of interaction with ionic surfactants [4]. The strong synergy is of great importance in formulations but its strength makes it more difficult to treat quantitatively than nonionic–ionic surfactant interactions.

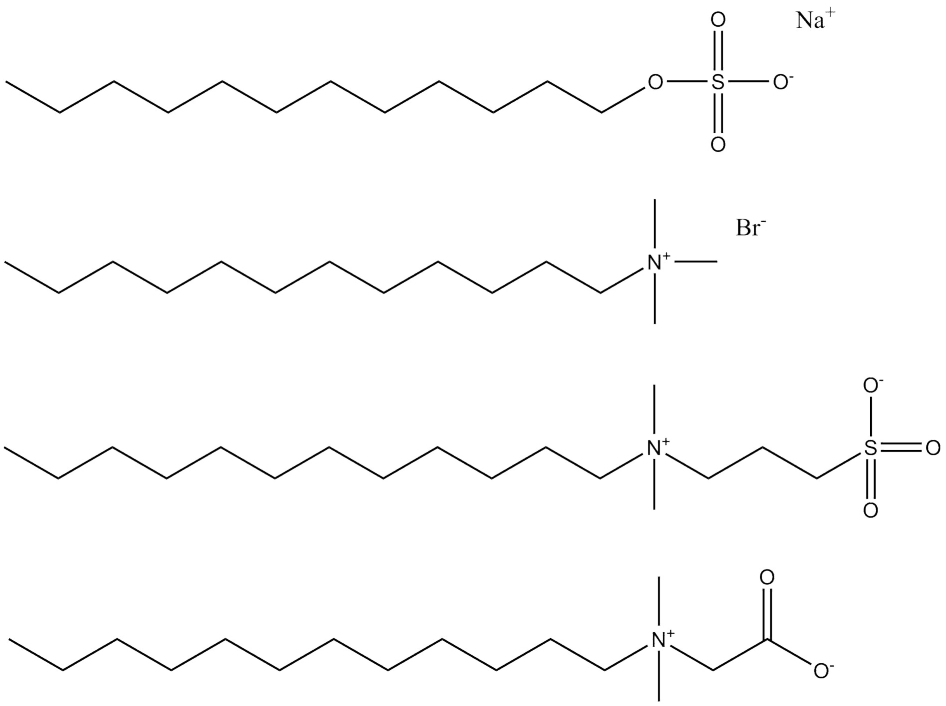


Figure 4.1: The structure of the surfactants studied. From top to bottom SDS, DTAB, DSB and DB.

The structures of the surfactants studied are shown in Figure (4.1). Although surface tension measurements in principle give the surface coverage of individual surfactants by application of the Gibbs equation, It has been show that there are serious limitations in applying the Gibbs equation accurately to surface tension data of ionic surfactants to obtaining the limiting surface excess [5–7]. By applying this method to the surface tension data of mixed surfactant systems, one can obtain the coverage and composition. These results are then used in ther-

modynamic models of surface tension or micellization in order to understand the mixing behaviour. The most frequently used model is the pseudophase approximation combined with the regular solution theory. However, the composition information for mixed systems from surface tension measurements is even more inaccurate, hence the conventional model could not provide satisfactory description of the mixing behaviour. It has been shown by Hines et al. that the excess free energy of mixing is asymmetrical, which is contradict to the result from regular solution model [1]. The failure of the conventional model could be attributed to two factors. Firstly, the model can only strictly be applied to non–ionic surfactant mixtures. Secondly, the representation of excess free energy, G_E, as a simple quadratic may not be realistic.

The pseudophase approximation with an expansion of the excess free energy is introduced to fit the two sets of data simultaneously. To apply the expanded expression of excess free energy, some additional experimental information is required. The most important one would be the composition of the surface. The neutron reflection was shown to be methodologically sound and accurate for measuring the surface coverage and composition, which can be further applied to understand the mixing behaviour thermodynamically.

4.2 Adsorption of DSB Surfactant

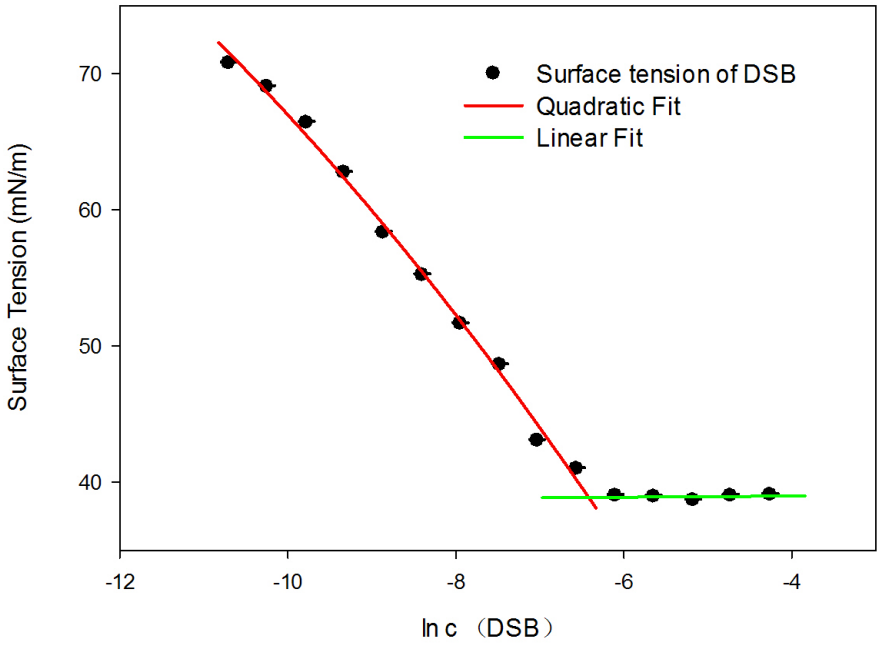


Figure 4.2: Surface tension plot of DSB at 298K

The plot of surface tension, γ, against $\ln C$ is shown in Figure (4.2), where C is the concentration of surfactant. The CMC was calculated using a quadratic fit to the data below the CMC and a linear fit above [8]. The method assumes that the surface coverage increases up to or reaches a limit at the CMC. The surface coverage, or area per molecule, can then be calculated by applying the Gibbs equation on the surface tension plot below the CMC, using

$$\Gamma_i = -\frac{1}{nRT}\frac{d\gamma}{d\ln C_i} \tag{4.1}$$

where $n = 1$ for the zwitterionic surfactant because no counterion adsorption is expected. The surface excess Γ_i can be obtained by first fitting the second order polynomial curve in the surface tension below the CMC and then substituting the best fitted $\gamma - \ln C$ into the Gibbs equation (4.1). The area per molecule, A may be obtained by applying the relationship

$$A_i = \frac{1}{\Gamma_i N_A} \tag{4.2}$$

.

From the data shown in Figure(4.2), the CMC of surfactant is calculated to be $2.2 \pm 0.2\ mM$ and $\gamma_{lim} = 38.9 \pm 0.5\ (mN\ m^{-1})$. The values of area per molecule and surface excess calculated from surface tension data by applying the Gibbs equation using a prefactor of 1 and fitting a quadratic in $\ln C$ are listed and compared with those from neutron experiments in Table (4.1), the corresponding fitting diagrams are given in Appendix A.

Conc. (mM)	$\tau \pm 2$ (Å)	$\Gamma \pm 0.25/10^{-6}$ (mol/m^2)(NR)	$A \pm 3$ (Å^2)(NR)	$\Gamma \pm 0.25/10^{-6}$ (mol/m^2)(ST)	$A \pm 3$ (Å^2)(ST)
0.022				2.5	66
0.22	11	2.8	60	3.1	54
0.66	13	3.3	50	3.3	50
2.2	14	3.7	45	3.5	48
6.6	15	4.0	42		

Table 4.1: Surface excess and areas per molecule for DSB from the NR and ST measurements at 298K.

The surface excess was measured over a range of concentration from 1/10 CMC to 3 times CMC using neutron reflection. The optical matrix method with a single

layer model was used to determine the area per molecule using

$$A_i = \frac{\sum_i b_i}{\rho\tau} \tag{4.3}$$

where $\sum_i b_i$ is the scattering length of the surfactant and ρ is the scattering length density and τ is the layer thickness. The reflectivity fits and calculated results are listed in Figure (4.3) and Table (4.1). The close agreement between NR and ST measurements indicates that DSB carries no nett charge at natural pH. Zhao et al. have recently obtained the values of 1.383 mM for the CMC, 38.64 mN m^{-1} for the limiting surface tension and 63.57 Å for the area per molecule (abbreviated to APM) for a purified commercial sample of DSB with no given error [9]. There is a large discrepancy between this value of the limiting area and those in Table (4.1). This problem has been discussed elsewhere [5,6] and it may be associated with an inaccurate determination of the limiting slope of the $\gamma - \ln C$ plot by Zhao et al. In general, the correct value of the limiting slope can only be obtained by fitting the surface tension curve to a quadratic in $\ln C$, but there is no detail given in the original paper. Yaseen et al. used three methods to analyse their surface tension and neutron reflection results for C_{12}PC and found limiting areas of 65, 53 and 52 $Å^2$ from ST analysis with a simple linear plot, ST analysis with a quadratic fit, and direct measurements with NR respectively. These values suggest that Zhao et al. may have used a linear plot to analyse their ST data and this could account for the surprisingly high value of area per molecule they obtained. In agreement with this conclusion, the limiting APM value in Table (4.2) of 45 $Å^2$ is much closer to the corresponding values of 52 $Å^2$ for C_{12}PC and 50 $Å^2$ for C_{12}CB [1]. Qu et al. obtained values of 1.6 mM , 32.8 mN m^{-1} and 105 $Å^2$ for CMC, limiting ST and APM respectively [10], the large discrepancy in the limiting ST suggests that there is something faulty in their calibration of the tensiometer (drop volume

method), since the limiting value of the ST for other zwitterionics tends to be closer to 40 mN m^{-1}. Graciani et al. obtained 2.7 mM for the CMC of DSB at 298K [11]. Taking the three previous measurements together gives a mean value of 1.9mM , within error of the values obtained here from ST data. There are two more noticeable points in Table (4.1). First, NR can be used above the CMC and this shows that there is a further decrease in A between 2.2 and 6.6 mM and therefore the plateau of adsorption has not been reached at the CMC. Secondly, the thickness of the layer is significantly smaller than for ionic surfactants with the C_{12} chain. Thus, SDS and dC_{12}hTAB (chain–deuterated) have a layer thickness at the CMC of 18 and 17.5 Å at limiting areas of 44 and 48 $Å^2$ respectively, about 20% higher than for DSB. This suggests that the alkyl chains in the adsorbed layer of DSB are more strongly tilted than in the two ionic surfactants. In general, a strong tilting of this magnitude is associated with a significantly large APM but this may not be the case here, because the tilting of DSB can be interpreted in terms of the long headgroup taking up a vertical orientation in the water and the alkyl chain is therefore forced to tilt.

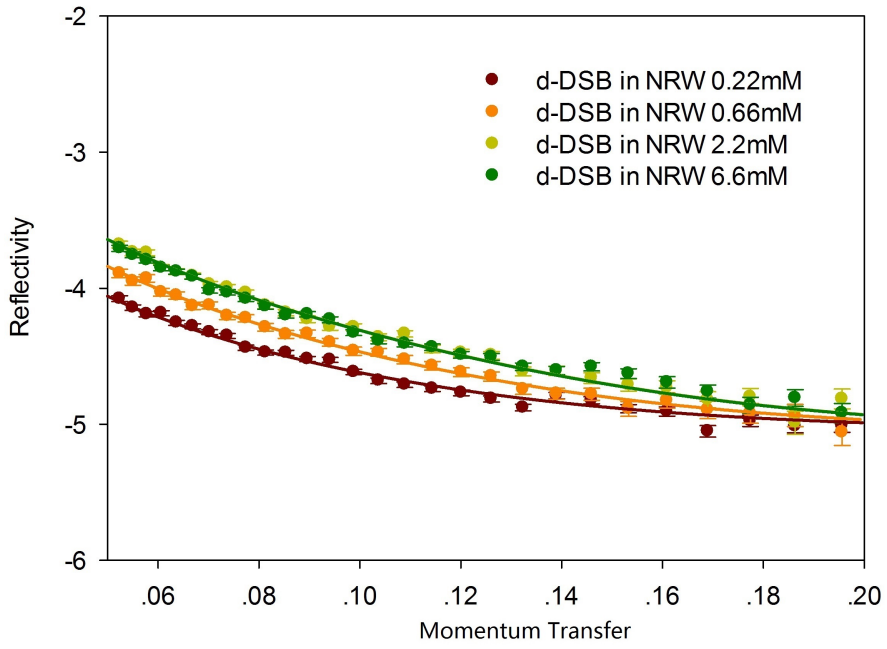


Figure 4.3: Reflectivity fits for deuterated DSB at air/liquid interface

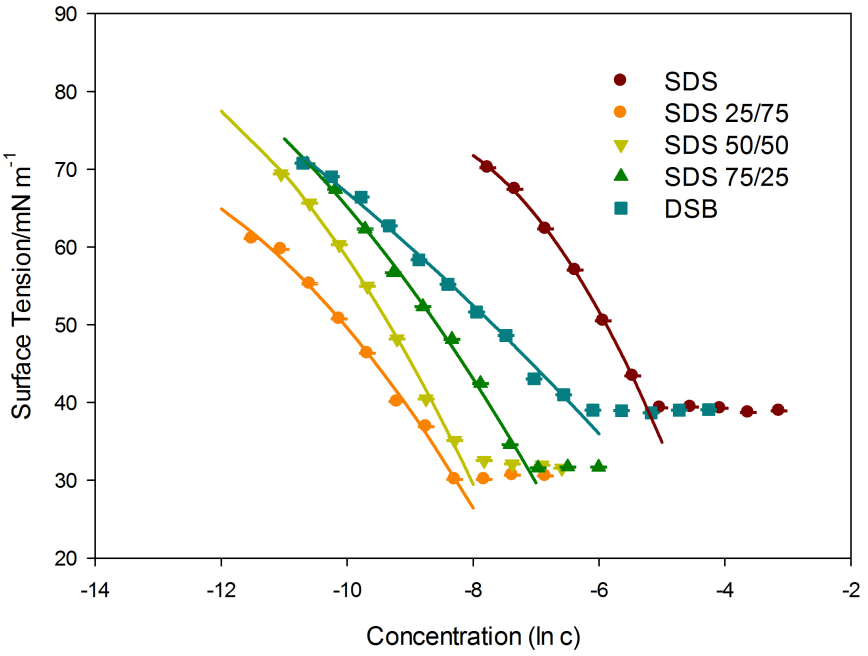
4.3 Adsorption of Surfactant Mixtures at Air-liquid Interface

4.3.1 Mixtures at CMC

The plots of surface tension, against $\ln C$ are shown in Figure (4.4) and (4.5) for SDS/zwitterionic and DTAB/zwitterionic mixtures respectively. Both of the mixed systems were studied over a range of surfactant composition. Also shown for comparison are the corresponding plots for the individual components. The CMCs were calculated using a second order fit to the data below the CMC and a horizontal line above [8], and the results are given in Table (4.2) with calculated ideal mixing CMCs for different values of α, where α is the bulk mole fraction of ionic surfactant in mixed systems. The CMC of mixtures are much lower compared to the two individual surfactants, which shows that there is strong synergy between the zwitterionics and the ionic surfactants. The interaction is significantly stronger with SDS than with DTAB for both zwitterionics because of the larger size of the DTAB headgroup.

α	SDS/DSB		SDS/DB	
	CMC ± 0.2 (mM)	Ideal (mM)	CMC ± 0.2 (mM)	Ideal (mM)
0	2.2		1.9	
0.25	0.2	2.7	0.2	2.3
0.5	0.3	3.3	0.3	3.0
0.75	0.8	4.5	0.8	4.2
1	7.0		7.0	
α	DTAB/DSB		DTAB/DB	
	CMC ± 0.2 (mM)	Ideal (mM)	CMC ± 0.2 (mM)	Ideal (mM)
0	2.2		1.9	
0.25	2.0	2.8	2.0	2.4
0.5	2.7	3.8	2.8	3.4
0.75	3.2	6.1	4.9	5.5
1	14.9		14.9	

Table 4.2: Measured CMC and calculated ideal values at different compositions for SDS and DTAB with the two zwitterionic surfactants, DSB and DB. Measurements are made at 298K except for DB with SDS, which was done at 313K. because the strong interaction leads to a raised Krafft point for the mixed system.



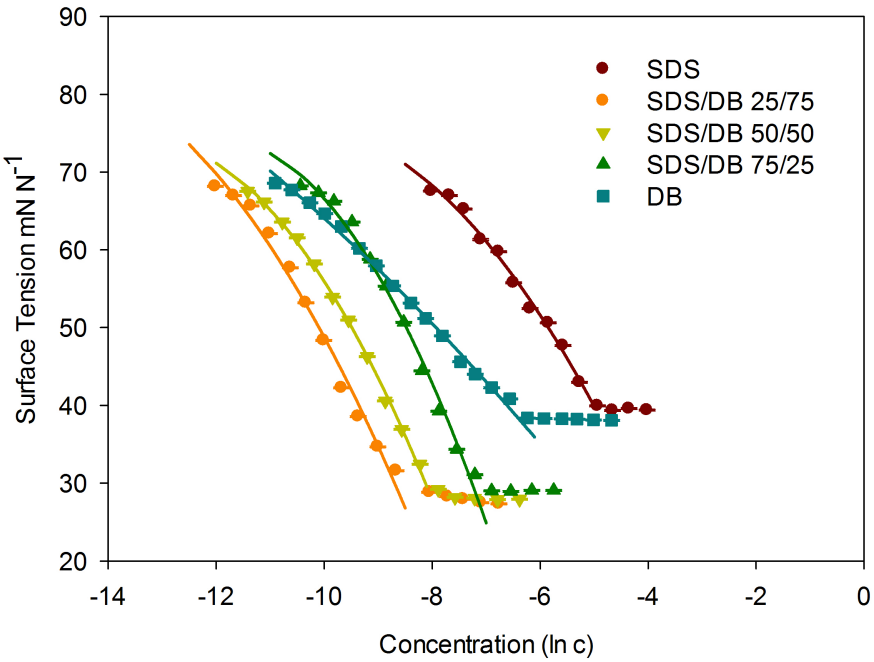


Figure 4.4: Surface tension plots of SDS/zwitterionic mixtures at 298K and 313K as a function of $\ln c$

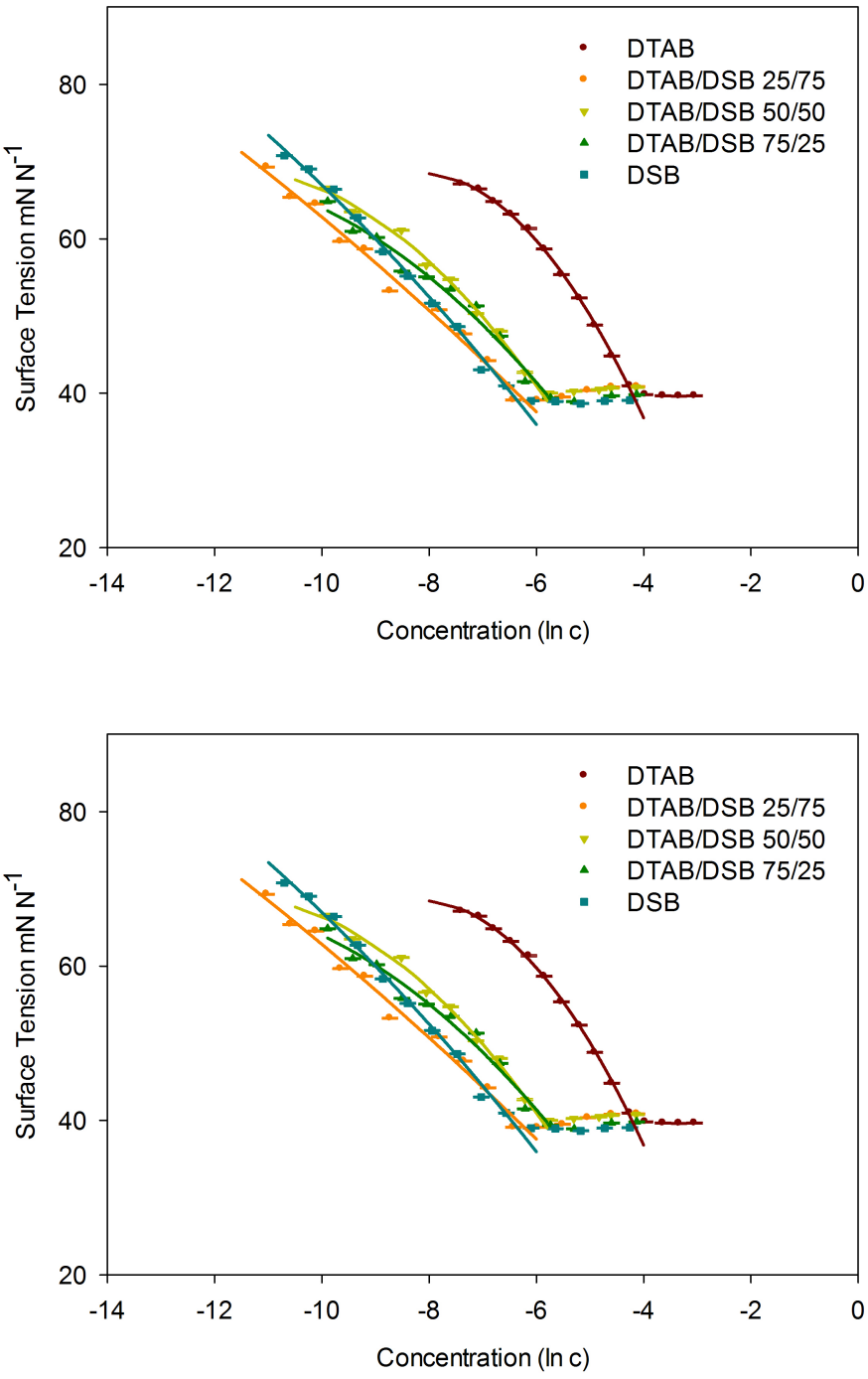


Figure 4.5: Surface tension plots of DTAB mixtures at 298K and 313K as a function of $\ln c$

As described in Chapter 1, for a mixed micelle consisting only of two nonionic surfactants, the pseudophase approximation gives the following equation at the mixed CMC(C^M_{mix}) [12–14],

$$\frac{\alpha_1}{f_1 C_1^M} + \frac{\alpha_2}{f_2 C_2^M} = \frac{1}{C^M_{mix}} \tag{4.4}$$

where α_i are the bulk mole fractions of surfactant i and C_i^M are the CMCs of the corresponding compound. The activity coefficients, f_i in the micelle are determined by the excess free energy of mixing, G_E, which is assumed to be a single quadratic term in the regular solution approximation, i.e.

$$G_E = RTBx_1x_2 \tag{4.5}$$

which gives the activity coefficients as

$$\ln f_i = Bx_j^2 \tag{4.6}$$

where x_i is the concentration of species i in the micelles and B is a constant. It has been shown that the pseudophase approximation gives a minimum in the plot of CMC against bulk concentration when $\alpha_i = x_i$ [15], i.e. the compositions of micelle and bulk solution are identical at the CMC. Applying this approximately to the SDS/DSB mixture the experimental points in Figure (4.6) indicate that the minimum occurs well below $x_i = 0.5$ in the micelle. Because the regular solution model equation (4.5) is symmetrical in the micelle composition it tends to force the minimum in the CMC to occur closer to $x_i = 0.5$ for the observed CMC ratio of about 3.5. This then B_m to be large and negative, which corresponds to a very strong attractive interaction. In order to improve such a simple fit more information is needed. The surface adsorption above the CMC is extremely sensitive to any fractionation of the composition of the micelles relative to the bulk

composition, and offers the possibility of fitting the CMC behaviour with a better model.

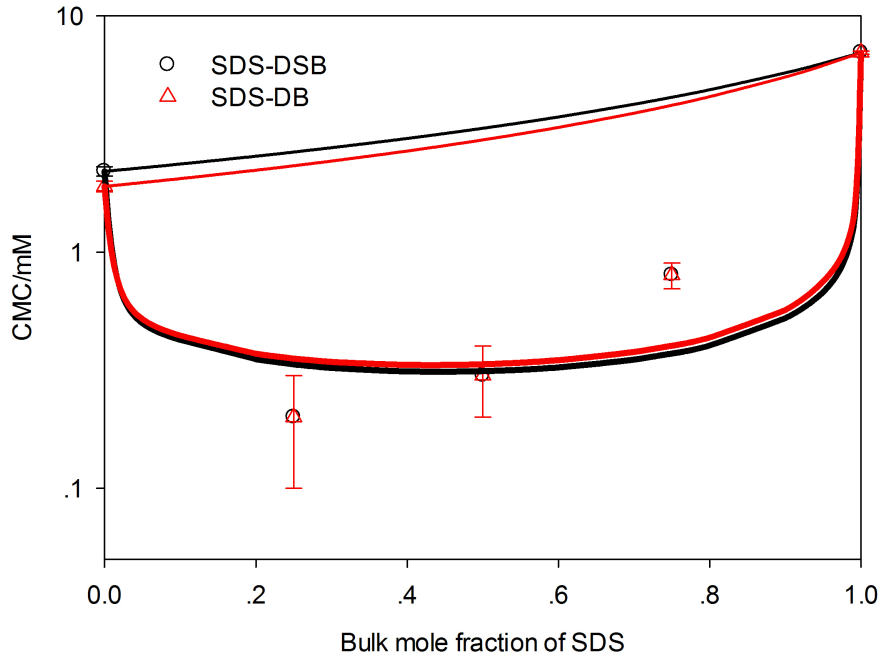


Figure 4.6: The variation of CMC (points) with composition for mixtures of SDS with DSB (black) and DB (red). The thin lines show the variation of the CMC for ideal mixing of the surfactants and the heavy lines show fits using the regular solution model with values of the interaction parameter B/RT of -10 and 9.4 for DSB and DB respectively

The procedure for applying the regular solution approximation is to make an iterative fit of equation (4.4) to a set of CMC data to obtain a value of B_m and the composition of micelle, x_i. An effective form for the iteration is discussed in Chapter 1 and it can be done as described in Chapter 2.

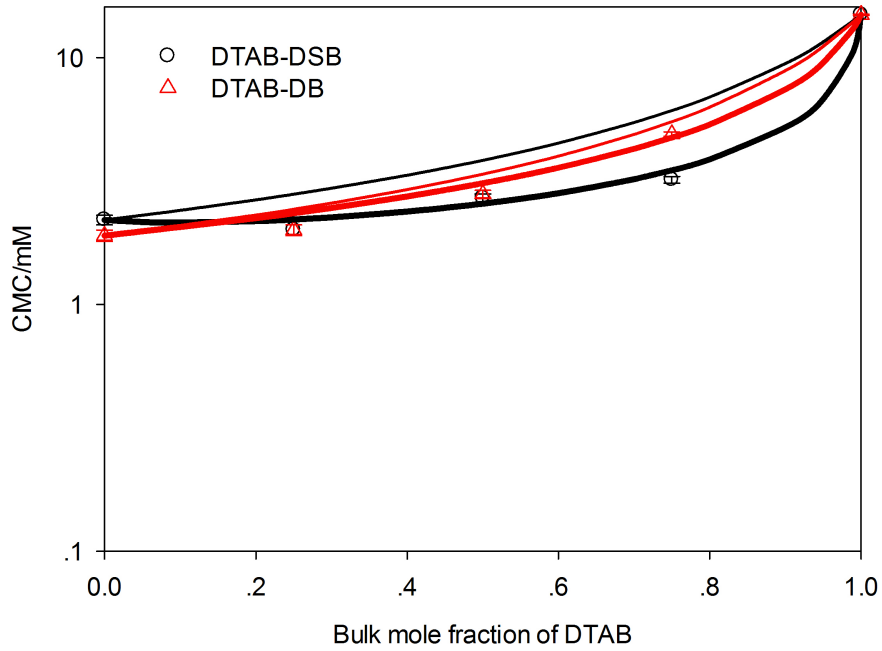


Figure 4.7: The variation of the CMC with composition for mixtures of DTAB with DSB (black) and DB (red). The thick lines show fits using the regular solution model with values of -2.4 and -0.7 for DSB and DB respectively. The thin lines show the variation of the CMC for ideal mixing.

In Figures (4.6) and (4.7) the results are compared with calculations from both ideal and nonideal mixing using the regular solution model with a single interaction parameter, equation (4.5). The fit for the more strongly interacting system SDS/zwitterionic is poor. An alternative way of dealing with this is to use a different value of B_m for each composition in which case the magnitude of B_m decreases significantly with the bulk mole fraction of ionic surfactant. This was done by Hines for SDS/DB, by Lopez–Diaz et al. for SDS/DSB and DTAB/DSB , and by Li et al. for SDS/DSB (at 313K) [1,16,17]. The values for SDS/DSB using

this method are -11,-10 and -7 (units of RT) for mole fractions of SDS of 0.25, 0.5 and 0.75 respectively, which give good agreement with the calculated results from ST data, as shown in Table 4.3. Hines et al. suggested that the asymmetry in the regular solution model is the result of either the ionization of the micelle or a less symmetrical excess free energy than given by just a quadratic term in G_E.
The values of the mixed CMC are almost identical for the DSB and DB mixtures. Although a sulfonate group is generally ionized more than a carboxylate, close approach of carboxylate to the permanent positive charge of the quaternary ammonium group in the zwitterionic molecule can reduce the difference significantly [18]. For the DTAB mixture systems the interaction parameter is much lower. This may be because the headgroups are of similar size so that the charge on the cationic headgroup feels the effects of both two charged parts on the zwitterionic.

α	SDS/DSB		SDS/Betaine	
	$B \pm 0.5$	$x_{SDS} \pm 0.05$	$B \pm 0.5$	$x_{SDS} \pm 0.05$
0		0.0		0.0
0.25	-11.3	0.41	-11.5	0.41
0.5	-10.6	0.45	-9.3	0.44
0.75	-7.1	0.49	-7.2	0.48
1		1.0		1.0

Table 4.3: Calculated values of B and x_{SDS} for each bulk composition

4.3.2 Mixtures: Surface Tension and Composition at and below the CMC

The pseudophase approximation can also be applied to the surface tension and/or surface excess of a surfactant mixture. It is relatively simple using either neutron reflection or surface tension measurements below the CMC. In the concentration range below the CMC, the iterative method can be applied to the surface tension data if the C_i^M in equations (1.12) and (1.13) are replaced by C_i^π where C_i^π is the concentration at which the surface pressure, π, reaches a particular value. Such a set of measurements of C_i^π for different compositions at a fixed surface pressure can be fitted in terms of a parameter B_s to solve equation (1.13). The details are discussed in chapter 1. Such a set of data is assembled in Table (4.4) based on the surface tension curves given above. The C_i^π in Table (4.4) were obtained by interpolation of the surface tension curves using fitted quadratics in $\ln C$ at the highest possible surface pressure in each case, i.e. close to the limiting surface tension at the CMC of the less surface active component.

SDS/Z	DSB C_i^π	$x_1 \pm 0.04$	DB C_i^π	$x_1 \pm 0.04$
0/100	1.5_5	0.0	1.4	0.0
20/80	-	-	-	0.26^c
25/75	0.1	0.32	0.1	-
50/50	0.2	0.32	0.1_5	0.32^c
75/25	0.4	0.39^a	0.4	-
80/20	-	-	-	0.39^c
100/0	7.0	1.0	7.0	1.0
DTAB/Z	DSB C_i^π	$x_1 \pm 0.04$	DB C_i^π	$x_1 \pm 0.04$
0/100	1.6	0.0	1.4	-
25/75	1.8	0.25^a	1.5_5	-
50/50	2.8	0.30^b	2.1	-
75/25	3.0	0.33^b	4.1	-
100/0	14.9	1.0	14.9	-

Table 4.4: Measured C^π (mM) for SDS and DTAB with the zwitterionic surfactant (DSB and DB) and surface compositions,x_1, below the mixed CMC from neutron reflection, all at 298K except SDS/DB at 313K. The measurements were made at an surface tension of 40 mN m^{-1}. The superscript a denotes an average over values at total concentrations of 0.22 and 0.66 mM, b denotes an average over 0.22, 0.66 and 2.2mM (full details of the neutron reflection measurements are given in Table (4.5)), and c denotes results recalculated from the reflectivity data of Hines et al [1]. The error in C^π are the same as for the CMC measurements in Table (4.2)

An important difference from the analysis of the CMC data is that the concentration of the individual surfactants at the surface , i.e. the x_i in equations, can be determined using NR both above and below the CMC. As an example, Figure (4.8) and (4.9) show the NR profiles for 50/50 mixtures for each of SDS/DSB and DTAB/DSB at a concentration of 0.66 mM plotted for three isotopic combinations, two where one of the components has a deuterated chain, and the third where both chains are deuterated. In Figure (4.8) the fraction of SDS in the adsorbed layer is higher than that in DTAB/DSB mixture but the surface is still rich in DSB.

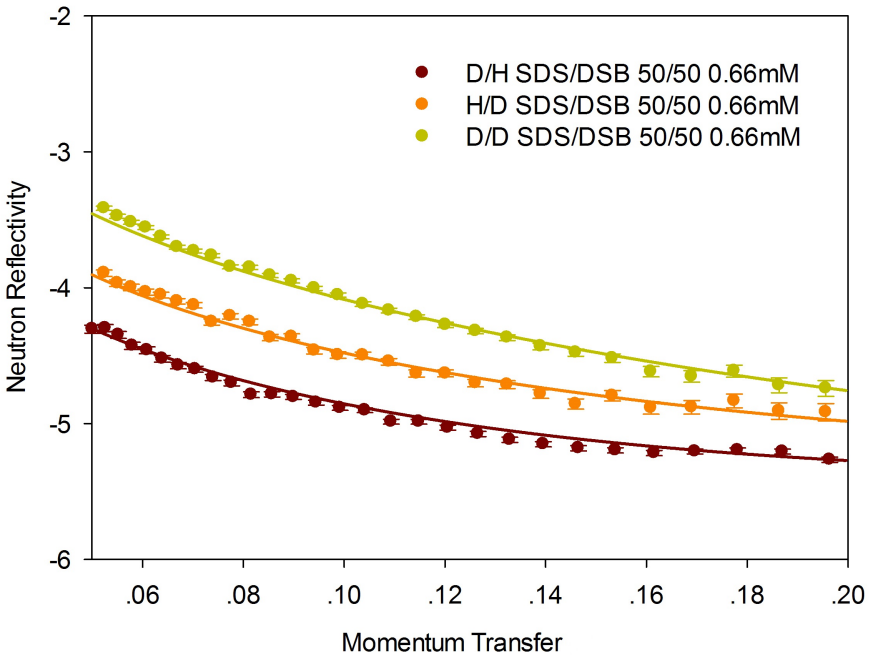


Figure 4.8: Neutron reflectivity profiles from 50/50 mixture of SDS/DSB at a concentration of 0.66 mM (above the mixed CMC)

In Figure (4.9) for 50/50 DTAB/DSB there is only a small difference between the total adsorbed amount and that of just DSB, and this is consistent with the low level of adsorption of DTAB. Finally, since the scattering lengths of the three molecules are almost the same, the total adsorption in SDS/DSB is higher than in DTAB/DSB.

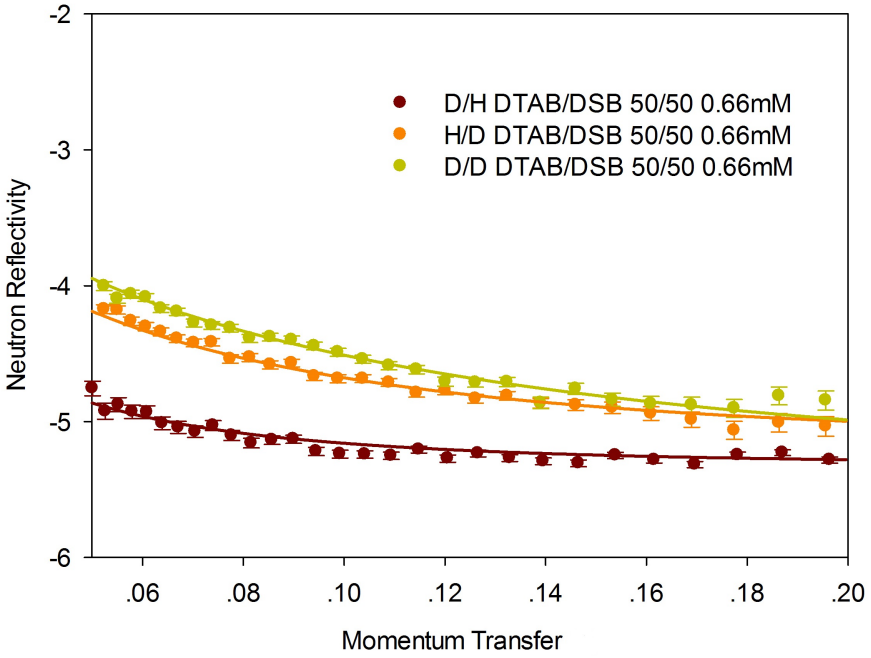


Figure 4.9: Neutron reflectivity profiles from 50/50 mixture of SDS/DSB at a concentration of 0.66 mM (below the mixed CMC)

The set of three isotopic profiles gives independent measures of the total coverage and the complete set of results is given in Table (4.5). The corresponding fitted diagrams are given in Appendix A. Ideally, the measured total adsorption amount should equal the sum of the individual surface excesses but, as shown in Table (4.5), there are discrepancies and the final composition then depends on the way

the results are combined. Here the total surface excess is first determined from the average of the total measurement and the sum of the individual measurements to give the result in the last column in Table (4.5), then this is used to determine the individual fractions and finally the sum of these fractions is normalized to unity. The NR values used in Table (4.4) are averages of the values below the mixed CMC from Table (4.5). These should be corrected for the surface pressure term but the effect seems to be small here and there is no systematic change in the fractional coverages over the concentrations studied. Hines et al. observed changes in the SDS/DB system at concentrations well below the CMC. In addition, re–analysing of the NR data from Hines et al. using the method above gives different values of x from the original paper, especially at the two lower compositions.

Table 4.5: Surface excesses and fraction of ionic surfactant at the surface(x_S) measured by NR for three isotopic compositions of the systems SDS/DSB and DTAB/DSB. Sets of figures in italics are measurements at or below the mixed CMC.

System (Composition)	C/mM	Γ (d/d) ± 0.25	Γ (d/h) ± 0.15	Γ (h/d) ± 0.2	x_S (ionic) ± 0.03	Γ_{total} ± 0.2
	0.22	*4.3*	*1.4*	*3.0*	*0.32*	4.3_5
SDS/DSB	0.66	4.7	1.7	3.3	0.34	4.8_5
25/75	2.2	5.0	1.8	3.3	0.35	5.0_5
	6.6	5.2	2.1	3.3	0.39	5.3
	0.22	*4.9*	*1.4*	*3.0*	*0.32*	4.6_5
SDS/DSB	0.66	5.2	2.0	3.0	0.40	5.1
50/50	2.2	5.2	2.0	3.3	0.38	5.2_5
	6.6	5.6	2.3	3.3	0.41	5.6
	0.22	*4.3*	*1.7*	*2.7*	*0.39*	4.3_5
SDS/DSB	*0.66*	*5.0*	*1.9*	*2.9*	*0.40*	4.9
75/25	2.2	5.3	2.2	3.0	0.42	5.2_5
	6.6	5.4	2.5	3.0	0.45	5.4_5

Table continues on next page

System (Composition)	C/mM	Γ (d/d) $\pm$ 0.25	Γ (d/h) $\pm$ 0.15	Γ (h/d) $\pm$ 0.2	x_S (ionic) $\pm$ 0.03	Γ_{total} $\pm$ 0.2
	0.22	*2.9*	*0.8*	*2.2*	*0.27*	2.9_5
DTAB/DSB	*0.66*	*3.3*	*0.8*	*2.7*	*0.23*	3.4
25/75	2.2	3.9	1.1	3.1	0.26	4.0_5
	6.6	4.2	1.4	2.9	0.33	4.2_5
	0.22	*2.6*	*0.7*	*2.0*	*0.27*	2.9_5
DTAB/DSB	*0.66*	*3.0*	*0.9*	*2.1*	*0.30*	3.0
50/50	*2.2*	*3.9*	*1.3*	*2.4*	*0.35*	*3.8*
	6.6	4.3	1.7	2.7	0.39	4.3_5
	0.22	*2.2*	*0.75*	*1.5*	*0.33*	2.2_5
DTAB/DSB	*0.66*	*2.6*	*0.9*	*1.8*	*0.33*	2.6_5
75/25	*2.2*	*3.5*	*1.2*	*2.4*	*0.33*	3.5_5
	6.6	3.9	1.4	2.7	0.34	4.3_5

Table 4.6: Values of $\rho \times \tau$ for SDS/DB at 0.2 mM, calculated from the reflectivity data from Hines et al. but using an identical method of calculation to that in this chapter [1]. Scattering lengths used are 0.267 and 0.012 Å for dSDS and hSDS respectively, and 0.259 and 0.004 Å for dDB and hDB respectively.

Composition	$((\rho\tau)_{dh}\Gamma_{SDS})$	$((\rho\tau)_{hd}\Gamma_{DB})$	$((\rho\tau)_{dd}\Gamma_{total})$	$x_{SDS}(x_{SDS})^1$
20/80	15 (0.91)	42 (2.63)	51(3.24)	0.26±0.08 (0.10)
50/50	17 (1.06)	36 (2.29)	60(3.82)	0.32±0.08 (0.22)
80/20	24 (1.49)	36 (2.31)	59(3.75)	0.39±0.05 (0.36)

The reflectivity profiles of Hines et al. were therefore refitted using the same procedure as for SDS/DSB mixtures. Allowance was made for the small contributions from the weakly scattering component in the hd and dh samples, but the correction is small. The errors in this determination are significantly larger for the earlier data than those presented in this chapter, mainly because of considerable improvement in the neutron relfectometers. The calculation was done at the single total concentration of 0.2 mM. The large differences in the calculation of the 20/80 and 50/50 compositions from that of Hines et al. stem from the fact that the sum of the individually measured surface excesses of SDS and DB do not add up to the total surface excess in the dd experiment. The results are listed in Table (4.6)

The application of the pseudophase approximation usually uses the C^{π} data combined with the regular solution model. As already described, this can lead to the problem that B_s varies with coverage. If coverage data are also available, there may also be a discrepancy between the values of B_s needed to fit the two different sets of data. For example, Hines et al. found that $B_s = -8$ for the C^{π} data on the SDS/DB system whereas it was only -1.6 for the coverage data obtained from neutron experiments. This discrepancy can be explained by taking the SDS/DSB data here as an illustration. At the concentration where the minimum of C^{π} occurs, the composition of the bulk solution and the composition of the surface layer are identical in the regular solution model equation. At this point the surface composition x_{1min} and B_s are related by

$$x_{1min} = \frac{1}{2} + \frac{1}{2B_s} \ln\left(\frac{C_1^{\pi}}{C_2^{\pi}}\right) \tag{4.7}$$

The behaviour of x_{1min} when B_s is negative, for the value of C_1^{π}/C_2^{π} for SDS/DSB, is shown in Figure (4.10), where x_1 is x_{SDS}. For the large magnitude of B_s observed for this system x_{1min} is between 0.4 and 0.5, which indicates that the strong attraction between the surfactants causes the surface layer to tend towards being equimolar even though DSB is much more surface active than SDS. The mixed C^{π} is obtained directly by substituting the values of x_{1min} from equation (4.7) into the surface version of equation (4.4)

$$\frac{x_{1min}}{C_1^{\pi} \exp(-B_s x_{2min}^2)} + \frac{1 - x_{1min}}{C_2^{\pi} \exp(-B_s x_{1min}^2)} = \frac{1}{C_{min}^{\pi}} \tag{4.8}$$

where the C_i^{π} refer to the individual components. The resulting value of C_{min}^{π} relative to the C^{π} of DSB is also plotted in Figure (4.10). It shows that a value of x_{1min} of about 0.2 correlates with a weak interaction of B_s of about -2, while low values of C_{min}^{π} in the range 0.05-0.08 correspond to values of x_{1min} of about 0.45.

Therefore the experimental results of x_{1min} for all the SDS systems in Table (4.4) require the $-B_s$ to be small, whereas the corresponding C^{π}_{min} values require $-B_s$ to be large. Thus the coverage and C^{π} data cannot even agree approximately in the regular solution model.

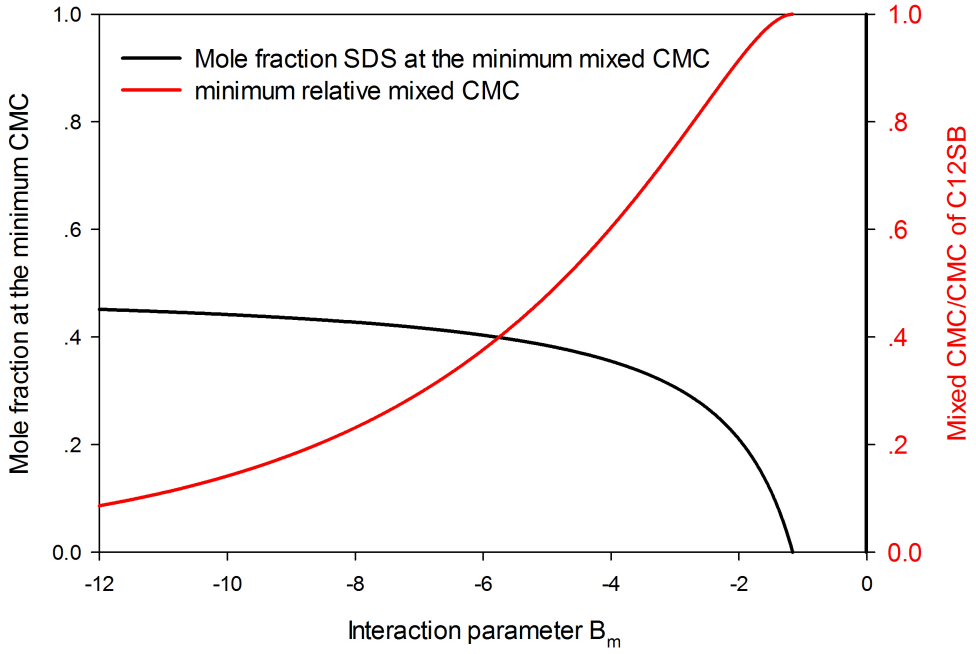


Figure 4.10: The behaviour of the minimum value of C^{π} at a mixed surface and of the surface composition of the less surface active component (component with the higher C^{π}) as a function of the interaction parameter, B_s, calculated using the exact solution of the regular solution approximation, equations (4.7) and (4.8), and the observed C^{π}_1/C^{π}_2 ratio.

The possible explanations for this failure of the regular solution model have all been discussed previously by many authors, especially by Hines et al. [19]. These are (i) the model strictly only applies to nonionic surfactant systems, (ii) the ex-

pression of excess free energy as a simple quadratic may not be realistic, and (iii) the hydration of the layer may change on mixing and this makes the assumption that the layer only consists of the two surfactants incorrect. One solution for the first difficulty is to do all the measurements in swamping electrolyte, but this is also likely to affect the interaction, which is the major interest in studying ionic/zwitterionic mixtures. Hines et al. showed that the dissociation can be treated quantitatively if its variation with composition is available. The symmetric G_E can be overcome by using a more extensive expansion of G_E. There are no models for the change of hydration although Hines et al. used neutron reflection to obtain the information about structure of the layer, from which they showed that there were large hydration changes associated with the mixing of SDS and DB at the air–liquid interface. They also showed that the first two factors have similar effects on the apparent G_E.

As described in Chapter 1, an expansion for G_E that is well established for bulk binary mixtures [20–23] is

$$G_E = RTx_1x_2\left[B_s + C_s(x_1 - x_2) + D_s(x_1 - x_2)^2 + ...\right] \tag{4.9}$$

where B_s, C_s and D_s are constants appropriate to the surface layer. The use of this fuller expression in equation (4.9) does not change the procedure for solving equation (4.4) except that the activity coefficients are now [22, 23]

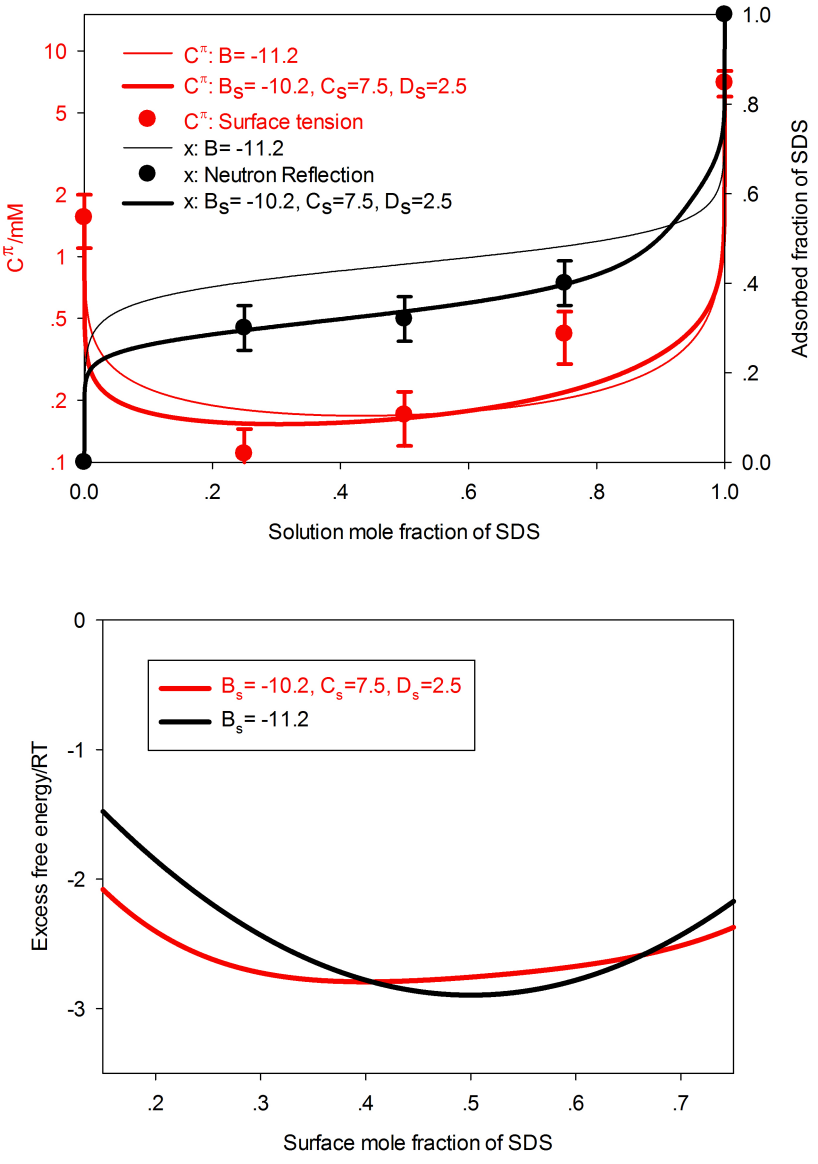
$$\ln f_1 = B_s x_2^2 + x_2^2(3 - 4x_2)C_S + x_2^2(5 - 16x_2 + 12x_2^2)D_S \tag{4.10}$$

with a parallel expression for f_2 but the sign changes for the C term. The simultaneous solution of equation (4.4) can still be done accurately by iteration method described above. The simultaneous fitting of NR and ST data described below

were conducted with software written by Dr. R K Thomas.

In Figure 4.11 (a), the thick lines show the best fit of the pseudophase model to SDS/DSB using the full expression, equation (4.9), for the excess free energy, and the thin lines represent fitting using the regular solution model. By introducing the extra parameters in G_E, i.e. C_s and D_s, the fit of the composition of the surface is improved. The reason is that these parameters shift the minimum in G_E so that it matches the observed surface compositions, as shown in Figure 4.11 (b), where the corresponding excess free energies are plotted over the range of accessible surface composition. It is easier to understand the data in terms of G_{min} and x_{min} and the fits for the four systems are given in Table (4.7) therefore include the derived values of G_{min} and x_{min} as well as the set of parameters, B_s, C_s and D_s.

Figure 4.11: (a) Fitting of the values of C^{π} from surface tension (red) and for x_i from NR(black) for SDS/DSB mixtures below the CMC and (b) the excess free energy of mixing at the surface plotted against the surface composition over the range accessible to the surface tension and neutron reflection. In (a) thin lines use the regular solution approximation and thick lines use the full excess free energy of equation (4.9) using the values of the parameters in the Figure.



The asymmetry is effectively fitted in terms of its depth and composition at the minimum but in a way that is thermodynamically consistent with the pseudophase approximation. However, the doubts over the validity of the pseudophase approximation and the limited range of surface concentration probed might allow a more flexible choice of expressions for G_E than those from bulk liquid mixtures. The most obvious causes of the asymmetry in G_E are different lateral dimensions for the two surfactants and the optimization of electrostatic screening. For example, a 1:2 lattice is particularly stable for a regular two dimensional lattice of one charged and one uncharged component, and local structures with this conformation will persist in a liquid–like layer [24].

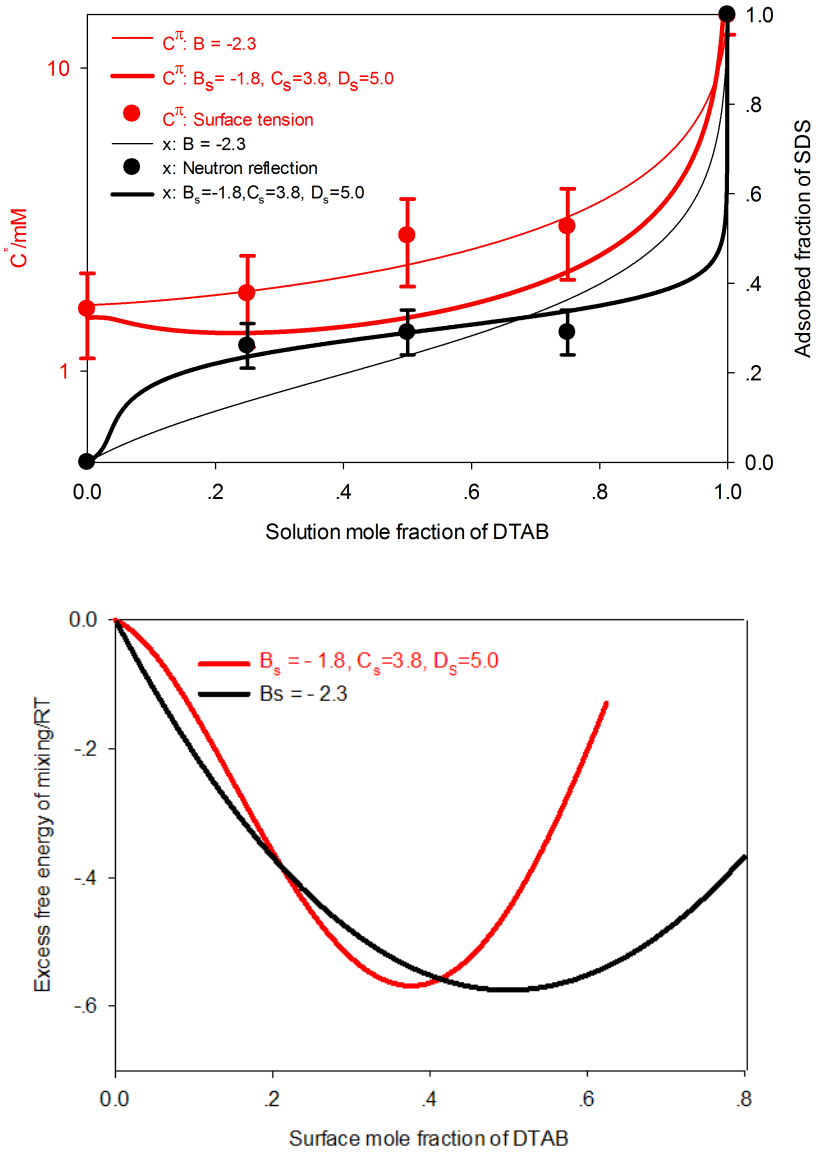
By fitting the combination of surface coverage obtained from neutron reflection and surface tension data to a single model using a fuller expansion of G_E, the limitation of regular solution approximation of G_E has been overcome [14]. Although the model also neglects dissociation, Hines et al. applied a dissociation model based on the theoretical work of Hall to neutron and surface tension data on SDS/DB and found that it was similar to the use of the fuller expansion of G_E [1, 25, 26]. The advantages of using the full expansion is that the interaction between the surfactants is more accurately parametrized without the necessity to introduce a model for the dissociation. Hines et al. noted that the expansion of G_E in equation (4.9) cannot be used in conjunction with the dissociation model. The simultaneous fitting of C^{π} and surface composition with the implicit inclusion of dissociation into the higher coefficients of equation (4.4) for nonionic mixing seems to be a more practicable option.

System	B	B_s, C_s, D_s	x_{min}	$G_{Emin} \pm 0.3$
SDS/DSB	-11.2	-10.2, 7.5, 2.5	0.38	-2.8
SDS/DB	-10.9	-10.8, 3.8 -4.5	0.38	-2.8
DTAB/DSB	-2.3	-1.8, 3.8, 5.0	0.38	-0.6
DTAB/DB	-1.0	-	0.5	-0.25

Table 4.7: Two sets of parameters characterizing the excess free energy of mixing, G_E. Columns 2 and 4 are the interaction parameter for the regular solution model, B, and the composition of the minimum energy mixture, x_{min}, which refers to the first component of the mixture. Columns 3 and 5 give the corresponding parameters for a free energy of mixing with quadratic (B_s), cubic(C_s) and quartic(D_s).

The interactions in the DTAB/DSB systems are weaker versions of those discussed above for SDS/DSB and the parallel calculations and the data are shown in Figure (4.12). It can be seen that the maximum depth of G_E is much reduced compared with SDS/DSB. The fitting parameters are given in Table(4.7). In some cases the extrapolation of equation (4.9) to regions outside those that can be explored in the accessible bulk composition range indicates that there might be phase separation. However, this involves extrapolation outside the normal range of bulk concentrations. It suggests that an exploration of very low or very high fractions would be useful. However, measurements in these regions would be vulnerable to surface contamination, surface depletion and slow equilibration.

Figure 4.12: (a) Fitting of the values of C^{π} from surface tension (red) and for x_i from NR(black) for DTAB/DSB mixtures below the CMC and (b) the excess free energy of mixing at the surface plotted against the surface composition over the range accessible to the surface tension and neutron reflection. In (a) thin lines use the regular solution approximation and thick lines use the full excess free energy of equation (4.9) using the values of the parameters in the Figure.



4.4 Conclusions

Surface tension and neutron reflection measurements were made on a series of mixtures of two ionic surfactants, one anionic (SDS) and one cationic (DTAB), with the two zwitterionic surfactants, DSB and DB at air–liquid interface. The anionic SDS interacts unusually strongly with both zwitterionics and the DTAB less strongly. By simultaneously fitting the surface tension and neutron reflection data of the mixed system SDS/DSB, it is possible to use the pseudophase approximation with an expansion of the surface free energy, G_E, up to and including the quartic term, which is much better and able to account quantitatively for the observed behaviour. It was found that G_E is asymmetric for the adsorbed layer and the minimum occurs at a surface mole fraction, x_{SDS}, of 0.28 with a depth of -2.8RT. Neutron reflection data on SDS/DB showed that G_E for both surface and micelles are similarly asymmetric to those of SDS/DSB. These results have been recently published in J. Phys. Chem. B [27]. The analysis from the NR and ST measurements here also provides a basis for a more accurate quantitative analysis of the adsorption behaviour of mixtures at the solid–aqueous interface.

Bibliography

[1] J. D. Hines, R. K. Thomas, P. R. Garrett, G. K. Rennie, and J. Penfold. Investigation of mixing in binary surfactant solutions by surface tension and neutron reflection: strongly interacting Anionic/Zwitterionic mixtures. *The Journal of Physical Chemistry B*, 1998.

[2] L. M. Hjelmeland. A nondenaturing zwitterionic detergent for membrane biochemistry: design and synthesis. *Proceedings of the National Academy of Sciences*, 77(11):6368–6370, 1980.

[3] L. M. Hjelmeland, D. W. Nebert, and J. C. Osborne Jr. Sulfobetaine derivatives of bile acids: Nondenaturing surfactants for membrane biochemistry. *Analytical biochemistry*, 130(1):72–82, 1983.

[4] D. J. Hodge, R. G. Laughlin, R. H. Ottewill, and A. R. Rennie. Micellization of ultralong chain surfactants. *Langmuir*, 7(5):878–884, 1991.

[5] P. X. Li, Z. X. Li, H.i Shen, R. K. Thomas, J. Penfold, and J. R. Lu. Application of the gibbs equation to the adsorption of nonionic surfactants and polymers at the air–water interface: Comparison with surface excesses determined directly using neutron reflectivity. *Langmuir*, 29(30):9324–9334, 2013.

[6] H. Xu, P. X. Li, K. Ma, R. K. Thomas, J. Penfold, and J. R. Lu. Limitations in the application of the gibbs equation to anionic surfactants at the air/water surface: sodium dodecylsulfate and sodium dodecylmonooxyethylenesulfate above and below the cmc. *Langmuir*, 29(30):9335–9351, 2013.

[7] P. X. Li, R. K. Thomas, and J. Penfold. Limitations in the use of surface tension and the gibbs equation to determine surface excesses of cationic surfactants. *Langmuir*, 30(23):6739–6747, 2014.

[8] J. N. Phillips. The energetics of micelle formation. *Transactions of the Faraday Society*, 51:561–569, 1955.

[9] J. Zhao, C. Dai, Q. Ding, M. Du, H. Feng, Z. Wei, A. Chen, and M. Zhao. The structure effect on the surface and interfacial properties of zwitterionic sulfobetaine surfactants for enhanced oil recovery. *RSC Advances*, 5(18):13993–14001, 2015.

[10] G. Qu, J. Cheng, J. Wei, T. Yu, W. Ding, and H. Luan. Synthesis, characterization and surface properties of series sulfobetaine surfactants. *Journal of Surfactants and Detergents*, 14(1):31–35, 2011.

[11] M. del Mar Graciani, A. Rodríguez, M. Muñoz, and M. L. Moyá. Micellar solutions of sulfobetaine surfactants in water-ethylene glycol mixtures: surface tension, fluorescence, spectroscopic, conductometric, and kinetic studies. *Langmuir*, 21(16):7161–7169, 2005.

[12] von H. Lange and K-H. Beck. Zur mizellbildung in mischlösungen homologer und nichthomologer tenside. *Kolloid-Zeitschrift und Zeitschrift für Polymere*, 251(6):424–431, 1973.

[13] J. H. Clint. Micellization of mixed nonionic surface active agents. *Journal of the Chemical Society, Faraday Transactions 1: Physical Chemistry in Condensed Phases*, 71:1327–1334, 1975.

[14] D. N. Rubingh. Mixed micelle solutions. In *Solution chemistry of surfactants*, pages 337–354. Springer, 1979.

[15] C. M. Nguyen, J. F. Rathman, and J. F. Scamehorn. Thermodynamics of mixed micelle formation. *Journal of colloid and interface science*, 112(2):438–446, 1986.

[16] F. Li, G. Z. Li, and J. B. Chen. Synergism in mixed zwitterionic–anionic surfactant solutions and the aggregation numbers of the mixed micelles. *Colloids and Surfaces A: Physicochemical and Engineering Aspects*, 145(1):167–174, 1998.

[17] D. Lopez-Diaz, I. Garcia-Mateos, and M. M. Velázquez. Synergism in mixtures of zwitterionic and ionic surfactants. *Colloids and Surfaces A: Physicochemical and Engineering Aspects*, 270:153–162, 2005.

[18] J. G. Weers, J. F. Rathman, F. U. Axe, C. A. Crichlow, L. D. Foland, D. R. Scheuing, R. J. Wiersema, and A. G. Zielske. Effect of the intramolecular charge separation distance on the solution properties of betaines and sulfobetaines. *Langmuir*, 7(5):854–867, 1991.

[19] K. Ogino and M. Abe. *Mixed surfactant systems*. CRC Press, 1992.

[20] P. M. Holland. Nonideality at interfaces in mixed surfactant systems. In *Mixed surfactant systems*, volume 1, pages 327–341. American Chemical Society Washington, DC, 1992.

[21] O. Redlich and A. T. Kister. Algebraic representation of thermodynamic properties and the classification of solutions. *Industrial & Engineering Chemistry*, 40(2):345–348, 1948.

[22] J. A. Barker. Determination of activity coefficients from total pressure measurements. *Australian Journal of Chemistry*, 6(3):207–210, 1953.

[23] J. S. Rowlinson and F. L. Swinton. *Liquids and Liquid Mixtures: Butterworths Monographs in Chemistry*. Butterworth-Heinemann, 2013.

[24] A. Patist, S. Devi, and D. O. Shah. Importance of 1: 3 molecular ratio on the interfacial properties of mixed surfactant systems. *Langmuir*, 15(21):7403–7405, 1999.

[25] D. G. Hall. Thermodynamic and kinetic aspects of micellisation in solutions of ionic surfactants. *Colloids and Surfaces*, 4(4):367–378, 1982.

[26] D. G. Hall and R. W. Huddleson. A regular-solution treatment of the micelle point in surfactant mixtures of different types. *Colloids and surfaces*, 13:209–219, 1985.

[27] P. Li, K. Ma, R. K. Thomas, and J. Penfold. Analysis of the asymmetric synergy in the adsorption of zwitterionicionic surfactant mixtures at the air-water interface below and above the critical micelle concentration. *J. Phys. Chem. B*, Doi: 10.1021/acs.jpcb.6b00762.

Chapter 5

Mixtures of Anionic/Zwitterionic surfactants at the Solid-liquid Interface

5.1 Introduction

In this chapter, the results of neutron reflection experiments at the interface between a hydrophilic silicon/silica block and aqueous solutions containing different surfactant mixtures are discussed. The surfactants used were the anionic surfactant Sodium n-Dodecyl Sulphate (SDS), the zwitterionic surfactant N-Dodecyl-N,N-dimethyl-3-ammonio-1-propanesulfonate (DSB) and n-dodecyl-N,N-dimethylamino acetate (DB). Solutions containing individual zwitterionics, and the mixtures involving ionic surfactants are investigated at different concentrations and compositions. The results are compared with the results from the air-liquid interface described in chapter 4.

It is known that the adsorption of surfactants at the interface between the hydrophilic silica substrate and aqueous solution is driven by the combination of several factors. Firstly, the interaction between the headgroup of individual surfactant and the surface leads to low levels of adsorption. Secondly, the cooperative hydrophobic interaction between the hydrophobic units, leads to the formation of aggregated structures and much higher levels of adsorption [1, 2]. The higher levels of adsorption are highly cooperative and regarded as a surface critical micelle/aggregate concentration (abbreviated to sCMC), which is analogous and often close to the critical micelle concentration of the bulk solution [3]. This higher adsorption is often greater than a monolayer and as deduced from non–structural techniques analysis, it is often associated with the formation of hemimicelles at the interface [2]. However, with the help of structural techniques such as neutron reflection and null ellipsometry, the surface structures at the silica–water interface are found to be essentially closer to fragmented bilayer structures rather than hemimicelles [4–6], although atomic force microscopy (AFM) has indicated that spherical micelles and hemimicelles of cationic surfactants occur on silica and mica respectively [7, 8]. Tyrode et al. have used a full set of spectroscopic experiments to confirm the fragmented bilayer structure of cationic surfactants on silica and Speranza et al. have used x–rays to show that the fragmented bilayer is also the correct structure for a quiescent layer on mica [9, 10], when the structure has not been disturbed by a physical probe relying on force.

The adsorption of charged surfactant ions on a solid surface at low concentrations is thought to be driven by the affiliation between charged surfactant and the oppositely charged site on surface. However, with an increase of concentration,

the level of adsorption rises much higher than the known charge on the surface, and ion exchange, which indicates that ionization is reduced on the surface and the adsorption of surfactant ion–counterion pairs, all of which related to electrostatic and entropic contributions, must be involved [11]. The investigation of interfacial behaviour of anionic–nonionic surfactant mixtures at negatively charged silica substrates shows that the surfactant and surface do not need to be oppositely charged for adsorption to occur [12]. Thus, although anionic SDS does not adsorb on silica, a mixed SDS–$C_{12}E_6$ bilayer containing up to about a third of SDS will adsorb, which is driven by the hydrophobic interaction despite the apparently unfavourable electrostatics. A recent study has shown that SDS adsorbs on sapphire and forms a complete bilayer with a concentration dependence that suggests a much lower adsorption of counterions and the involvement of surface ionization during the process, because the surface charge density on sapphire in the absence of SDS is insufficient to neutralize the layer [13]. This mechanism of adsorption is associated with a sharp maximum at the CMC and may be difficult to distinguish from the type of maximum produced by impurities or mixtures [11, 14–19].

The formation of fragmented bilayer structures of ionic surfactants raises the issue of what happens to the charge distribution on a surface. Unless an ionic surfactant adsorbs with its counterion a bilayer patch may lead to reversal of the charge in the corresponding area of the surface. Tulpar and Ducker have explained the low adsorption region of charged surfactants at low concentrations in terms of an initial low ion exchangeable charge on the bare solid–aqueous surface, and a separate cooperative adsorption at high concentrations associated with mobile charges, which move to counter the large excess of charge that occurs when bilayer regions form.

This offers a mechanism for the initial strong but low adsorption of a charged surfactant on a surface carrying opposite charge, and explains the phenomenon that a surface is covered by a patchy instead of a complete bilayer. The total coverage varies with the concentration and is probably limited by the capacity of the surface to produce the necessary mobile charge. Another consequence of this mechanism is that the patches may be mobile and can lead to oppositely charged patches on the surface. Both of these features have been observed for cationic surfactants on mica surfaces [20, 21].

The application of mixed systems gives considerable flexibility for probing the effects of charge at a surface because the interaction can be used to tune the composition of the adsorbed layer, especially when the interaction between the two surfactants is strong as in the combination of ionic and zwitterionic surfactants. The interfacial behaviour of such mixtures at the air–liquid interface has been extensively studied [22–27]. Adsorption of such mixtures at the air–liquid interface and their micellization are strongly enhanced compared to the individual components and this has been quantified by means of the charge interaction by Mulqueen and Blankschtein [28]. There are several studies that show that zwitterionic surfactants show cooperative adsorption around the CMC on the negatively charged silica substrate [29–32]. Zajac et al. have found the expected weak adsorption of zwitterionic surfactants at low concentration as well as the positive enthalpy characteristic of a cooperative hydrophobic interaction at around the CMC [33]. Harwigsson et al. have described the cooperativity of the adsorption of a series of dodecyl dialkylammonium alkanecarboxylates on a single silica surface in terms of sCMC [3]. Lokar and Ducker have shown the adsorption of mixtures of cationic

dodecylpyridine chloride and dodecyl dimethylammonium propanesulfonate (DS-B) is enhanced relative to the separate components at the hydrophilic silica and mica surfaces [34].

5.2 Experimental Details

The neutron reflection measurements were made on the reflectometer INTER at the ISIS pulsed neutron source as described in Chapter 2, using the "white beam time-of-flight" method. The measurements were made using a single detector at two different grazing angles of incidence, at 0.7° and 2.3° and a neutron waveband length ranging from 1-15 Å. This gives a momentum transfer Q range of 0.03-0.5 Å^{-1}. The reflectivity measurements were made at three different sets of bulk solution composition for both anionic-zwitterionic surfactant mixture systems (mol% SDS/DSB or SDS/DB) 25/75, 50/50, 75/25, and for each combination, three different solution concentrations were measured. In all cases the isotopic combinations of d-SDS/h-DSB, h-SDS/h-DSB, d-SDS/h-DB and h-SDS/h-DB in D_2O were measured. All the neutron reflection data were fitted using the analysis package Motofit, which relies on the Abeles matrix method that provides identical results to the traditional Parratt formalism (see Chapter 2). The model curve generated is then compared to the measured reflectivity data and the fitting assessed using the least-squares method (χ^2). The fitting parameters used for each layer were the instrumental scale factor, the number of layers, the layer thickness (τ), the inter-facial roughness (δ), the scattering length density ρ of the material, and the solvent volume fraction (ϕ). Data fitting was optimized by varying the parameters within physically reasonable ranges until an adequate physical description was reached. Although any single profile may not provide a unique solution, the

use of different isotopic contrasts usually ensures that an unambiguous model of the interface is obtained.

The simplest model that is consistent with all the data in this chapter is a fragmented inter-penetrating bilayer. The main features of the model are as follows: The adsorbed layer can be described by three layers, a layer of thickness τ_1 adjacent to the solid surface containing both surfactant head-groups and associated hydration, a layer of thickness τ_2 containing hydrocarbon chains over-lapping from both sides of the bilayer, a third layer of thickness τ_3 adjacent to the aqueous solution and again containing head-groups and hydration. This structure of the bilayer contains some disorder, and an additional parameter is required to account for the inter-mixing between head-groups and hydrocarbon chains. This is described by f_c which is the fraction of alkyl chains in the head-group region. Overall, the model is then described by three thickness, τ_1, τ_2 and τ_3, the area per molecule A_a for SDS and A_z for DSB or DB, the fractional coverage, (1-f), where f is the fraction of surface covered by flattened micelle, f_c. The basic parameters such as scattering length densities, molecular volumes, and scattering lengths of the samples studied in this chapter are listed in Table (5.1)

Materials	Volume/Å^3	Length/Å	$10^4 b$/Å	$10^6 \rho$/Å
H_2O	30		-0.618	-0.56
D_2O	30		1.915	6.35
$Water_{2.07}$	30		0.621	2.07
$Water_{4.00}$	30		1.200	4.00
Si	47		0.415	2.07
SiO_2	96		1.585	3.41
-carboxybetaine	165		1.7	1.03
-sulfobetaine	260		2.1	0.81
-SO_4ONa	64		2.5	3.91
$C_{12}H_{25}$	350	16.7	-1.37	-0.39
$C_{12}D_{25}$	350	16.7	24.1	6.88
h-SDS	414		1.2	0.29
h-DB	515		0.4	0.08
d-DB	515		25.8	5.13
h-DSB	610		0.79	0.13
d-DSB	610		26.2	4.30

Table 5.1: Properties of Surfactants used in this thesis

5.3 Results and Discussion

5.3.1 Characterization of the Oxide layer

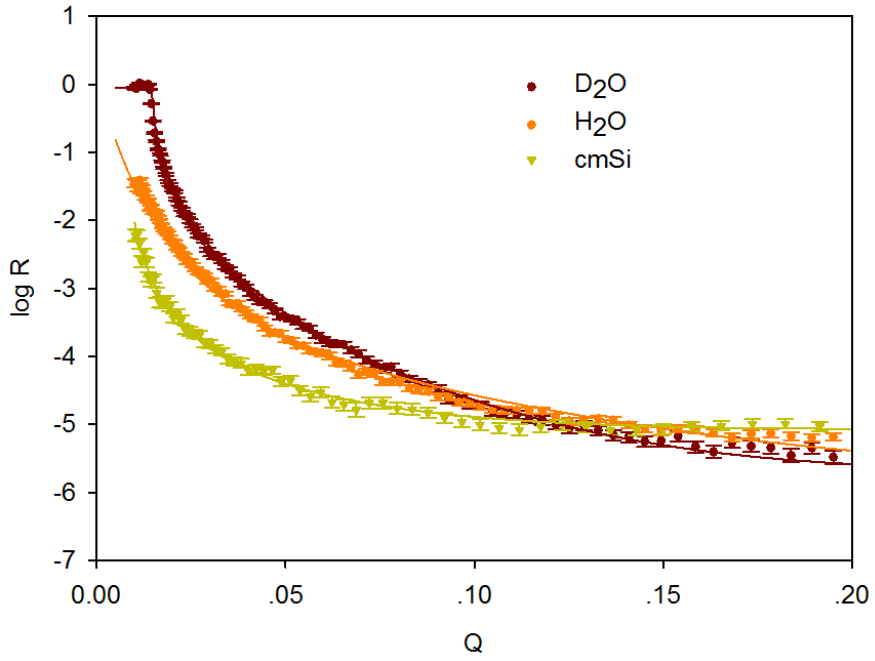


Figure 5.1: Neutron reflection at three different contrasts of the oxide layer. The continuous lines are calculated using the parameters in the text.

Before the neutron reflection measurements of surfactant mixtures at the hydrophilic solid surface, several silicon blocks with an oxide layer were characterized. Although the contribution to the reflectivity at the silicon-solution interface from the oxide layer is small because its scattering length density is not very different from that of the underlying silicon, it is essential to characterize the oxide layer as fully as possible to ensure correct fitting of the structure and composition of any subsequently adsorbed layers. Neutron reflection measurements of the silicon-liquid

interface with different water contrasts (D_2O, H_2O, and water index matched to silicon, cmSi) were made. The simultaneous fit of a single model to the three profiles gave a thickness of 17 ± 3 Å for the oxide layer, and the volume fraction of water was found to be 0.15 ± 0.05, which corresponds with the silicon blocks used in previous reports [35–38]. All these values and the small roughness between oxide and water interface indicates that the bare oxide surface is reasonably smooth.

5.3.2 Surfactant Adsorption at the Interface

Measurements of components h-DB and h-DSB at the hydrophilic silicon interface were conducted at 313K and 308K respectively in a wide range of concentrations below and above their CMCs. The temperatures were raised from room temperature in order to avoid the chance of precipitation in the mixtures because crystallization in some of the SDS/DB composition at 298K had been reported by Hines et al. These measurements give estimates of the adsorbed amount of the surfactant components at the hydrophilic solid-liquid interface. The reflectivity profiles are shown in Figure (5.2) with the best fits using the parameters given in Table (5.2), the corresponding fitting diagrams are given in Appendix B. Measurements on anionic surfactant SDS were not conducted because it is known not to adsorb at the negatively charged hydrophilic surface. Each complete set of data was fitted using a three layer model, with an analysis process similar to the method used for characterizing the underlying oxide layer.

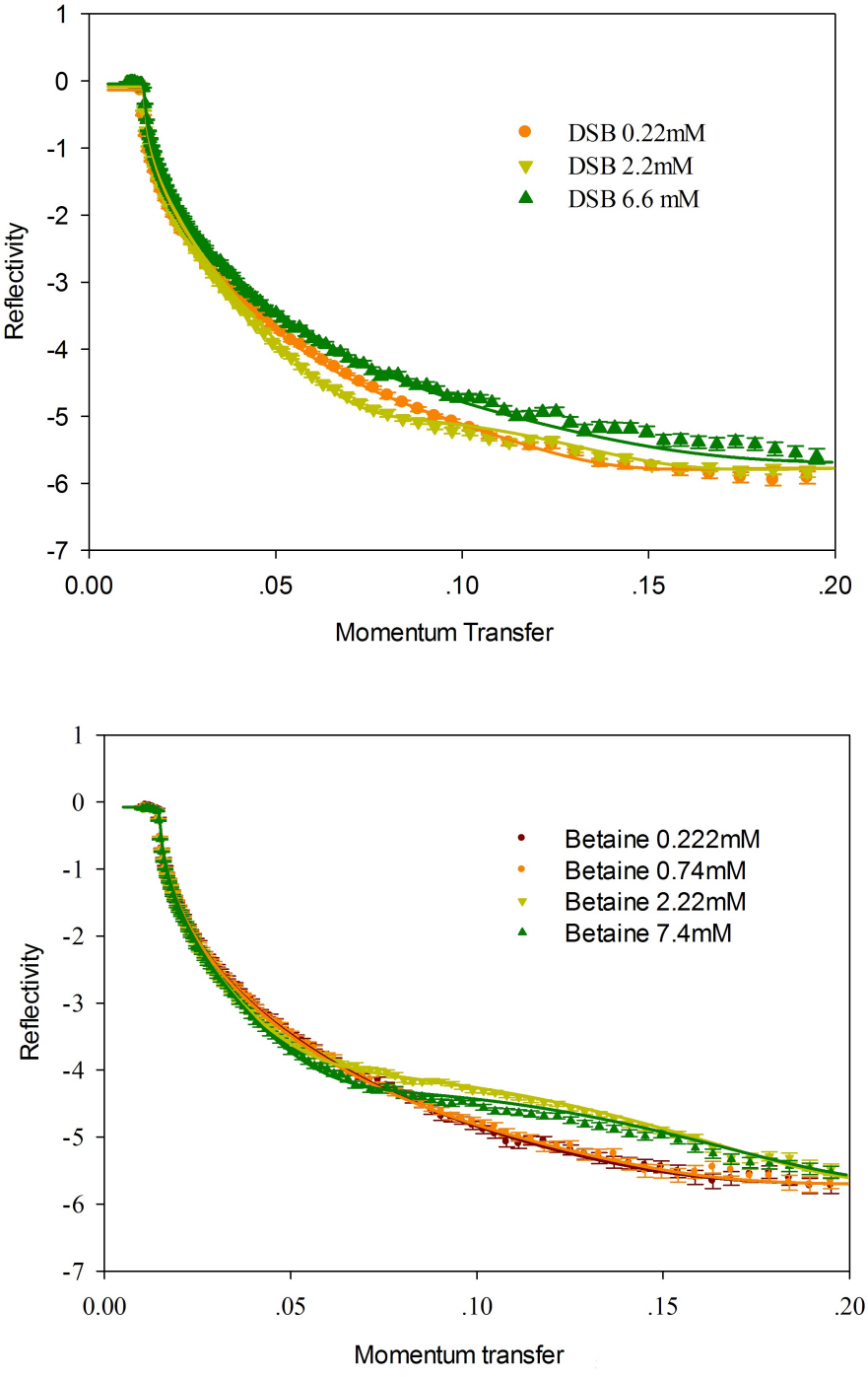


Figure 5.2: Neutron reflectivity profile measured for DSB and DB solutions at solid–liquid interface. The temperature was set at 308K and 313K for DSB and DB respectively.

Surfactant	Conc. mM	Coverage ±7%	τ_1 ±2Å	τ_2 ±2Å	τ_3 ±2Å	Surface Excess $\mu mol\ m^{-2}$
h-DB	*0.22*	0.02	7	18	5	0.2± 0.2
h-DB	*0.74*	0.03	8	18	4	0.3± 0.2
h-DB	2.2	0.86	5	18	8	7.3± 0.5
h-DB	7.4	0.81	5	18	7	6.8± 0.5
h-DSB	*0.22*	0.19	6	14	6	1.3± 0.3
h-DSB	2.2	0.33	4	19	8	3.0± 0.4
h-DSB	6.6	0.48	4	20	9	2.1± 0.4

Table 5.2: Adsorbed layer characteristics derived from neutron reflectivity data using a three layer model of DB at 313K and DSB at 308K. τ_1 and τ_3 refer to the headgroup thickness, τ_2 to the alkyl chain region and surface excess (Γ). Italics indicate that the measurement is below the CMC at 1.9 and 2.2 mM for DB and DSB respectively.

The zwitterionic DB shows very strong adsorption at two higher concentrations as can be seen from the last column in Table (5.2) and DSB only shows weak adsorption. At lower concentrations, DB also shows significant adsorption though the concentrations are well below its CMC at 1.9 mM. The surface excess then increased to around 7 μmol m^{-2} at the CMC and this level of adsorption is comparable with that for cationic surfactant, e.g. C_{16}TAB, and is close to a complete bilayer [5, 39]. Combined with the result that the thickness of the hydrocarbon region is about the fully extended length of the C_{12} chain, it is suggested that the structure is an interdigitated bilayer. These results also suggest that the quater-

nary ammonium group of the surfactant is in close contact with the surface but the molecules are still able to maintain a packing that allows a strong cooperativity of the hydrophobic interaction. The individual molecular configuration of the surfactant adjacent to the surface may be as shown for DB in Figure (5.3), in which the headgroup is bent rather than a extended conformation. This allows the quaternary ammonium group to be close to the surface and interact laterally with the carboxy groups within the immediate surface layer. The key factor is that the various contributions to the interactions within the headgroup and surface region should enable the strong hydrophobic interaction between the chains to be maximized.

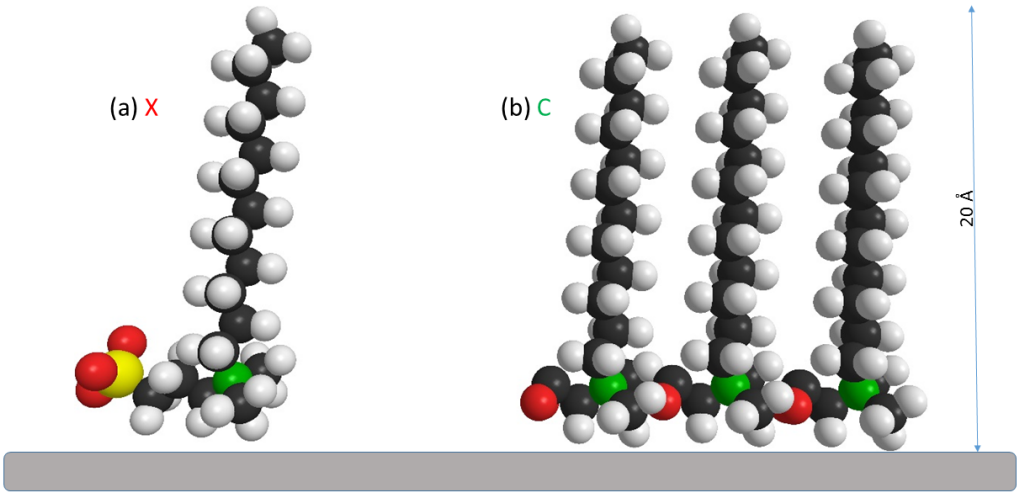


Figure 5.3: Possible configurations of the DSB and DB molecules in the layer next to the surface (inner layer) at the silica–aqueous solution interface, (a) DSB, (b) DB. Cooperative adsorption is marked with a green C and no or little adsorption with a red X. The colours are black/grey for C, red for O, green for N and yellow for S

The adsorption of DSB at low concentrations is larger than DB, indicating a stronger individual interaction between DSB and the surface, but there is little effect of cooperative hydrophobic interaction occurs when the concentration rises close to the CMC, and the adsorption at 3 times CMC is significantly lower than for DB. The stronger individual interaction is consistent with the positive part of the headgroup being attached to the surface while the negative part is held further away from the surface by the flexible three carbon spacer in a way that hinders the close approach of other molecules, as shown in Figure (5.4). The larger spacer thus blocks self–assembly of the layer. From the results of Chapter 4, these two surfactants form quite well packed monolayers at the air–liquid interface with similar limiting areas per molecule, indicating that the headgroups adopt the fully extended conformation in these circumstances. This should also be the case for the outer set of molecules in the bilayer adsorbed on the solid but the much larger spacing of the inner layer is evidently still sufficient to prevent self-assembly.

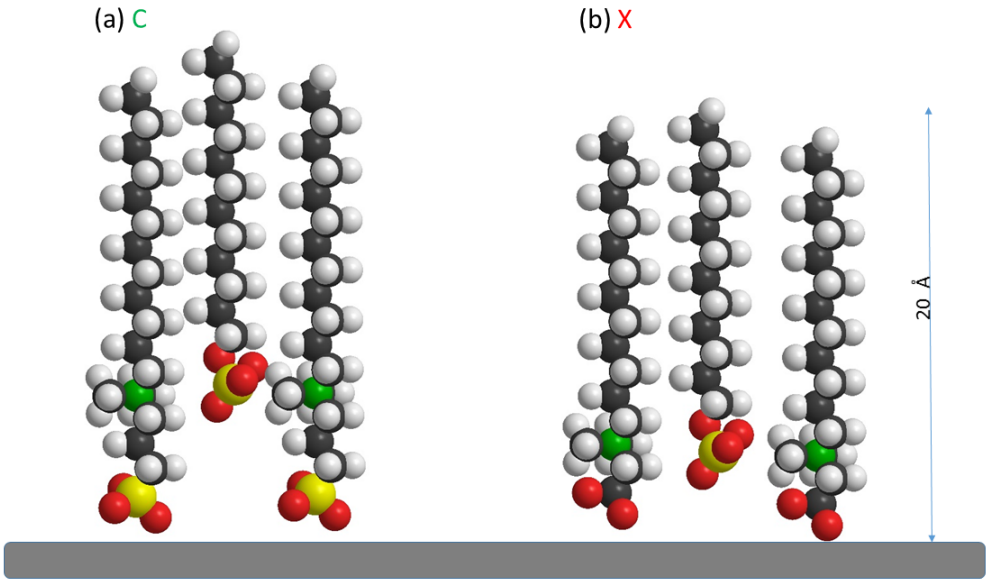


Figure 5.4: Possible configurations of mixed systems in the layer next to the surface (inner layer) at the silica–aqueous solution interface, (a) a mixture of SDS and DSB, (b) a mixture of SDS and DB. Cooperative adsorption is marked with a green C and no or little adsorption with a red X. The separation and stoichiometry in the two mixtures approximately matches those observed and the colours are black/grey for C, red for O, green for N and yellow for S

Harwigsson et al. have previously used ellipsometry to determine the level of adsorption of a set of dodecyl carboxybetaine ($C_{12}C_nB$) with varying length of carbon spacer in the betaine headgroup on silica as substrate [3]. The same sharp onset with concentration was reported for $C_{12}CB$ (DB), although their limiting surface excess was slightly less at 5 μmol m^{-2}. Lokar and Ducker have found some signs of cooperative adsorption of DSB on oxidized silicon up to a higher limiting value at 4 μmol m^{-2} by using attenuated infrared spectroscopy [34]. The limiting adsorption on silica is sensitive to factors such as roughness and is also

expected to be sensitive to differences in the underlying substrate and thickness of the oxide layer [40]. The silica (111) planes used in neutron experiments here have a thickness of about 15 Å but on the Si (100) face used for ellipsometry it is about 300 Å thick. Harwigsson et al. also showed that their pattern of adsorption was similar to those for typical nonionic surfactants where at higher concentrations the formation of structure depends on the cooperativity of the hydrophobic interaction and can be approximately regarded as a critical aggregation concentration on the surface [3].

5.3.3 Adsorption of SDS/Zwitterionic Mixtures

Mixtures containing zwitterionic surfactant have been much less studied than ionic/nonionic systems, especially at the hydrophilic interface. Just as for the adsorption of individual surfactant, the mixtures were expected to adsorb as a 'patched bilayer' at the interface. All the neutron reflectivity profiles were therefore fitted using the three–layer model discussed in the previous section.

It is instructive to discuss reflectivity data in D_2O qualitatively before more detailed data analysis is discussed. Figure(5.5) shows the reflectivity profiles of three different SDS/DSB mixtures at 0.22 mM which is below the mixed CMCs of solutions with different composition. Since the signal from the surfactant layer is identical with that of the bare oxide layer, it is clear that at this concentration, all three samples with different solution compositions show little or no adsorption at the interface.

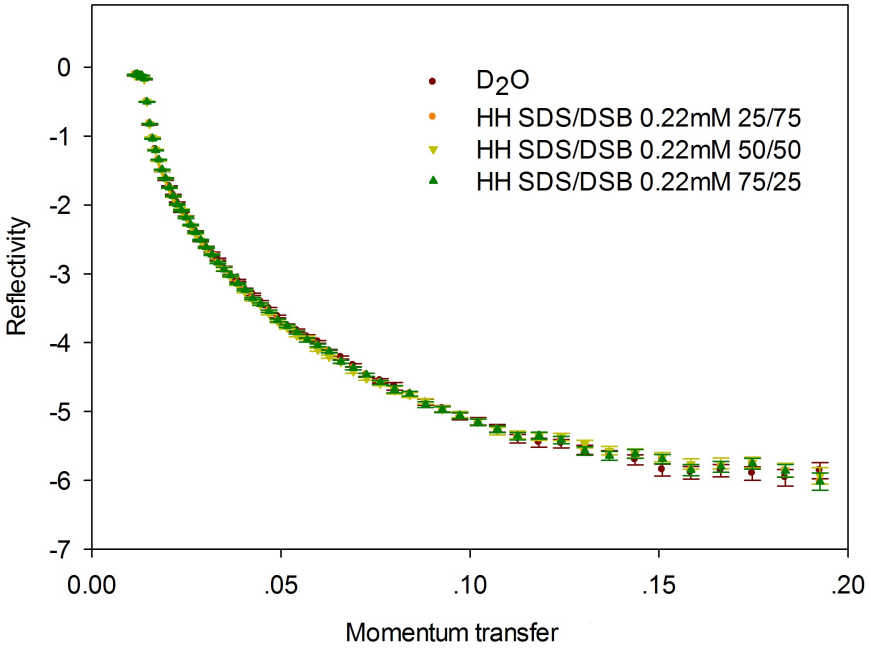


Figure 5.5: Neutron reflectivity profiles for h-SDS/h-DSB 0.22mM of different solution composition

Figure (5.6) shows the reflectivity profiles of SDS/DSB mixtures in D_2O at 0.66 mM at three different solution compositions, 25, 50 and 75 mol% SDS. Now it can be seen directly that there is a noticeable difference between the adsorbed layer and the silicon/D_2O bulk phases, and that the adsorption is greater than for DSB alone (see Figure 5.2). This indicates that, although SDS does not adsorb on the hydrophilic interface by itself, in the presence of zwitterionic surfactant DSB there is co-adsorption. Further fitting of the data shows that the total adsorption is strong at 25 and 50% SDS but weaker at 75% SDS.

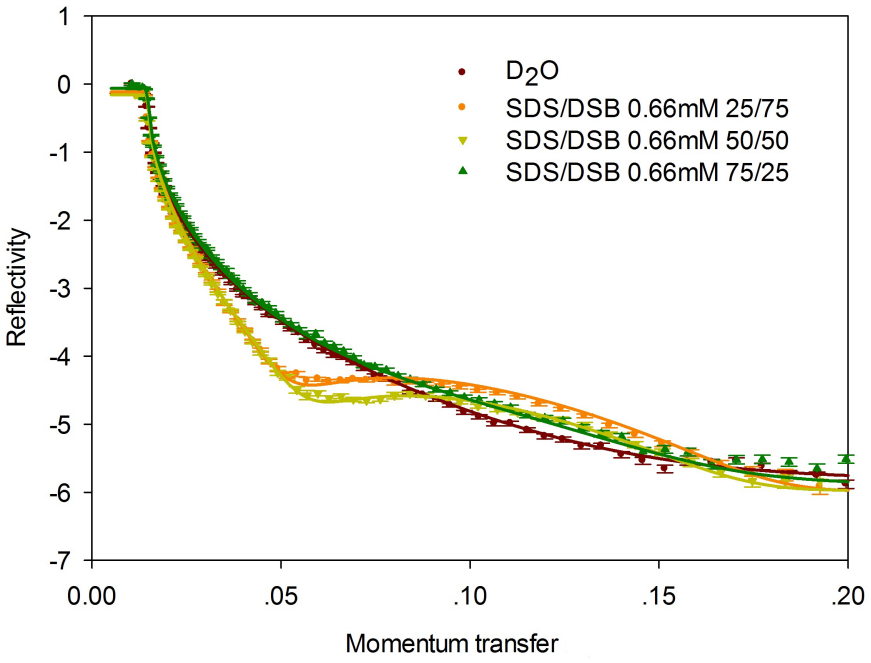


Figure 5.6: Neutron reflectivity profiles for h-SDS/h-DSB 0.66mM of different solution composition

The same fitting procedures and qualitatively analysis have been conducted on the mixture systems of SDS/DB. The complete range of different isotopically labelled combinations using the three–layer model fitting gave the results shown in Table (5.3) for SDS/DSB and Table (5.4) for SDS/DB. Also included in the Tables are the calculated mole fraction of SDS in the bulk solution and observed mole fractions of SDS adsorbed at the air–liquid interface from Chapter 4. The complete set of fitting diagrams are given in the Appendix B.

x_{SDS} bulk	Conc. mM	τ_1 ±2 Å	τ_2 ±2 Å	τ_3 ±2 Å	Γ $\mu mol\ m^{-2}$	x_{SDS} ads±0.05	x_{SDS} air±0.03	x_{SDS} soln(calc)
25	*0.22*	-	-	-	<0.1	-	0.32	0.25
25	0.66	8	19	10	7.7±0.5	0.47	0.34	0.28
25	2.2	7	17	9	5.3±0.5	0.41	0.35	0.41
25	6.6	9	17	7	2.6±0.5	0.35	0.39	0.55
50	*0.22*	-	-	-	<0.1	-	0.32	0.50
50	0.66	10	19	6	5.2±0.4	0.42	0.40	0.63
50	2.2	9	19	11	4.0±0.4	0.28	0.38	0.86
50	6.6	6	17	8	2.2±0.4	0.20	0.41	0.96
75	*0.22*	-	-	-	<0.1	-	0.39	0.75
75	*0.66*	7	21	7	1.9±0.3	0.33	0.40	0.75
75	2.2	7	15	4	0.8±0.3	0.21	0.42	0.94
75	6.6	7	14	5	0.3±0.2	0.13	0.45	0.99

Table 5.3: Mean Values of Parameters from model fits from SDS/DSB Mixtures together with the calculated mole fraction of SDS in the bulk solution, based on data given in Chapter 4, and the observed mole fractions of SDS adsorbed at the air–liquid interface, also from Chapter 4. The concentrations in italic are below the mixed CMC of the systems

x_{SDS} bulk	Conc. mM	τ_1 ±2 Å	τ_2 ±2 Å	τ_3 ±2 Å	Γ $\mu mol\ m^{-2}$	x_{SDS} ads±0.05	x_{SDS} air±0.03	x_{SDS} soln(calc)
25	*0.074*	-	-	-	<0.1	-	-	0.25
25	0.22	6	22	8	0.2±0.2	0.13	0.26[a]	0.25
25	0.74	5	21	5	0.3±0.2	0.19	-	0.24
25	2.22	7	19	7	0.8±0.3	0.24	-	0.21
50	*0.074*	-	-	-	<0.1	-	-	0.50
50	*0.22*	5	20	7	0.2±0.2	0.17	0.32	0.50
50	0.74	9	19	7	0.5±0.2	0.24	-	0.69
50	2.22	8	20	9	0.9±0.3	0.33	-	0.93
75	*0.074*	-	-	-	<0.1	-	-	0.75
75	*0.22*	4	15	4	0.1±0.1	0.27	0.39[a]	0.75
75	0.74	5	17	8	0.6±0.2	0.39	-	0.75
75	2.22	4	17	4	2.9±0.4	0.40	-	0.96

Table 5.4: Mean Values of Parameters from model fitting from SDS/DB mixtures together with the observed fractions of SDS adsorbed at the air–liquid interface from Chapter 4 and Hines et al [25]. [a] are values for 20:80 and 80:20 rather than 25:75 and 75:25

There are three interesting features of the adsorption pattern in the results. Firstly, the presence of anionic surfactant SDS enhance the total adsorption of DSB but suppress the total adsorption of DB. Secondly, for the mixture of SDS/DSB. A sharp maximum in the total adsorbed amount occurs around a concentration region of 1–3 times mixed CMC in all compositions studied, as shown in Figure (5.7). Thus, the DB on its own shows strong cooperative adsorption and reaches

nearly a complete bilayer structure on the surface, whereas DSB on its own shows no sign of cooperativity and does not even attain the equivalent of a complete monolayer. The arrangement of the headgroups close to the surface is invoked to explain these changes of interfacial behaviour for the mixed systems. The third is that in the SDS/DSB systems, the total adsorbed amount increases with the fraction of adsorbed SDS, as shown in Figure (5.8), even though SDS on its own does not adsorb. The similar behaviour was also observed for mixtures of SDS and the nonionic $C_{12}E_6$ and these results are included in Figures (5.8) and (5.9) for comparison [12].

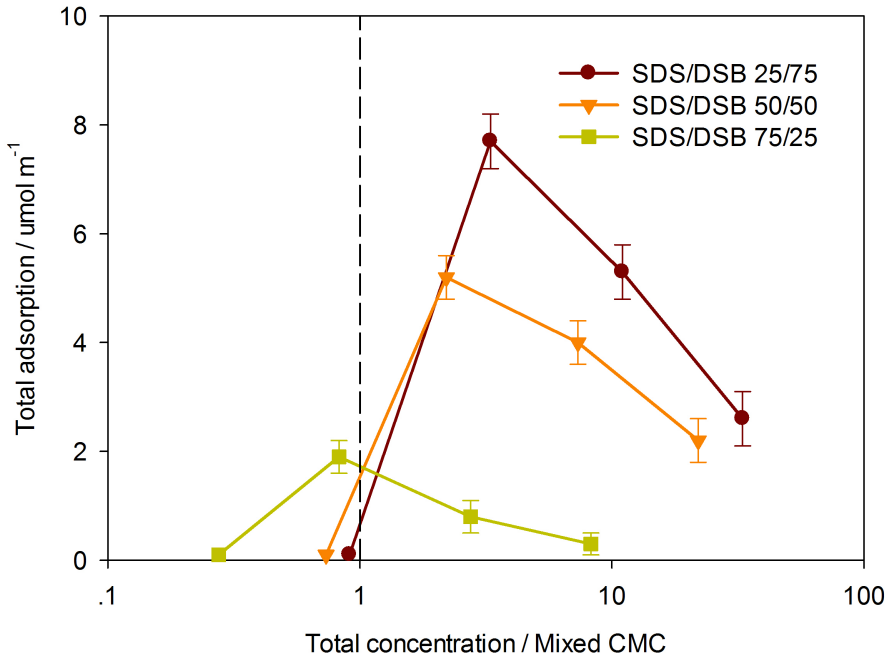


Figure 5.7: Total adsorbed amount at the silica–aqueous interface as a function of concentration relative to the mixed CMC for three compositions of SDS/DSB. A vertical line is drawn for guidance at C/CMC=1

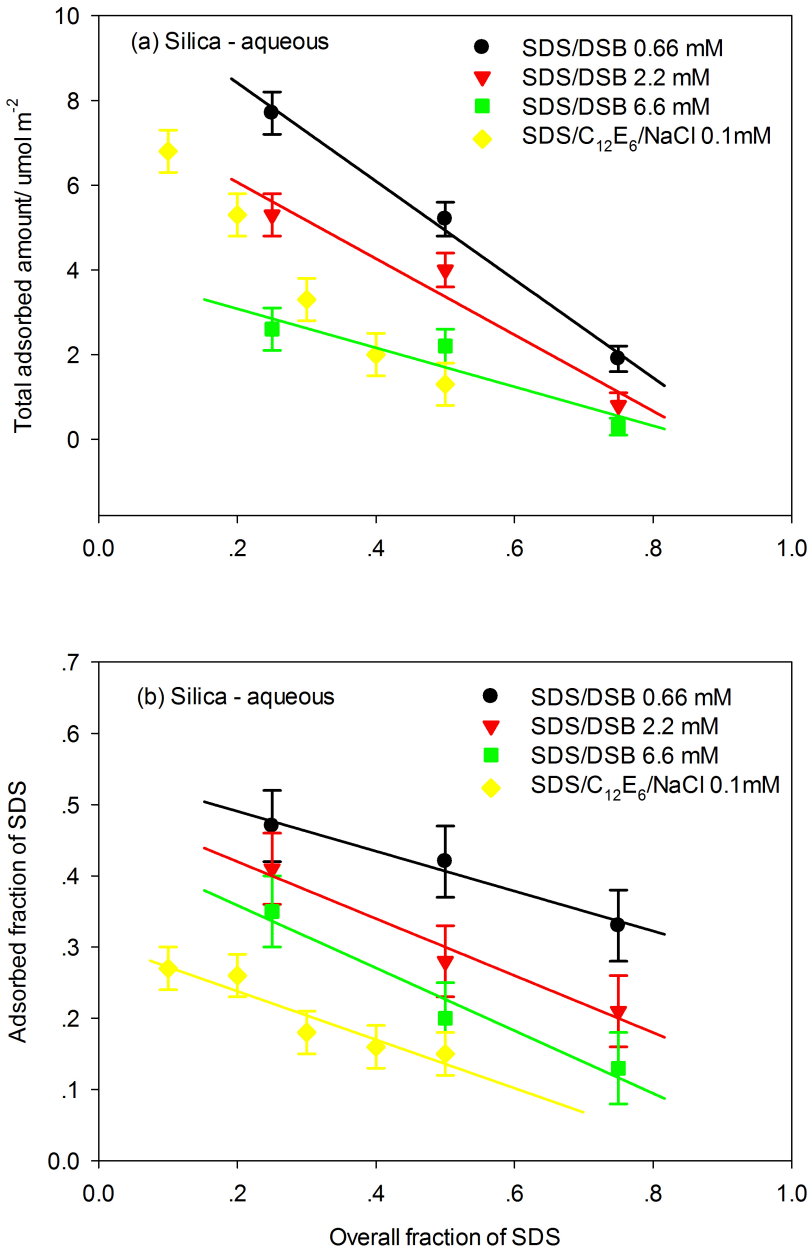


Figure 5.8: (a) Total amount adsorbed at the silica–aqueous interface and (b) adsorbed fraction of SDS plotted against the overall fraction of SDS in the system for three overall concentrations of SDS/DSB, all above the mixed CMC, and for some concentration for SDS/$C_{12}E_6$/NaCl, also well above the CMC [12, 41].

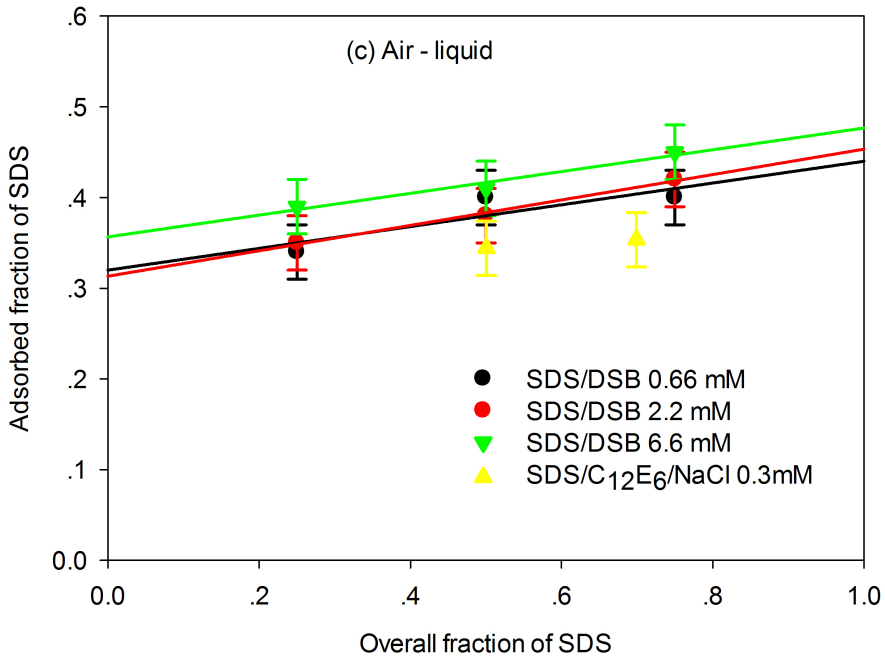


Figure 5.9: Plots of the adsorbed fraction of SDS against the overall fraction of SDS for the air–aqueous interface [12].

As shown in Figures (5.3) and (5.4), it is more difficult for the neighbouring DSB molecules to pack together than for DB due to the configuration of the individual DSB molecule. However, with the presence of anionic SDS, whose headgroup is able to interact preferentially with the quaternary ammonium on the zwitterionic, the spacer may be forced to be more fully extended as in Figure (5.4). The configuration of the SDS/DSB mixture could significantly improve the packing of the alkyl chains and therefore promote cooperativity and self–assembly, but the layer would be presenting a negative charge to the surface. Although the cooperativity is improved, the layer with the structure shown in Figure (5.4) may not show adsorption on the surface as SDS on its own does not adsorb. However, it is known

that the mixed layer of SDS and the nonionic surfactant $C_{12}E_6$ shows strong adsorption up to a nominal negative charge of about one third of a monolayer [12]. This structure of the mixture reduces the interaction of the sulfate group with the surface and, given the weaker activity of SO_3 compared with SO_4, this may be sufficient to sustain the 2/3rd coverage of charge implied by Figure (5.4). The spacer in the headgroup of DB is shorter than that of DSB, therefore the alkyl chains of neighbouring are expected to pack well, as indicated in Figure (5.3), and the interaction between SDS and the cationic part is of similar strength for the sulfo– and carboxybetaine. As the sulfate group of SDS is much closer to the surface than for the sulfobetaine mixture as shown in Figure (5.4), this configuration reduces the effect of the attachment to the surface and causes desorption.

Maxima in adsorption shown in Figure (5.7) are usually treated with suspicion because they are often associated with impurities, whether these are ones that could be regarded as insoluble or whether they are soluble, e.g. other surfactants. The classic impurity is dodecanol in SDS and, depending on its concentration, this produces a strong adsorption maximum below the CMC of SDS at the air–liquid interface [42]. Trogus et al., and Paria and Khilar have suggested that adsorption maxima can also occur in surfactant mixtures and these have a different origin from those of insoluble impurities such as dodecanol [11, 19]. Another explanation of maxima at the solid–aqueous interface is that in the adsorption of ionic surfactant the two ion activities are different because of preferential segregation of the surfactant ion into micelles [15, 16]. If the adsorbed layer on a solid surface contains more surfactant ion than counterion, the adsorption will then decrease with increasing total concentration above the CMC. A recent study has explained

the maxima occurs in three MDS and sodium decylsulfonate on a sapphire surface with this mechanism [13]. Close examination of the present data suggest that the maxima in the SDS/DSB system may result in part from the mixture and in part from ion segregation in the micelles.

The zwitterionic DSB is considered to be the major component in the micelles due to its lower CMC but the strong interaction between SDS and DSB limits the extent of preferential incorporation of DSB into the micelles. When the SDS fraction is 0.25 the composition of monomers and micelles stays in a narrow range from the CMC to 10 times CMC, i.e. over this concentration range there is little change of the fractionation. This is also confirmed by the fact that the total adsorption at the air–liquid interface only increases slightly from 4.8 to 5.3 μmol m^{-2}. However, in the exactly same concentration range, the adsorbed amount at the silica–aqueous interface drops drastically from 7.7 to 2.6 μmol m^{-2}. Thus the possibility of preferential solubilization of DSB can be eliminated.

The characteristic feature of dodecanol as a surfactant impurity is that the solubility of the dodecanol is so low that, even when present at a low fraction in the surfactant, it reaches its solubility limit at or below the CMC of the surfactant. At the solubility limit its activity is 1, much higher than that of the surfactant, and if it is surface active it will form a saturated monolayer and/or precipitate. The effect of the impurity dodecanol on adsorption at the air–liquid interface is reasonably well understood [42–44]. The solubility limit of a dodecanol solution of concentration greater than 0.15 wt% is reached below the CMC of SDS. At this stage its activity approaches unity and a complete monolayer is formed except

that SDS also competes for the surface. Above the CMC, dodecanol is solublized into SDS micelles and SDS increasingly takes up the dominance of the surface. At concentrations below 0.15 wt% the solubility limit of dodecanol is not reached until the SDS has micellized and it will be largely removed by solubilization into the micelles. Therefore the adsorption maxima of SDS–dodecanol mixtures often occurs at or below the CMC [42], which is different from the phenomenon in Figure (5.7). The effect of dodecanol on the surface tension becomes negligible at about 0.01 wt % [44]. Although there is no experimental investigation on the effect of dodecanol on the interfacial behaviour of mixture systems, it must have a much lower effect because the wt % of the dodecanol impurity is reduced by mixing with DSB and the CMC of a synergistic mixture is much lower than for SDS. Hence the solubility limit of the dodecanol is reached at a higher concentration under these conditions than in SDS alone. In the case of 0.015 wt % dodecanol in SDS, where there is negligible effect on the surface tension of just SDS, in order to achieve the equivalent effect in an SDS/DSB mixture the wt % is required to be about 0.9 wt % for 50/50 SDS/DSB mixture. Such a high concentration would make the surface tension curve almost unrecognizable but will be negligible in the mixed system. This makes the effect of dodecanol easy to eliminate in a synergistic mixture. Also, the direction of the effect on changing from 0.75 to 0.25 SDS would be in the opposite direction to the size of the maximum in Figure (5.7).

Based on the discussion above, the origin of the maximum then must lie in some pattern of behaviour of either the cooperativity of the two components and/or their activities. For an independent component in any phase, the form of its chemical potential consists of a fixed term, μ^* and a concentration dependent term

$RT \ln a$, where a is the activity. For the independent components of such a phase the Gibbs–Margules equation gives [45]

$$x_1 \frac{d \ln a_1}{dx_1} = -x_2 \frac{d \ln a_2}{dx_2} \tag{5.1}$$

Since $dx_1 = -dx_2$ this means that as x_1 increases the changes in $\ln a_1$ and $\ln a_2$ must be opposite in sign. In the case of SDS/DSB system, the SDS mole fraction is denoted by using x_1, if $\ln a_1$ is increasing with SDS concentration then $\ln a_2$ must be decreasing and this may be what is happening to the monomers in the bulk solution. If one of the components is an electrolyte its x and a are replaced by the equivalent mean values $x\pm$ and $a\pm$. Therefore although pseudophase approximation is assumed only to apply to nonionic species, the two component equation (5.1) also applies when the mean activity can be used for the ionic surfactant. Some information can be obtained by analysing the surface adsorption of SDS at the air–liquid and solid–aqueous interfaces. In the case of air–liquid interface, the neutral SDS ion pair is adsorbed at the surface and therefore the adsorption is determined by $a\pm$. As shown in Chapter 4 the fraction of adsorbed SDS increases with total concentration above the CMC, i.e. its mean activity must also increase with bulk solution concentration. Since the measurements on solid–aqueous interface are conducted using identical solutions, the increase of $a\pm$ must also be true in this circumstance. However, this is not observed in the experiments. The only possible conclusion is that it is not the SDS ion pair that is adsorbed.

The thermodynamic discrepancy can be explained by the incorrectness of the assumption that SDS is adsorbed in the same form at both air–liquid and silica–aqueous interfaces, i.e. the Na^+DS^- ion pair, which is the cause of the requirement that the direction of change in activity of SDS must be the same at the two

different interfaces. Pethica et al. argued that the ionization of water means that one can never be sure that the counterion of anionic surfactant that adsorbs at the air–liquid interface is the original counterion rather than H^+ or OH^- [46]. It is generally easy to establish this occurs at the air–liquid interface but there seem to have been no attempts to determine if this is the case at solid–aqueous interface [47]. For SDS at the silica–aqueous interface, the activity controlling the adsorption is effectively only that of the DS^- if either the coadsorbed counterion is H^+ or sufficient H^+ counterions are generated by the surface that no Na^+ ions are adsorbed. It is known that micelles of ionic surfactants are dissociated above the CMC, which leads to a preferential fractionation of counterions in the bulk solution with an increase of overall concentration. When this happens and the adsorbed species is DS^- or DS^-H^+ the activity that controls adsorption decreases strongly with increasing overall concentration. At the air–liquid interface this is not the case as the adsorbing ion pair is usually DS^-Na^+. This effect has recently been identified for MDS species and sodium decylsulfonate adsorbed on sapphire [13]. Although sapphire is positively charged the adsorption of DS^- is much larger than the resident positive charge on the surface and therefore requires ionization at the surface or coadsorption of H^+. Unfortunately, there are no models in the literature for treating this effect quantitatively. Although the pseudophase approximation can be used in combine with an asymmetric excess free energy of mixing to analyse the mixing of SDS and DTAB with zwitterionics (see Chapter 4), the model does not include dissociation behaviour of ionic compounds and the mass action model applied in reference [13] cannot handle the relatively complicated situation here.

5.4 Conclusion

The interfacial behaviour of both the zwitterionic components, DSB and DB, and their mixture with anionic SDS have been examined respectively using neutron reflection experiments. Although the two zwitterionics are similar in molecular structure, the adsorption of each shows a different pattern through the concentrations studied. The structural features of the individual molecules in the inner layer are invoked to explain the large variation in adsorbed amount above the CMC. In the presence of anionic SDS, the adsorption patterns are completely different and are also associated with the interaction between SDS and neighbouring zwitterionic molecules. For the mixture of SDS/DSB, strong adsorption is observed for all three compositions studied just above each mixed CMC, which may be a combination of structural effects of the mixture and an ion segregation effect.

Bibliography

[1] M. R. Bohmer and L. K. Koopal. Adsorption of ionic surfactants on variable-charge surfaces. 1. charge effects and structure of the adsorbed layer. *Langmuir*, 8(11):2649–2659, 1992.

[2] P. Somasundaran and D. W. Fuerstenau. Mechanisms of alkyl sulfonate adsorption at the alumina-water interface1. *The Journal of Physical Chemistry*, 70(1):90–96, 1966.

[3] I. Harwigsson, F. Tiberg, and Y. Chevalier. Nature of the adsorption of zwitterionic surfactants at hydrophilic surfaces. *Journal of colloid and interface science*, 183(2):380–387, 1996.

[4] E. M. Lee, R. K. Thomas, P. G. Cummins, E. J. Staples, J. Penfold, and A. R. Rennie. Determination of the structure of a surfactant layer adsorbed at the silica/water interface by neutron reflection. *Chemical Physics Letters*, 162(3):196–202, 1989.

[5] A. R. Rennie, E. M. Lee, E. A. Simister, and R. K. Thomas. Structure of a cationic surfactant layer at the silica-water interface. *Langmuir*, 6(5):1031–1034, 1990.

[6] F. Tiberg, J. Brinck, and L. Grant. Adsorption and surface-induced self-assembly of surfactants at the solid–aqueous interface. *Current opinion in colloid & interface science*, 4(6):411–419, 1999.

[7] S. Manne and H. E. Gaub. Molecular organization of surfactants at solid-liquid interfaces. *Science*, 270(5241):1480, 1995.

[8] J. Liu and W. A. Ducker. Surface-induced phase behavior of alkyltrimethylammonium bromide surfactants adsorbed to mica, silica, and graphite. *The Journal of Physical Chemistry B*, 103(40):8558–8567, 1999.

[9] E. Tyrode, M. W. Rutland, and C. D. Bain. Adsorption of ctab on hydrophilic silica studied by linear and nonlinear optical spectroscopy. *Journal of the American Chemical Society*, 130(51):17434–17445, 2008.

[10] F. Speranza, G. A. Pilkington, T. G. Dane, P. T. Cresswell, P. X. Li, R. M. J. Jacobs, T. Arnold, L. Bouchenoire, R. K. Thomas, and W. H. Briscoe. Quiescent bilayers at the mica–water interface. *Soft Matter*, 9(29):7028–7041, 2013.

[11] S. Paria and K. C. Khilar. A review on experimental studies of surfactant adsorption at the hydrophilic solid–water interface. *Advances in Colloid and Interface Science*, 110(3):75–95, 2004.

[12] J. Penfold, E. Staples, I. Tucker, and R. K. Thomas. Adsorption of mixed anionic and nonionic surfactants at the hydrophilic silicon surface. *Langmuir*, 18(15):5755–5760, 2002.

[13] N. N. Li, R. K. Thomas, and A. R. Rennie. Neutron reflectometry of anionic surfactants on sapphire: A strong maximum in the adsorption near

the critical micelle concentration. *Journal of Colloid and Interface Science*, 471:81–88, 2016.

[14] R. C. Murray and G. S. Hartley. Equilibrium between micelles and simple ions, with particular reference to the solubility of long-chain salts. *Transactions of the Faraday Society*, 31:183–189, 1935.

[15] M. L. Corrin, E. L. Lind, A. Roginsky, and W. D. Harkins. Adsorption of long-chain electrolytes from aqueous solution on graphite of known area and on polystyrene. *Journal of Colloid Science*, 4(5):485–495, 1949.

[16] F. H. Sexsmith and H. J. White. The absorption of cationic surfactants by cellulosic materials: Iii. a theoretical model for the absorption process and a discussion of maxima in absorption isotherms for surfactants. *Journal of Colloid Science*, 14(6):630–639, 1959.

[17] D. F. Evans and H. Wennerstrom. *Colloidal domain*. Wiley-Vch, 1999.

[18] R. D. Vold and N. H. Sivaramakrishnan. The origin of the maximum in the adsorption isotherms of association colloids. *The Journal of Physical Chemistry*, 62(8):984–989, 1958.

[19] F. J. Trogus, R. S. Schechter, and W. H. Wade. A new interpretation of adsorption maxima and minima. *Journal of Colloid and Interface Science*, 70(2):293–305, 1979.

[20] S. Perkin, N. Kampf, and J. Klein. Stability of self-assembled hydrophobic surfactant layers in water. *The Journal of Physical Chemistry B*, 109(9):3832–3837, 2005.

[21] S. Perkin, N. Kampf, and J. Klein. Long-range attraction between charge-mosaic surfaces across water. *Physical review letters*, 96(3):038301, 2006.

[22] K. Tajima, A. Nakamura, and T. Tsutsui. Surface activity of complex in mixed surfactant solution. *Bulletin of the Chemical Society of Japan*, 52(7):2060–2063, 1979.

[23] M. J. Rosen. Synergism in mixtures containing zwitterionic surfactants. *Langmuir*, 1991.

[24] J. D. Hines, R. K. Thomas, P. R. Garrett, G. K. Rennie, and J. Penfold. Investigation of mixing in binary surfactant solutions by surface tension and neutron reflection: Anionic/Nonionic and Zwitterionic/Nonionic mixtures. *The Journal of Physical Chemistry B*, 1997.

[25] J. D. Hines, R. K. Thomas, P. R. Garrett, G. K. Rennie, and J. Penfold. Investigation of mixing in binary surfactant solutions by surface tension and neutron reflection: strongly interacting Anionic/Zwitterionic mixtures. *The Journal of Physical Chemistry B*, 1998.

[26] P. Wydro and M. Paluch. A study of the interaction of dodecyl sulfobetaine with cationic and anionic surfactant in mixed micelles and monolayers at the air/water interface. *Journal of colloid and interface science*, 286(1):387–391, 2005.

[27] D. Lopez-Diaz, I. Garcia-Mateos, and M. M. Velázquez. Synergism in mixtures of zwitterionic and ionic surfactants. *Colloids and Surfaces A: Physicochemical and Engineering Aspects*, 270:153–162, 2005.

[28] M. Mulqueen and D. Blankschtein. Prediction of equilibrium surface tension and surface adsorption of aqueous surfactant mixtures containing zwitterionic surfactants. *Langmuir*, 16(20):7640–7654, 2000.

[29] A. Amin-Alami, N. Kamenka, and S. Partyuka. Interfacial properties of zwitterionic surfactants: N-dodecylbetaine. *Thermochimica Acta*, 122(1):171–179, 1987.

[30] P. F. Brode III. Adsorption of ultra-long-chain zwitterionic surfactants on a polar solid. *Langmuir*, 4(1):176–180, 1988.

[31] S Partyka, M Lindheimer, and B Faucompre. Aggregate formation at the solidliquid interface: The calorimetric evidence. *Colloids and Surfaces A: Physicochemical and Engineering Aspects*, 76:267–281, 1993.

[32] M. Chorro, N. Kamenka, B. Faucompre, S. Partyka, M. Lindheimer, and R. Zana. Micellization and adsorption of a zwitterionic surfactant:n-dodecyl betaineeffect of salt. *Colloids and Surfaces A: Physicochemical and Engineering Aspects*, 110(3):249–261, 1996.

[33] J. Zajac, C. Chorro, M. Lindheimer, and S. Partyka. Thermodynamics of micellization and adsorption of zwitterionic surfactants in aqueous media. *Langmuir*, 13(6):1486–1495, 1997.

[34] W. J. Lokar and W. A. Ducker. Forces between glass surfaces in mixed cationic-zwitterionic surfactant systems. *Langmuir*, 20(11):4553–4558, 2004.

[35] J. R. Lu, T. J. Su, P. N. Thirtle, R. K. Thomas, A. R. Rennie, and R. Cubitt. The denaturation of lysozyme layers adsorbed at the hydrophobic sol-

id/liquid surface studied by neutron reflection. *Journal of colloid and interface science*, 206(1):212–223, 1998.

[36] G. Fragneto, J. R. Lu, D. C. McDermott, R. K. Thomas, A. R. Rennie, P. D. Gallagher, and S. K. Satija. Structure of monolayers of tetraethylene glycol monododecyl ether adsorbed on self-assembled monolayers on silicon: a neutron reflectivity study. *Langmuir*, 12(2):477–486, 1996.

[37] J. Penfold, E. J. Staples, I. Tucker, and L. J. Thompson. Adsorption of mixed cationic and nonionic surfactants at the hydrophilic silicon surface from aqueous solution: Studied by specular neutron reflection. *Langmuir*, 13(25):6638–6643, 1997.

[38] J. Penfold, E.J. Staples, I. Tucker, and R. K. Thomas. Adsorption of mixed cationic and nonionic surfactants at the hydrophilic silicon surface from aqueous solution: The effect of solution composition and concentration. *Langmuir*, 16(23):8879–8883, 2000.

[39] D. C. McDermott, J. McCarney, R. K. Thomas, and A. R. Rennie. Study of an adsorbed layer of hexadecyltrimethylammonium bromide using the technique of neutron reflection. *Journal of colloid and interface science*, 162(2):304–310, 1994.

[40] G. Fragneto, R. K. Thomas, A. R. Rennie, and J. Penfold. Neutron reflection from hexadecyltrimethylammonium bromide adsorbed on smooth and rough silicon surfaces. *Langmuir*, 12(25):6036–6043, 1996.

[41] J. Penfold, E. Staples, L. Thompson, I. Tucker, J. D. Hines, R. K. Thomas, and J. R. Lu. Solution and adsorption behavior of the mixed surfactant

system sodium dodecyl sulfate/n-hexaethylene glycol monododecyl ether. *Langmuir*, 11(7):2496–2503, 1995.

[42] J. R. Lu, I. P. Purcell, E. M. Lee, E. A. Simister, R. K. Thomas, A. R. Rennie, and J. Penfold. The composition and structure of sodium dodecyl sulfate-dodecanol mixtures adsorbed at the air-water interface: a neutron reflection study. *Journal of Colloid and Interface science*, 174(2):441–455, 1995.

[43] G. D. Miles and L. Shedlovsky. Minima in surface tension–concentration curves of solutions of sodium alcohol sulfates. *The journal of physical chemistry*, 48(1):57–62, 1944.

[44] P. X. Li, R. K. Thomas, and J. Penfold. Limitations in the use of surface tension and the gibbs equation to determine surface excesses of cationic surfactants. *Langmuir*, 30(23):6739–6747, 2014.

[45] P. Rysselberghe. Activity coefficients in mixed solutions and the gibbs-duhem and duhem margules formulas. *The Journal of Physical Chemistry*, 38(9):1161–1168, 1934.

[46] B. A. Pethica. The adsorption of surface active electrolytes at the air/water interface. *Transactions of the Faraday Society*, 50:413–421, 1954.

[47] H. Xu, P. X. Li, K. Ma, R. K. Thomas, J. Penfold, and J. R. Lu. Limitations in the application of the gibbs equation to anionic surfactants at the air/water surface: sodium dodecylsulfate and sodium dodecylmonooxyethylenesulfate above and below the cmc. *Langmuir*, 29(30):9335–9351, 2013.

Chapter 6

Mixtures of Cationic/Zwitterionic Surfactants at the Solid-liquid Interface

6.1 Introduction

The adsorption of cationic surfactant at hydrophilic and hydrophobic solid-liquid interfaces has been extensively studied. It is generally known that the cationic surfactant interacts with the hydrophilic silica interface strongly by itself due to the electrostatic interaction between the positively charged headgroup and the negatively charged sites on the surface. The adsorbed layers are known to form a patchy bilayer structure [1–3]. The conclusion is based not only on the amount adsorbed and the force distance curves in force balance measurements [4–6], but also more recent results from FTIR, NMR and neutron reflection [2, 7, 8].

6.2 Experimental Details

The neutron reflection measurements were made on the reflectometer INTER at the ISIS pulsed neutron source [9], using the "white beam time-of-flight" method as described in chapter 5. The reflectivity measurements were made at three sets of bulk solution composition for both surfactant mixture systems (mol% DTAB/DSB or DTAB/DB) 25/75, 50/50, 75/25, and for each combination, four different concentrations were measured. In all cases the isotopic combinations of d-DTAB/h-DSB, h-DTAB/h-DSB, d-DTAB/h-DB and h-DTAB/h-DB in D_2O were measured. By deuterating the hydrocarbon chain of one surfactant, the reflection signal of the other one is highlighted in D_2O. All the neutron reflection data were fitted using the analysis package Motofit, which relies on the Abeles matrix method that provides identical results to the traditional Parratt formalism (see Chapter 2). The fitting parameters used for each layer were the instrumental scale factor, the number of layers, the layer thickness (τ), the inter-facial roughness (δ), the scattering length density ρ of the material, and the solvent volume fraction (ϕ). The model used here is the same one described in chapter 5 and the parameters are listed in Table(5.1)

6.3 Adsorption of DTAB/Zwitterionic Mixtures

Figure (6.1) shows the reflectivity profiles of h–DTAB/h–DSB mixture in D_2O at 0.66mM for three different solution compositions, 25, 50 and 75 mol% DTAB. The neutron reflection profile of pure D_2O is also included for comparison. The neutron reflection profiles of the three mixtures show deviations from the D_2O profile, indicating that there are significant total adsorption at the interface.

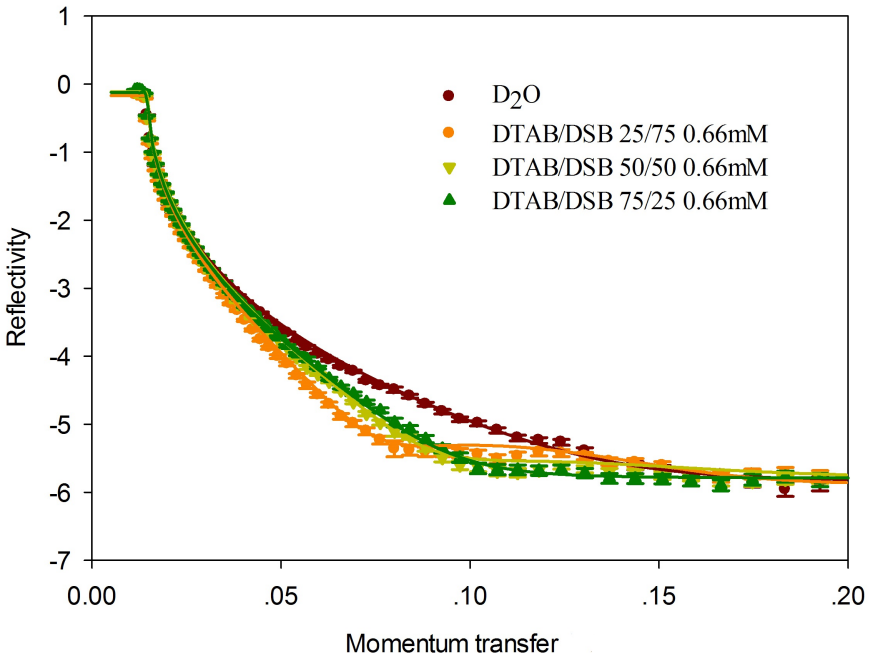


Figure 6.1: Neutron reflectivity profiles for h-DTAB/h-DSB 0.66mM of different solution composition

Figure (6.2) shows the reflectivity profiles of h–DTAB/h–DB mixtures in D_2O at 0.74 mM for three different solution compositions, 25, 50 and 75 mol% DTAB. The adsorption pattern of this system is very different from the profiles for the DTAB/DSB mixture. Thus although DB and DSB are very similar in their molecular structure, the mixture system of DTAB/DB shows little or no adsorption at the lower concentration, whereas DTAB/DSB shows a significant amount of adsorption.

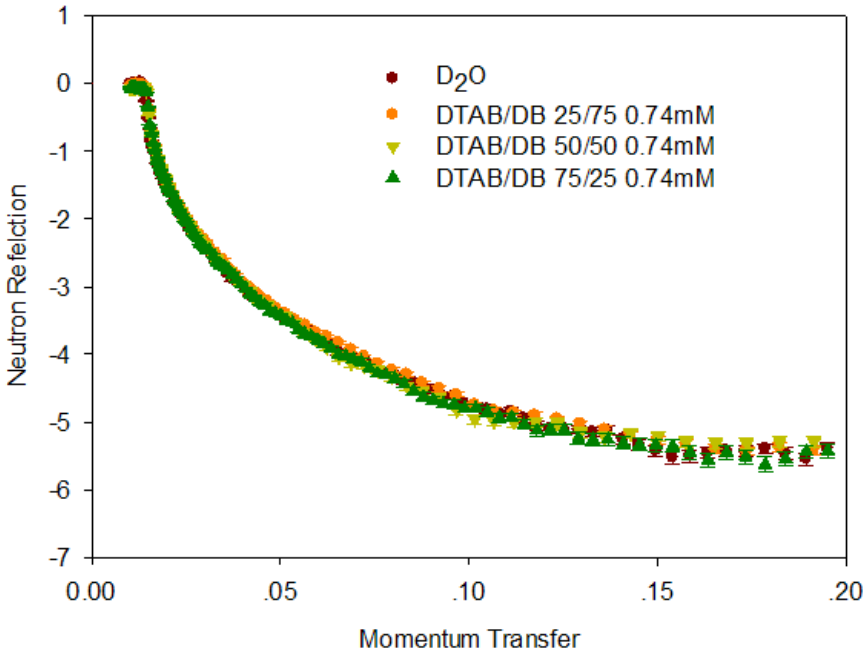


Figure 6.2: Neutron reflectivity profiles for h-DTAB/h-DB 0.74mM of different solution composition

The individual results from fitting the data are given in the Appendix and combined results are given in Tables (6.1) and (6.1) for DTAB/DSB and DTAB/DB, where concentrations below or at about the mixed CMC are given in italics. The Tables also include experimental measurements of the adsorbed fraction of cationic surfactant and the calculated mole fraction of monomer DTAB in solution at the air–liquid interface from Chapter 4. The complete set of fitted diagrams are given in Appendix B. The thickness of the hydrocarbon region is found to be about the length a of a single approximately normally oriented chain which suggests that it is an interdigitated layer.

x_{DTAB} bulk	Conc. mM	τ_1 ± 2 Å	τ_2 ± 2 Å	τ_3 ± 2 Å	Γ $\mu mol\ m^{-2}$	x_{DTAB} ads± 0.1	x_{DTAB} air± 0.03[a]
25	*0.22*	7	14	6	3.13	0.69 (0.58)	0.27
25	0.66	6	16	7	4.47	0.81 (0.56)	0.23
25	2.2	5	14	5	4.95	0.86 (0.75)	0.26
25	6.6	7	13	7	4.94	0.85 (0.77)	0.33
50	*0.22*	6	15	6	1.11	0.80 (0.56)	0.26
50	*0.66*	6	13	7	1.65	0.85 (0.62	0.30
50	2.2	8	14	9	3.32	0.93 (0.83)	0.36
50	6.6	5	12	6	3.48	0.92 (0.84)	0.39
75	*0.22*	7	12	7	1.01	0.83 (0.52)	0.33
75	*0.66*	5	12	5	2.85	0.92 (0.58)	0.33
75	*2.2*	6	10	8	3.16	0.90 (0.59)	0.33
75	6.6	6	14	7	3.84	0.93 (0.60)	0.34

Table 6.1: Mean Values of Parameters from Model Fits to DTAB/DSB Mixtures

x_{DTAB} bulk	Conc. mM	τ_1 ± 2 Å	τ_2 ± 2 Å	τ_3 ± 2 Å	Γ $\mu mol\ m^{-2}$	x_{DTAB} ads± 0.05
25	*0.22*	7	19	8	0.1	0.05
25	*0.74*	6	19	6	0.2	0.16
25	2.2	6	19	6	0.3	0.31
25	7.4	8	17	7	1.8	0.38
50	*0.22*	9	18	6	0.5	0.11
50	*0.74*	8	19	9	0.6	0.21
50	*2.2*	8	15	7	3.7	0.28
50	7.4	6	13	8	3.6	0.39
75	*0.22*	5	17	7	0.1	0.06
75	*0.74*	6	19	8	0.3	0.16
75	*2.2*	5	18	8	0.3	0.18
75	7.4	5	15	5	1.1	0.33

Table 6.2: Mead values of parameters from fits to neutron reflectivity from DTAB/DB mixtures.

Tables (6.1) and (6.2) show that the presence of DTAB at the solid–aqueous interface enhances the total adsorption of DSB but suppresses the total adsorption of DB. The different interfacial behaviour between these two systems can be attributed to different structure features in the inner layer, which is adjacent to the surface, as shown schematically in Figure (6.4). A difference from the SDS/DSB system is that the adsorbed amount of the system DTAB/DSB does not change much with increasing fraction of DTAB in the adsorbed layer, as shown in Figure (6.3).

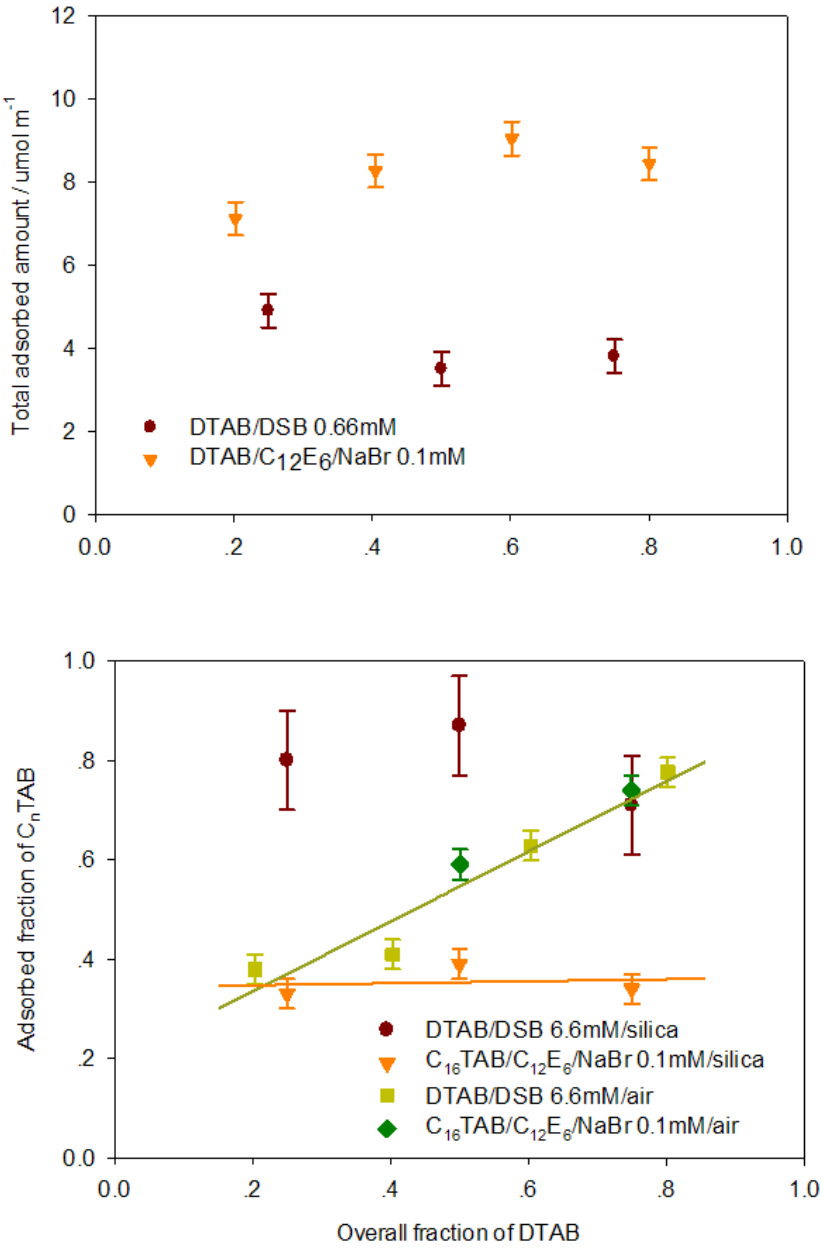


Figure 6.3: (a) Total adsorbed at the silica–aqueous interface and (b) adsorbed fraction of C_nTAB plotted against the overall fraction for total concentration each of DTAB/DSB and C_{16}TAB/$C_{12}E_6$/NaBr above the CMC for both the silica–aqueous and air–liquid interfaces. The data for C_{16}TAB/$C_{12}E_6$ are from Penfold et al. [10, 11]

In the schematic diagrams of DTAB/DSB, the stoichiometry reflects the strong interaction of DTAB with the surface. A possible configuration shows that the spacer group of DSB is partially bent so that some interaction between the sulfonate and the DTAB headgroups is allowed, while maintaining a reasonable close spacing of the alkyl chains. Thus cooperativity is gained with respect to DSB on its own and the cationic groups ensure adsorption, although overall the adsorption is less strong compared with the mixed SDS/DSB system.

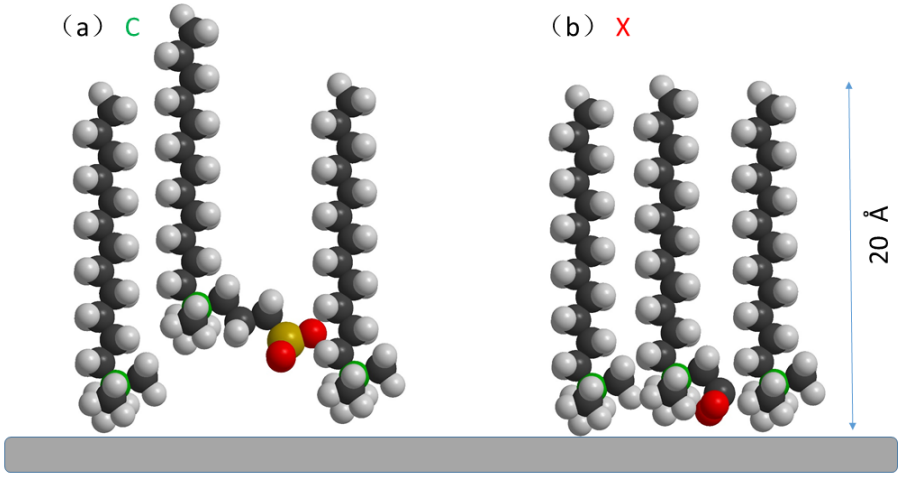


Figure 6.4: Possible configurations of molecules in the layer next to the surface (inner layer) at the silica–aqueous solution interface, (a) a mixture of DSB and DTAB, (b) a mixture of DB and DTAB. Cooperative adsorption is marked with a green C and no or little adsorption with a red X. The separation and stoichiometry in the two mixtures approximately matches those observed and the colours are black/grey for C, red for O, green for N and yellow for S

In the case of DTAB/DB mixtures, there is little total adsorption. The reason for

this is that the close proximity of the negatively charged surface to the carboxyl group will tend to make it revert to being a weaker acid. The natural pK_a of carboxyl group is about 4.5 but it drops to 2.4 when the carboxyl group is separated with the quaternary ammonium with a single CH_2 spacer [12]. Harwigsson et al. also found that by lowering the pH, the adsorption of carboxybetaine is reduced and it is therefore possible that the destabilization of adsorption is a result of combination of the close approach of the carboxy group to the surface and a reduction in the pK_a by the negatively charged surface [13].

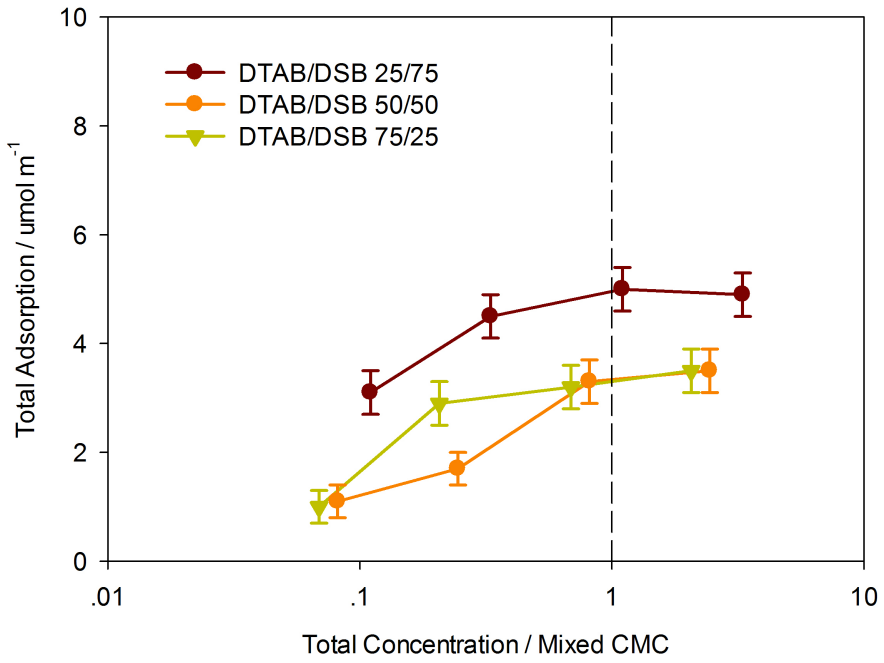


Figure 6.5: Total amount adsorbed at the silica–aqueous interface as a function of concentration relative to the mixed CMC for three compositions of DTAB/DSB, a vertical line is drawn for guidance at c/CMC=1.

Although a certain amount of adsorption occurs for DTAB/DSB, the pattern is

different from the SDS/DSB in a number of ways. As shown in Figure (6.5), at all compositions studied, the adsorbed amount is substantially lower and, given that the adsorbed layer still adopts three layer structure, must be in patches. However, the DTAB/DSB adsorption approximately rises to a plateau or a weak maximum instead of the sharp maximum of the SDS/DSB. Following the discussion in Chapter 5 that the sharp maximum is caused by adsorption depending on the concentration of just the surfactant ion, this indicates that both surfactant and its counterion Br^- are adsorbed at the surface.

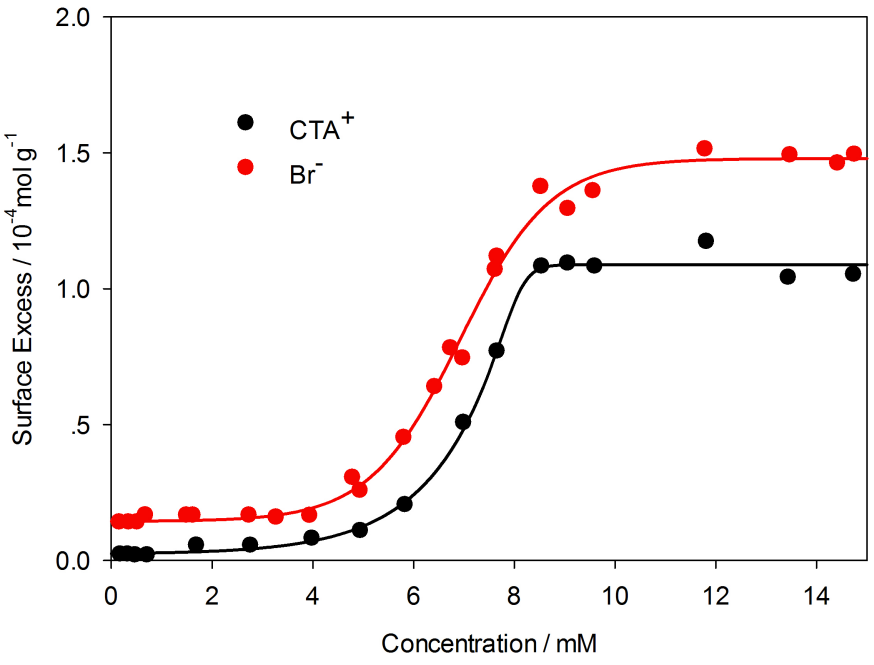


Figure 6.6: Adsorption isotherm of CTA^+ from aqueous solution no silica and the corresponding adsorption of Br^-. The plot is adapted from [15]

Rupprecht et al. proposed a mechanism of adsorption of cationic surfactants onto negatively charged hydrophilic surface [14]. The adsorption isotherm of cationic

surfactant can be characterized by a two step process. The first layer is adsorbed under the driven of direct electrostatic interaction between the surfactant cations and the negatively charged sites on the surface. The charge on the surface is therefore neutralized with coverage of hydrophobic groups and then the next step would then be adsorption of a second layer of surfactant ions at these hydrophobic sites, with the attractive force operating between the chains. Bijsterbosch has conducted a investigation on the mechanism of adsorption of DTAB and cetyltrimethylammonium bromide (CTAB) onto silica surfaces at different pH values [6]. It was observed that the adsorption of counterion Br^- does not occur until the the DTA^+ adsorption starts to increase to the second plateau, as shown in Figure (6.6). The electrophoresis experiments indicate that at concentrations corresponding with the first plateau in the adsorption isotherm is reached , the electrophoretic mobility reverses sign, and the positive charges of the second layer will be compensated by negative counterions, which is consistent with the model. A similar phenomenon was reported by Gu et al. on CTAB adsorption at the silica/water interface [15]. Modified equations for calculation of the aggregation number, equilibrium constant and the standard free energy change were applied and the results indicated that the charge neutralization in first step of adsorption is between the negatively charged surface and surfactant cations. Therefore no significant counterions will be adsorbed at this stage. The positive charges have to be compensated by negative counterions, which corresponds to the increasing adsorption of Br^- ions in second step. The investigation was extended by Gu et al. on the ionic exchange coefficients of halide ions with cationic CTA^+ and the data indicated that Br^- has the largest binding coefficient on adsorbed CTA^+ ions. Although in the zwitterionic system the interfacial behaviour is less clear, the interaction of Br^- ions

with the adsorbed layer should be much stronger because of dispersion forces and would therefore be less likely to be replaced with OH^- ions.

6.4 Conclusion

The presence of cationic surfactant DTAB enhance the total adsorption of DSB but suppress the total adsorption of DB at the silica–aqueous interface. The headgroup of DSB may be partially bent so that interactions between sulfonate and DTAB headgroups is allowed and a reasonable close packing is allowed, therefore cooperativity is gained to ensure adsorption, although it is less strong than for SDS/DSB. The destabilization of DTAB/DB adsorption can be attributed to the combination of the close approach of the carboxy group to the surface and the reduction of pK_a by the negatively charged surface.

Bibliography

[1] F. Tiberg, J. Brinck, and L. Grant. Adsorption and surface-induced self-assembly of surfactants at the solid–aqueous interface. *Current opinion in colloid & interface science*, 4(6):411–419, 1999.

[2] G. Fragneto, R. K. Thomas, A. R. Rennie, and J. Penfold. Neutron reflection from hexadecyltrimethylammonium bromide adsorbed on smooth and rough silicon surfaces. *Langmuir*, 12(25):6036–6043, 1996.

[3] R. Atkin, V. S. J. Craig, E. J. Wanless, and S. Biggs. Mechanism of cationic surfactant adsorption at the solid–aqueous interface. *Advances in colloid and interface science*, 103(3):219–304, 2003.

[4] P. Kekicheff, H. K. Christenson, and B. W. Ninham. Adsorption of cetyltrimethylammonium bromide to mica surfaces below the critical micellar concentration. *Colloids and Surfaces*, 40:31–41, 1989.

[5] R. M. Pashley, P. M. McGuiggan, R. G. Horn, and B. W. Ninham. Forces between bilayers of cetyltrimethylammonium bromide in micellar solutions. *Journal of colloid and interface science*, 126(2):569–578, 1988.

[6] B. H. Bijsterbosch. Characterization of silica surfaces by adsorption from solution. investigations into the mechanism of adsorption of cationic surfactants. *Journal of Colloid and Interface Science*, 47(1):186–198, 1974.

[7] W. Kern. The evolution of silicon wafer cleaning technology. *Journal of the Electrochemical Society*, 137(6):1887–1892, 1990.

[8] K. H. S. Kung and K. F. Hayes. Fourier transform infrared spectroscopic study of the adsorption of cetyltrimethylammonium bromide and cetylpyridinium chloride on silica. *Langmuir*, 9(1):263–267, 1993.

[9] J. R. P. Webster, S. Langridge, R. M. Dalgliesh, and T. R. Charlton. Reflectometry techniques on the second target station at isis: Methods and science. *The European Physical Journal Plus*, 126(11):1–5, 2011.

[10] J. Penfold, E. Staples, P. Cummins, I. Tucker, L. Thompson, R. K. Thomas, E. A. Simister, and J. R. Lu. Adsorption of mixed cationic–non-ionic surfactants at the air/water interface. *J. Chem. Soc., Faraday Trans.*, 92(10):1773–1779, 1996.

[11] J. Penfold, E. J. Staples, I. Tucker, and L. J. Thompson. Adsorption of mixed cationic and nonionic surfactants at the hydrophilic silicon surface from aqueous solution: Studied by specular neutron reflection. *Langmuir*, 13(25):6638–6643, 1997.

[12] R. Wüstneck, J. Kriwanek, M. Herbst, G. Wasow, and K. Haage. The adsorption behaviour of long-chain n-alkyl betaines and their hydrobromides. *Colloids and surfaces*, 66(1):1–9, 1992.

[13] I. Harwigsson, F. Tiberg, and Y. Chevalier. Nature of the adsorption of zwitterionic surfactants at hydrophilic surfaces. *Journal of colloid and interface science*, 183(2):380–387, 1996.

[14] H. Rupprecht, E. Ullmann, and K. Thoma. Auswirkungen von elektrolyten auf das sorptionsvermögen kolloider kieselsäure aerosil. *Fortschrittsberichte über Kolloide und Polymere*, 55(1):45–48, 1971.

[15] T. Gu and Z. Huang. Thermodynamics of hemimicellization of cetyltrimethylammonium bromide at the silica gel/water interface. *Colloids and surfaces*, 40:71–76, 1989.

Chapter 7

Air/liquid Interface Experiments on Carboxybetaine with Different Inter-charge Spacer

7.1 Introduction

Among surfactants applied in the commercial field, the zwitterionic compounds have been widely recognized as especially stable against several external variations, e.g., ionic strengths and they do not precipitate in hard water media due to their overall electrical neutrality [1–3]. They also differ from the polyoxyethylene nonionc surfactants in that they are not so sensitive to environmental temperature [4].

Nonionic surfactants $C_{12}H_{25}(OC_2H_4)_mOH$, $C_{12}(EO)_m$, have been used extensively to study the effect of headgroup size on adsorption [5–8]. It was suggested that with an increase of m from 2 to 4, the layer thickness becomes smaller with

increasing area per molecule (abbreviated to APM). The headgroup layers also become smaller in thickness and less than their fully extended length, the origin of this being mainly the bulkiness of the headgroup [9].

The headgroups of zwitterionic surfactants contain a pair of opposite charges separated by a spacer. The surfactant generally carry no nett charge at the neutral pH if the length of spacer is not too large, and the adsorption behaviour at the air/liquid interface is therefore governed by the Gibbs equation. For a 1:1 ionic surfactant this is

$$\frac{d\gamma}{RT} = -\Gamma_s d\ln a_s + \Gamma_i d\ln a_i \approx 2\Gamma_s d\ln c_s \tag{7.1}$$

where γ is the surface tension, Γ is the surface excess defined relative to a surface plane for which Γ_{water} is zero, a is the activity and is approximated as concentration c, the subscripts s and i indicate surfactant ion and any other ions that are also adsorbed. If the surfactant counterion is the only one adsorbed apart from the surfactant then the equation simplifies as shown on the right as required by neutrality that the two surface excesses and the two concentrations should be identical. In the case of zwitterionic surfactant where both groups are ionized, there are no additional ions adsorbed therefore the prefactor in the expression on the right is 1. If only one of the zwitterionic groups is ionized then by the requirement of surface neutrality the adsorption of a counterion is necessary and, unless the concentration of this counterion is constant, the prefactor of Gibbs equation becomes 2, as for a 1:1 ionic surfactant. The strength of adsorption and the critical micelle concentration (CMC) tend to be intermediate between those of nonionic and ionic surfactants and the zwitterionics are very soluble due to the two charge groups [10]. These properties and the overall charge neutrality, which weakens

the interaction with proteins, gives a mildness on zwitterionic surfactants that is useful for biological application and in formations for personal care [11, 12].

In a carboxybetaine headgroup the quaternary ammonium is a strong base but the carboxyl group is a weak acid group. The length of the spacer between the two groups has a strong effect on the interaction between the charged groups especially if one of them is weak [13, 14]. If the carboxyl group is directly connected to an alkyl group, the pK_a is expected to be in the range of 4–5. However, if the carboxyl group is separated from the cationic group by one methlyne group, the pK_a drops substantially and the zwitterionic becomes fully charged at natural pH. For the α, ω– ammonioalkanoates, the pK_a varies from 2.3 to 4.5 with the number of methylene group increase from 1 to 6, which is close to the pK_a values of 4.7 for acetic acid [10]. In ammonioalkanotes both charged groups are weak electrolytes and the behaviour is expected to be slightly different if a quaternary alkylammonium group is introduced as the cationic group. However, for dodecyl carboxybetaine with a single methylene spacer, the pK_a drops to 2.4 and varies with the spacer length increasing similarly with ammonioalkanoates [15, 16]. Thus with the increasing of the spacer length, the added stabilization of the dissociated state is gradually lost.

The pK_a of the carboxylic acid group in the zwitterionic can be expected to increase by about 2 units when the spacer changes from 1 to more than about 6 methylene units. By changing the dissociation of the carboxylic acid part of the head–group an increase in the spacer length will affect not only the charge but may also affect the polarity of the headgroup, e.g. the carboxylic acid part of the

headgroup will be less hydrophilic/more hydrophobic and this may also contribute to a change of the surface properties. In addition, the dipole associated with the charge also varies linearly with the separation in a rigid spacer but more slowly in the typical flexible alkylene spacer of the zwitterionics that have been studied.

In previous reports, Chevalier focused on the influence of zwitterionic surfactant headgroup spacer on their micellar properties, i.e. Kraft point, CMC and APM at air/liquid interface [4, 9]. The investigations were conducted on two series of zwitterionics, phosphocholines and dodecyl carboxybetaines, where the spacer was varied from 1 to 10 methlyene groups. In both systems the CMC passes though a pronounced maximum at around n=4 where n is the number of methylene units. It was explained in terms of the repulsion between the zwitterionic dipoles at the micellar surface as a function of n. In the series of dodecyl carboxybetaine, the limiting APM at the critical CMC, A_{CMC}, shows a steady increase with spacer length from 52 at a spacer length of 1 carbon to 92 Å^2 at 10 carbons, but the CMC and the limiting surface tension at the CMC, γ_{CMC}, both show strong maxima in the region of 3–4 methylene groups [9]. The behaviour of CMC was explained as for the phosphocholine system but the more steady increase of A_{CMC} was interpreted as a result of a interplay of the dipolar repulsion and an increasing steric lateral repulsion with spacer length which eventually causes the more flexible long spacers to form a loop at the surface, demonstrating that the control of inter–facial layer properties through their molecular structure is possible. Given that the properties of these important surfactants can be manipulated by adjustment of the spacer length, the understanding of the surface and aggregation behaviour as a function of spacer length is important.

Neutron reflection with deuterium labelling offers a means for studying the distributions of surfactant fragments along the direction normal to the surface and should be able to identify structural changes associated with changes of the spacer orientation or position relative to the underlying water [17, 18]. The combination of neutron reflection with surface tension measurements also allows an accurate assessment of the application of the Gibbs equation to the surface tension data, which may also reveal interesting features of the surface behaviour, e.g. in the surface tension data of Chevalier et al. the curve for the largest of the spacers studied shows an unusual long linear stretch [19,20]. The surface tension measurements of Chevalier et al. have therefore been repeated for a selection of the same series of dodecyl carboxybetaines with spacers of 1, 4 and 8 methylene groups and neutron reflection from the surfaces of the deuterated species measured, using differently labelled molecules to separate the signals from the chain and spacer.

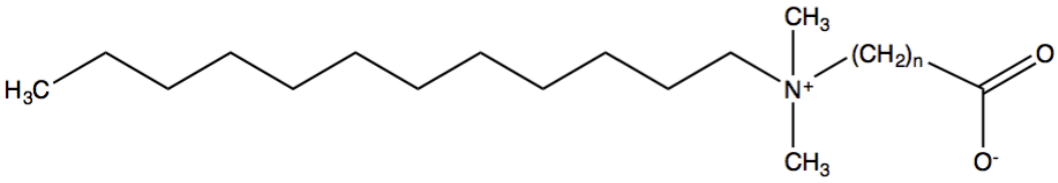


Figure 7.1: Conformation of dodecyl carboxybetaine with methylene spacer n as 1, 4 and 8.

7.2 Experiment details

The protonated and partial deuterated surfactants with n=1, 4 and 8 were synthesized as described in chapter 3 (designated $C_{12}C_n$betaine in the rest of the chapter). Owing to the difficulty of using ^{1}H NMR to determine the purity of perdeuterat-

ed materials the sequence of reactions detailed in chapter 3 was first done with protonated materials and then repeated exactly for the deuterated system. Surface tension were measured for each component at 25 °C using the du Noüy ring method. The absence of a surface tension minimum around the CMC indicates a high purity of the sample. Also the CMC of each component was calculated from the intersection of a second order fit to the data below the CMC and a horizontal line above [21].

Air–liquid interface neutron reflection experiments for different components were conducted using the procedures described in chapter 3 and 4. The conversion of measured signal to absolute intensity was made by calibration with D_2O. The protonated, chain deuterated and head–group deuterated carboxybetaine with n=1, 4 and 8 were measured in D_2O at three times CMC, respectively. In addition, each different component was measured in null reflection water (NRW) over a wide range of concentration from well below the CMC to three times CMC at 298K. Under these circumstances the reflected signal is entirely from the surfactant layer. The surface coverage of surfactant was determined by fitting the neutron reflectivity profiles with a simple slab model using the standard optical matrix method to calculate the reflectivity. A modification of the partial structure method was used to analysis the high concentration data and determine the structure.

Fragment (Component)	Volume ($Å^3$)	Scattering length ($b/10^{-4}Å$)	Scattering length density ($\rho/10^{-6}Å^{-2}$)
$C_{12}H_{25}$	350	-13.7	-0.39
$C_{12}D_{25}$	350	240.6	6.87
h–C_1Betaine	165	17.6	1.07
h–C_4Betaine	252	14.2	0.56
h–C_8Betaine	368	10.2	0.28
d–C_4Betaine	252	77.8	3.09
d–C_8Betaine	368	158.5	4.31
h–C_{12}h–C_1Betaine	515	3.9	0.08
h–C_{12}h–C_4Betaine	602	0.5	0.01
h–C_{12}h–C_8Betaine	718	-3.48	-0.05
d–C_{12}h–C_1Betaine	515	258.2	5.01
d–C_{12}h–C_4Betaine	602	254.8	4.23
d–C_{12}h–C_8Betaine	718	250.8	3.49
h–C_{12}d–C_4Betaine	602	65.7	1.09
h–C_{12}d–C_4Betaine	718	148.0	2.06

Table 7.1: The physical parameters of differently isotopic labelled dodecyl carboxybetaine

7.3 Discussion and Conclusion

7.3.1 Surface tension

The surface tension of dodecyl carboxybetaine surfactants with different spacer is plotted against $\ln C$ in Figure (7.2). The C_{10} spacer plot from Chevalier et al. is reproduced for comparison [9]. The calculated CMCs are 1.87 mM, 3.3 mM and 1.03 mM for carboxybetaine with n=1, 4 and 8, respectively. The values of the CMC are consistent with previous studies [9, 15, 22–24] and fall in line with the expected range for a dodecyl chain zwitterionic surfactants reported in the literature [25, 26]. The increase followed by a decrease of CMC with inter–charge spacers was also observed in the studies on similar zwitterionic surfactant phosphobetaines, namely (alkyldimethylammonioalkyl)-phenylphosphinates with inter–charge spacers varying from 1 to 10 with the maximum occurring in phosphobetaine at n=4 [4]. The results calculated by applying the Gibbs equation to the surface tension data are shown in Table (7.2). A feature of particular interest is that the $\gamma - \ln C$ plot for the largest spacer, C_8, is linear over a very long range of concentration and this was also found by Chevalier et al. for their largest spacer, C_{10}. Apart from the coverage for the C_4 compound and a constant shift in calibration of the surface tension the results are in good agreement.

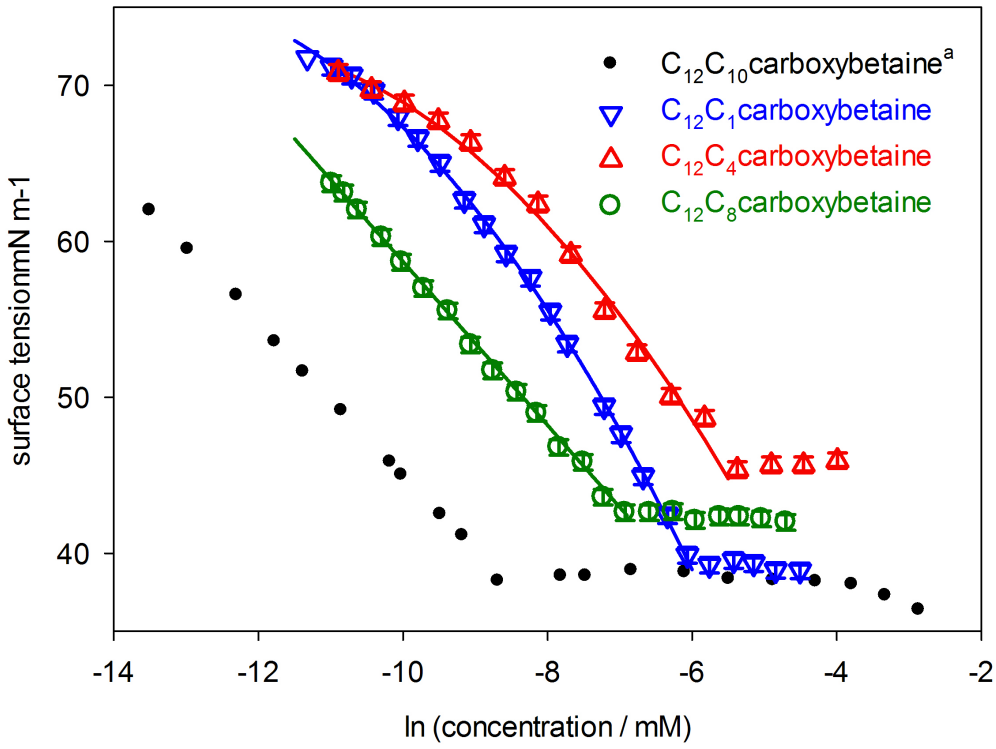


Figure 7.2: Surface tension plot of dodecyl carboxybetaines with different spacers measured at 298K and fits to the Gibbs equation using a quadratic in $\ln C$ and a prefactor of unity. Also included are surface tension data[a] from Chevalier et al. for the compound with a spacer of 10 methylene groups [9].

Components	CMC $\pm 20\%$ mM)	Surface tension ± 0.5 mN/m)	A_{CMC} $\pm 15\%$ (Å^2)	Γ_{CMC} $\pm 15\%$ (mol/m^2)
$C_{12}C_1$betaine	$1.9(2.0^a)$	$39.8(36.7^a)$	$44(52^a, 50^b)$	3.8
$C_{12}C_4$betaine	$3.3(3.4^a)$	$42.4(44.6^a)$	$53(68^a)$	3.13
$C_{12}C_8$betaine	$1.0(1.5^c)$	$42.1(41.6^b)$	$77(77^c)$	2.15

Table 7.2: Calculated APM and surface excess results by applying the Gibbs equation with prefactor of unity on the surface tension plots. . Results from Chevalier et al. are given in brackets for ^{a} the C_1 and C_4 compounds and ^{c} for the C_7 compound [9]. ^{b} Results from Hines et al. [27].The surface tension measurements were conducted at 298K in UHQ water.

It was suggested that the variation in CMC with different spacers is a interplay of two opposite contributions between the total hydrophobicity of the molecule and the dipole moment increase with n in headgroup regions. With an increasing number of methylene groups in the head–group region, the overall hydrophobicity of the zwitterionic surfactant molecule is enhanced, results in the decrease of the CMC. On the other hand, the distance between charged groups in headgroup grows, improving the strength of repulsive dipole–dipole interactions between the headgroups at the surface, leading to an increase of the hydrophilicity of molecule and therefore the CMC value. It was previously reported in the study of phosphobetaine using ^{13}C NMR that the variation of CMC with n is the consequence of the predominance of one effect or the other. The headgroup region is rigid when n is less than 3 and becomes flexible for larger n values [9], which in turn regulates the competition between two opposite contributions in micelle formation.

The surface tension values at the CMC for each component are broadly consistent with the CMC values: the larger the CMC, the higher the surface tension. It is straightforward to understand that surface tension is reduced when the surface adsorbs more compound (lower APM value) and therefore more hydrophobic chains oriented towards air, making the surface tension closer to that of hydrocarbons than that of water. The carboxybetaine with n=8 seems to contradict this rule with its larger APM but still relatively small surface tension at the CMC. The decreased surface tension of a surface is a result of a surface well covered by hydrophobic materials, therefore it is reasonable to assume that for the carboxybetaines with longer intercharge spacers, the coverage can be attributed to the polymethylene intercharge arms rather than the insufficiently dense surfactant alkyl chains. The larger intercharge arm adopts a conformation for which the hydrocarbon parts in the head–groups are oriented toward air, and Chevalier et al. suggested that these long chains make a loop inside the chains rich region of the interface [9]. Another factor that could contribute to the folding is the attraction between oppositely charged P and N atom centres of neighbouring head–groups at the interface [28].

It was also reported that the APM at air–liquid interface show an uprising trend with the increasing number of inter–charge spacers, indicating that the repulsive interactions increase with n from 1 to 10 for the carboxybetaine surfactants [9]. A similar trend was observed in the phosphocholine surfactant with inter–charge spacers of 2, 4 and 6 methylene groups [28]. This is a strong confirmation of the interpretation in terms of a competition between the two n-dependent factors, the total hydrophobicity of the molecule and the dipole–dipole moment between the

head–groups at the interface. However, there is no evidence that the repulsions between head–groups are only due to electrostatic dipole–dipole interactions. For the carboxybetaine with n=1 and 4, the APM values remain almost constant, suggesting that the folding of in head–group is not pronounced enough to allow head–groups to approach closer to each other. With larger head–groups, it is not clear that the the interactions between head–groups are only electrostatic dipole–dipole repulsions, steric repulsions due to the bulkiness of head–groups, or both. Since the APM values obtained directly from neutron reflection measurements are more accurate and some information on the conformation can be obtained via partial structure factor analysis, the neutron reflection results are now examined.

7.3.2 Neutron Reflection Experiments

Optical Matrix Method

The neutron reflection of partially deuterated dodecyl carboxybetaines was measured over a range of concentrations from well below to above the CMC of each component, namely $dC_{12}hC_1$betaine, $dC_{12}hC_4$betaine, $hC_{12}dC_4$betaine, $dC_{12}hC_8$ betaine and $hC_{12}dC_8$betaine in null reflection water, where d and h denote the deuterated and protonated part of the surfactant. By isotopic labelling part of the surfactant, its neutron reflection signal can be highlighted from the background and gives two independent and direct measurements of the coverage. The reflection data were fitted using a single uniform layer model. The results are listed in Table (7.3). The neutron reflectivity profiles of selected solutions were fitted with Motofit (see Chapter 2) and plotted in Figures (7.3) to (7.5). The value of surface excess, Γ, at this contrast depends on the product of scattering length density and layer thickness ($\rho \times \tau$ in the Table) and, although individually these have a signif-

icant error, the product is largely independent of the model used for the profile of the layer.

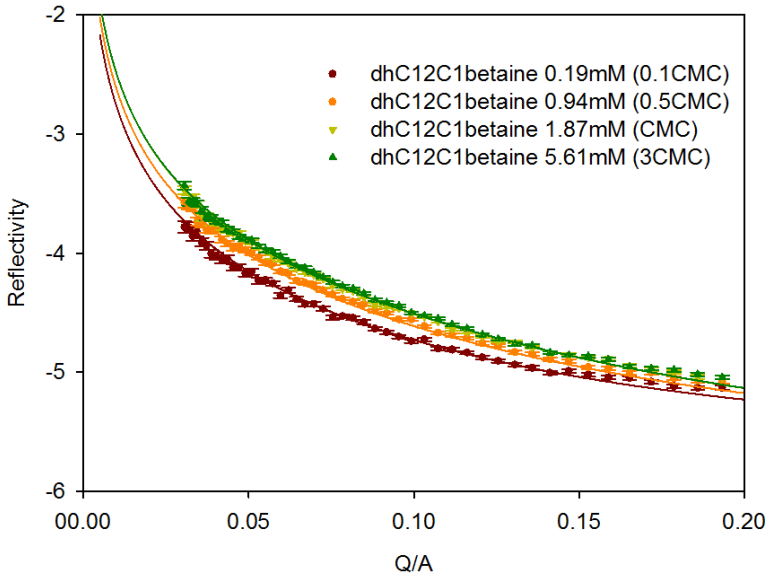


Figure 7.3: Neutron reflectivity profiles for dhC12C1Betaine in null reflection water at different concentrations, the curves were measured at 298K. The solid lines represent the best uniform model fits

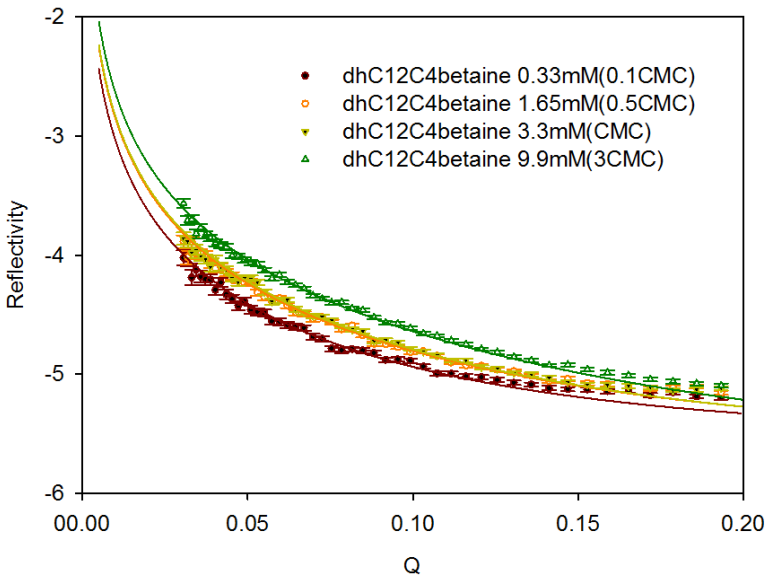


Figure 7.4: Neutron reflectivity profiles for dhC12C4Betaine in NRW.

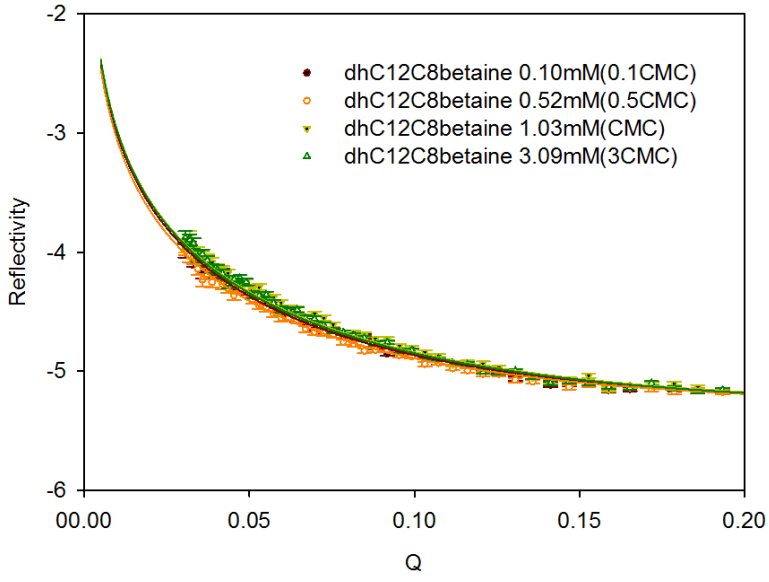


Figure 7.5: Neutron reflectivity profiles for dhC12C8Betaine in NRW.

Contrast	Conc. mM	τ $\pm 5\%$ Å^{-1}	$\rho \times \tau$ $\pm 5\%$ Å^{-1} $\times 10^6$	A $\pm 5\%$ Å^2	Γ $\pm 5\%$ $\mu mol\ m^{-2}$
dhC$_{12}$C$_1$Betaine	0.19	12	32.3	80	2.1
dhC$_{12}$C$_1$Betaine	0.56	12	46.8	55	3.0
dhC$_{12}$C$_1$Betaine	0.94	14	51.4	50	3.3
dhC$_{12}$C$_1$Betaine	1.40	15	55.4	47	3.5
dhC$_{12}$C$_1$Betaine	1.87	13	55.4	47	3.5
dhC$_{12}$C$_1$Betaine	5.61	14	57.8	45	3.7
dhC$_{12}$C$_4$Betaine	0.33	9	32.8	78	2.1
hdC$_{12}$C$_4$Betaine	0.33	8	8.0	82	2.0
dhC$_{12}$C$_4$Betaine	0.99	13	35.6	71	2.3
hdC$_{12}$C$_4$Betaine	0.99	12	9.6	68	2.4
dhC$_{12}$C$_4$Betaine	1.65	12	39.6	64	2.6
hdC$_{12}$C$_4$Betaine	1.65	10	10.0	66	2.5
dhC$_{12}$C$_4$Betaine	2.48	12	43.6	58	2.9
hdC$_{12}$C$_4$Betaine	2.48	11	11.2	58	2.9
dhC$_{12}$C$_4$Betaine	3.30	12	48.4	53	3.1
hdC$_{12}$C$_4$Betaine	3.30	16	12.5	52	3.2
dhC$_{12}$C$_4$Betaine	9.90	13	48.5	52	3.2
hdC$_{12}$C$_4$Betaine	9.90	14	12.6	52	3.2

Table continues on next page

Contrast	Conc. mM	τ $\pm 5\%$ Å^{-1}	$\rho \times \tau$ $\pm 5\%$ Å^{-1} $\times 10^6$	A $\pm 5\%$ Å^2	Γ $\pm 5\%$ $\mu mol\ m^{-2}$
dh$C_{12}C_8$Betaine	0.1	11	29.5	85	2.0
hd$C_{12}C_8$Betaine	0.1	9	17.2	86	1.9
dh$C_{12}C_8$Betaine	0.31	10	29.0	87	1.9
hd$C_{12}C_8$Betaine	0.31	10	17.5	85	2.0
dh$C_{12}C_8$Betaine	0.52	10	28.6	88	1.9
hd$C_{12}C_8$Betaine	0.52	9	17.7	84	2.0
dh$C_{12}C_8$Betaine	0.77	10	30.4	83	2.0
hd$C_{12}C_8$Betaine	0.77	13	17.7	84	2.0
dh$C_{12}C_8$Betaine	1.03	10	29.4	85	2.0
hd$C_{12}C_8$Betaine	1.03	12	17.5	85	2.0
dh$C_{12}C_8$Betaine	3.09	11	29.8	84	2.0
hd$C_{12}C_8$Betaine	3.09	15	17.6	84	2.0

Table 7.3: Uniform layer fitting results of a series of dodecyl carboxybetaine with different length of spacers. All measurements were conducted in null reflection water solution at 298K.

The results from two independent measurements at each concentrations are in good agreement. They are also in good agreement with the surface tension–Gibbs equation results from the surface tension data in Table (7.2). This is a confirmation that the prefactor in Gibbs equation is 1, i.e. that all three surfactants are fully disassociated in the bulk solution at natural pH despite the substantial increase in pK_a expected for the C_8 spacer. The straight surface tension curve of the compound with the longest spacer, which indicates constant surface excess

over the measured concentration range, is also replicated in the neutron reflection data. Thus, this compound reaches its plateau adsorption at around 1/10th of its CMC. Taking this data and those of Chevalier et al. for the C_{10} spacer indicates that this is a definite feature of the compounds with the long spacer. In previous reports discussing the application of the Gibbs equation, the evidence indicates that nonionic surfactants reach a plateau before but still close to CMC, whereas ionic species do not [19,29,30], although there is no thermodynamic reason why a plateau of adsorption should be associated with the CMC. A plateau in adsorption occurring well below the CMC suggests that compare with the saturated monolayer, the micelle is more unstable. This phenomenon may be explained in terms of difficulty in accommodating a long spacer chain in a micelle and this is discussed further below in connection with the layer structure.

Partial structure method

In order to have a better understanding of the structure of adsorbed layer at the air/liquid interface, the neutron reflection data of several different isotopic labelled $C_{12}C_n$betaine at 3×CMC were analysed using an extension of the kinematic approximation model. The basis of the direct fitting method is fully described in Chapter 2.

The betaines can be divided into two fragments as alkyl chain and the betaine headgroup, the latter includes the spacer chain and the two charged groups. In this case, Gaussian distributions can be used to represent the distributions of the two surfactant groups along the surface normal,

$$n_i(z) = n_i^0 \exp(\text{-}4z^2/\sigma_i^2) \tag{7.2}$$

where n_i^0 is proportional to the surface excess, σ_i is the width parameter (full width at (height) $/e$) and z is the distance along the surface normal. The distribution of water is taken to be determined by space filling up to a certain distance into the surface layer followed by a decay to zero,

$$\phi_w(z) = 1 - \phi_c - \phi_s; z \leq \xi \tag{7.3}$$

where ϕ are volume fractions and ξ is a cut–off distance [31], and

$$\phi_w(z) = \phi_w(\xi) \exp\left[-\frac{(z-\xi)^2}{\sigma^2}\right]; z \leq \xi \tag{7.4}$$

Then below the cut–off distance there is no empty space. Above this the decay of water follows a half–Gaussian. The region of water defined by this distribution can be thought as over which the capillary waves exert an effect. The Fourier transform of this has to be calculated numerically and one of the separations, δ_{cw} or δ_{hw} introduces another adjustable parameter into the cross partial structure parameter H_{cw} or H_{sw}. The procedure is to use a set of trial parameters and to compute R and optimize a simultaneous fit to the full set of reflectivity profiles. In this case, the number of independent parameters for the betaines is 7, which are the surface excess of surfactant, the width of the alkyl chain and betaine fragments, the separations of betaine from alkyl chain and from water, and the cut–off for the water and decay length for the water profile. In order to give a more explicit comparison of these three similar compounds, a different set of parameters are introduced within the framework of the same calculation.

The width of the distribution of a surfactant fragment is determined partly by the length of the projection of the fragment along the normal direction, denoted l, and partly by the thermal roughness, w, from the capillary waves such that the

parameter σ in equation (7.2) is given by

$$\sigma^2 = l^2 + w^2 \tag{7.5}$$

Since the whole layer is affected by the capillary waves, w can be taken to be the same for all fragments including the water decay in equation (7.4). In addition, since the two fragments of the surfactants are attached the distance between their centres is constrained to be

$$\delta_{cs} = \frac{1}{2}(l_s \pm l_c) \tag{7.6}$$

where the $\pm$ depends on whether the angle between the two projections along the surface normal is greater or less than 90°. There are now only 6 independent parameters, the surface coverage, the two fragment projections along the surface normal, the thermal roughness, the water cut–off and either the chain–water separation or the spacer–water roughness. Since the surface tensions of three betaine surfactants are not very different and the thermal roughness w is mainly determined by the surface tension, w can be assumed to be the same in all three sets, which further reduces the number of parameters for the set of surfactants. The reflectivity profiles were fitted using a program written by Dr. R. K. Thomas,using the model above and the corresponding fragment distributions based on this model are plotted in Figures (7.6) and (7.7) and the parameters are listed in Table (7.4). The fits should be judged as a set in that the unusually tight constraints put on the fitting model lead to some fits that could be improved either by relaxing the constant w restriction or allowing the independent variation of δ_{cs}. However, the constraints on the fitted parameters highlight the important differences in structure between the three surfactants.

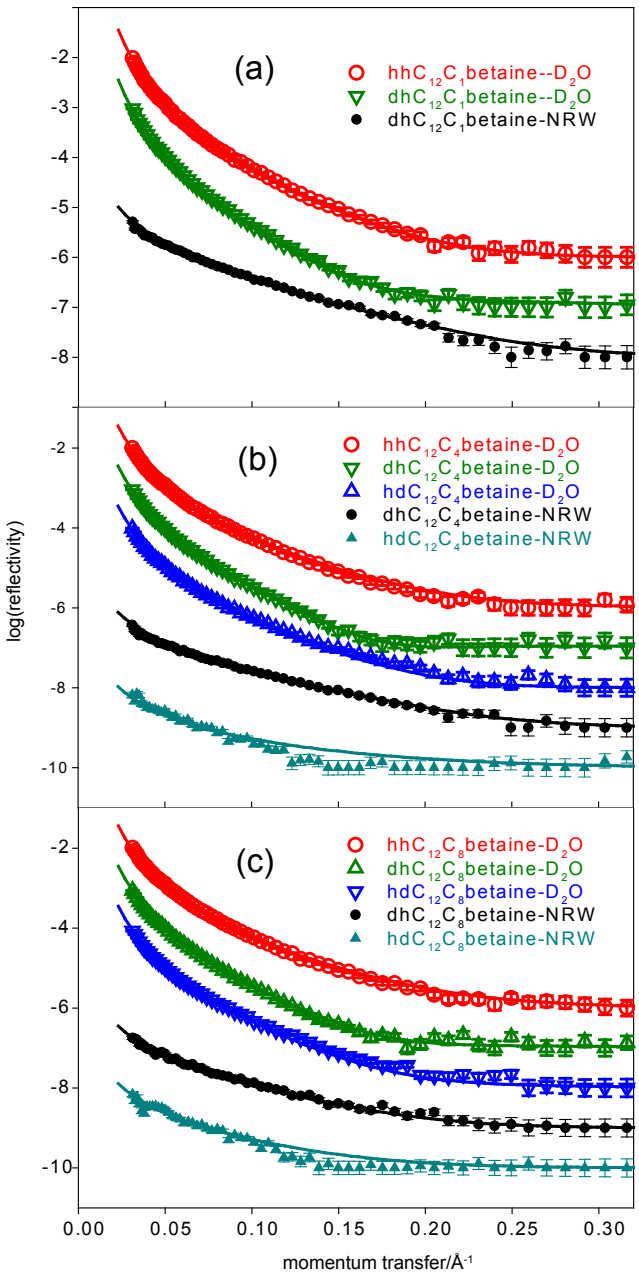


Figure 7.6: Neutron reflectivity profiles for different isotopic species of dodecyl carboxybetaines with methylene spacers of (a) 1, (b) 4 and (c) 8 units (points) and the best fits (lines) using the structures shown in Figure (7.7). For clarity, the individual profiles in each set are successively displaced downwards by 1 unit.

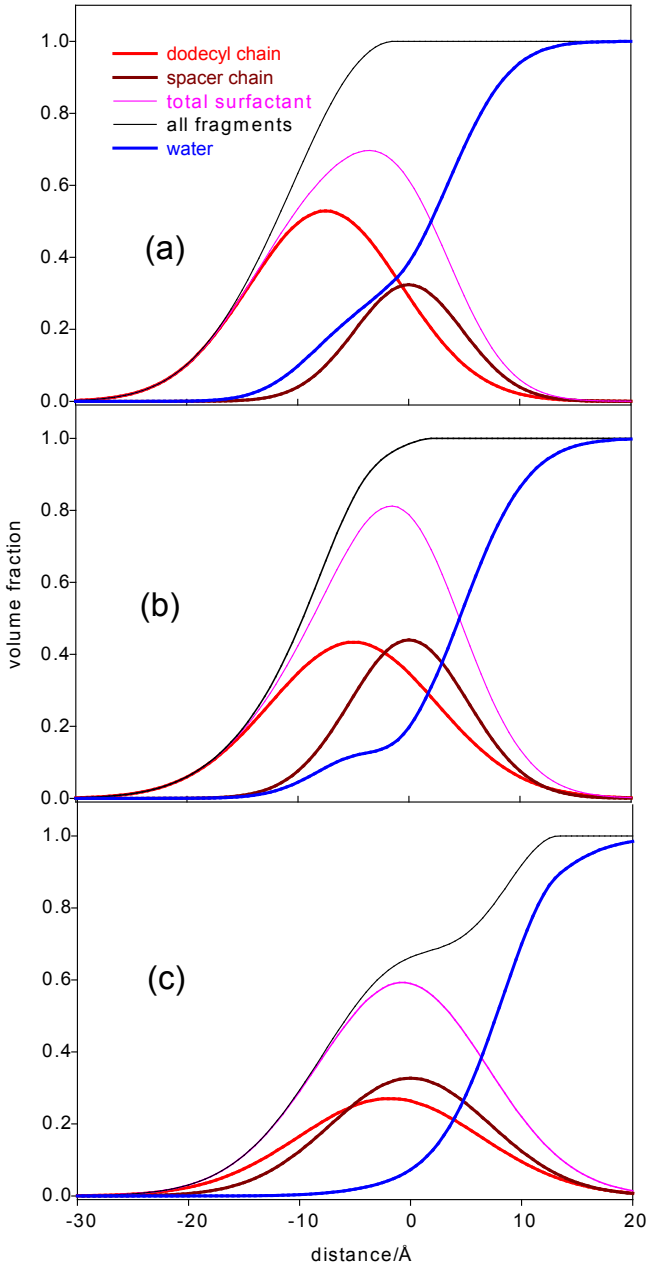


Figure 7.7: Distributions of the different fragments in layers of carboxybetaines at the air/liquid surface that best fir the reflectivity data of Figure (7.6).The spacer consists of the quaternary ammonium group and carboxy- groups separated by (a) 1, (b) 4 and (c) 8 methylene groups

Compound	$l_c \pm 3$ Å	$l_s \pm 3$ Å	$^a\delta_{cs}$	$^b\delta_{sw} \pm 1$ Å	$w \pm 3$ Å	$A \pm 3$ Å^2
$C_{12}C_1$Betaine	11	1	-6	-0.5	11	48
$C_{12}C_4$Betaine	13	5	-4	-3	11	52
$C_{12}C_8$Betaine	15	12	-1.5	-6	11	80

Table 7.4: structural parameters derived from fitting neutron reflection data from three betaines at 3×CMC. ^{a} depends directly on l_c and l_s. ^{b} The parameter defining the cut–off of the water space filling region is indirectly incorporated in to δ_{sw}

There are two trends in the fitted results. The first is that the projection of the C_{12} chain along the surface normal increases with the betaine spacer length. As the length defined by the $1/e$ width of a Gaussian distribution is around 90% of the true length and the fully extended length of C_{12} chain is known to be 16 Å [17]. Therefore, the C_{12} chain is tilted about 60 ° away from the horizontal with the presence of C_1 spacer. This changes to about 90 ° in the case of C_8 spacer. Another trend is that the spacer chain of the betaine group changes orientation more dramatically. For the C_1 compound the short length of the spacer determined that the thickness is close to the thermal roughness. In the case of C_8 compound, the fully extended length of the spacer is estimated to be around 15 Å (10 Å from the C_8H_{16} and 5 Å from the two charged groups). Thus the tilt of the spacer is about 60 ° away from the horizontal, almost the same as the C_{12} chain in the case of C_1 surfactant, indicating that the carboxyl group in $C_{12}C_8$betaine must in the direction completely out of the water, rather than suggested by Chevalier et al. that the long spacer forms a loop at the surface.

Another method to examine the nature of the surface layer is to measure the over-

lap of each unit with underlying water. If there is a small overlap between a hydrophobic unit and water, it indicates that the high energy surface of water is screened more effectively by the hydrophobic unit than if there is a large overlap. By using the distributions of Figure (7.7), the overlaps can be easily calculated, normalized and directly compared between the three systems. The calculated overlaps are 3.8, 3.3 and 3.0 between the dodecyl chain and water and 8.1, 5.3 and 3.7 between the spacer and water for the C_1, C_4 and C_8 spacers respectively, where the values are normalized both to the volume fraction per dodecyl chain and to the APM. These results show that the apparent effectiveness of the dodecyl chain is more or less the same within experimental error across the series. However, in the case of C_1 and C_4 spacers, the overlap of each spacers with water is strong and therefore the methylene groups of these spacers must be significantly immersed in water. This does not matter much for $C_{12}C_1$betaine but it leads to a large loss of surface energy for $C_{12}C_4$betaine, which leads to a larger limiting surface tension , γ_{CMC}, as seen in Figure (7.3) . However, the value of the overlap for C_8 spacer indicates that its effectiveness of screening of water per unit volume fraction is almost identical with that of the dodecyl chain. Therefore the overall screening of water per unit area of surfactant should approximately be the same for $C_{12}C_1$betaine and $C_{12}C_8$ betaine. However, due to the the exposed polar carboxyl at the surface, the contribution from the spacer group will be partially offset and the surface energy is higher than a methyl group, and overall γ_{CMC} value could be a bit higher for the $C_{12}C_8$ betaine as observed.

As the overlap of C_8 spacer with water is approximately the same as that of the dodecyl chain and this is well extended, it suggests that the carboxyl group must

be on average more or less completely out of the water. An ionized carboxyl group would be unstable in the low dielectric environment of the outer part of the layer. Combined with its higher pK_a, it is highly possible that the $C_{12}C_8$ betaine is adsorbed in its undissociated carboxylic acid form. This suggestion may contradict the argument that the prefactor in the Gibbs equation should be 2 if the betaine at the surface is in the cationic form. Wustneck et al. shown that the adsorption of the salt of $C_{12}C_1$ betaine , i.e. the salt with HBr or HCl does follow the Gibbs equation with a prefactor of 2. However, this is not appropriate unless the zwitterionic is in a salt form [16]. The equilibrium between the bulk and surface can be equivalently expressed either as

$$^{-}OOCC_8D_{16}NHMe_2^+(bulk) \rightleftharpoons^{-} OOCC_8D_{16}NHMe_2^+(surface) \qquad (7.7)$$

or

$$^{-}OOCC_8D_{16}NHMe_2^+ + H_2O \rightleftharpoons HOOCC_8D_{16}NHMe_2^+(surface) + OH^-(surface) \qquad (7.8)$$

The first case shows what is conventionally assumed and has a prefactor of 1 in corresponding Gibbs equation. However, the second case also produces a Gibbs prefactor of 1 because the concentration of OH^- ion in the bulk is constant at natural pH as neither the adsorbed amount nor the degree of hydrolysis (formation of COOH) is sufficient to affect the overall pH. Thus by using the Gibbs equation one can only tell if the $C_{12}C_8$betaine is fully dissociated in the bulk solution, but the equation does not help decide whether or not it is dissociated in the surface layer.

According to the neutron reflection results, the orientation of the spacer–head group in adsorbed layer of carboxybetaines with long spacers leads to the car-

boxyl groups being approximately aligned in a higher plane of the surface than the cationic quaternary ammonium groups. If the carboxyl groups lose their charge in the layer, there will be a large reduction in the lateral electrostatic repulsion, typically because at the level of the carboxylic groups there is no high dielectric constant from water. Gershevitz and Sukenik have also shown that the carboxyl terminated self–assembled monolayers are also mostly nonionized by using the more direct method of FTIR, although the situation is not the same [32]. For micellization, such an effect can only occur if the betaine is incompletely dissociated in the bulk solution and the Gibbs analysis indicates that it is not. The situation cannot be different in the micelle because the curvature at the surface of the micelle will tend to force the spacer groups to point outwards from the micelle and the high dielectric environment will then ensure that the carboxylate group remains fully ionized as pK_a is not too high. This difference suggests that at the air/water interface, the formation of a saturated monolayer is strongly favoured in comparison with micellization. This may be the reason for the unusually low concentration at which the adsorption reaches a plateau and hence the long straight line section is observed in the $\gamma - \ln C$ plot. In the more complete series studied by Chevalier et al. the straight line section starts to appear from about the C_4 spacer, i.e. about the same point as the maximum of in the CMC and γ_{CMC}. This link is consistent with the mechanism suggested by the neutron reflection results.

7.4 Conclusion

The structure of layers of three different dodecyl carboxybetaine surfactants adsorbed at the air/liquid interface have been measured by neutron reflection. Three surfactants each possessing a headgroup containing spacer with different length

between the quaternary ammonium and the carboxylate groups. By comparing the neutron experiments and corresponding surface tension data, the prefactors in the Gibbs equation are shown to be 1 in each case. An interesting observation is that the carboxybetaine with C_8 spacer reaches surface saturation at 1/10th of the CMC, which may be associated with the long spacer destabilizing the micelle relative to the surface layer. Through the results obtained from neutron reflection measurements on isotopic labelled compounds, the spacer is shown to be well immersed in water for C_1 and C_4 but significantly above water for the C_8, which has a distribution almost identical with that of the C_{12} chain. This contradicts with an earlier suggestion that the spacer forms a loop in the adsorbed layer. The comparison between overlaps of water with C_{12} chain and spacers also indicate that the C_8 spacer is oriented out of the water, which suggests that the anionic carbocylic acid group is not ionized in the adsorbed layer whereas it is dissociated in bulk solution. These results have been published recently in Langmuir [33].

Bibliography

[1] N. Parris, J. K. Weil, and W. M. Linfield. Soap based detergent formulations. v. amphoteric lime soap dispersing agents. *Journal of the American Oil Chemists Society*, 50(12):509–512, 1973.

[2] G. W. Fernley. Zwitterionic surfactants: structure and performance. *Journal of the American Oil Chemists Society*, 55(1):98–103, 1978.

[3] W. R. Noble and W. M. Linfield. Soap-based detergent formulations: Xxvi. hard water detergency of soap-lime soap dispersant combinations with builders and inorganic salts1. *Journal of the American Oil Chemists Society*, 57(10):368–372, 1980.

[4] Y. Chevalier, L. Germanaud, and P. Le Perchec. Micellar properties of zwitterionic phosphobetaine amphiphiles in aqueous solution: Influence of the intercharge distance. *Colloid and Polymer Science*, 266(5):441–448, 1988.

[5] J. R. Lu, Z. X. Li, T. J. Su, R. K. Thomas, and J. Penfold. Structure of adsorbed layers of ethylene glycol monododecyl ether surfactants with one, two, and four ethylene oxide groups, as determined by neutron reflection. *Langmuir*, 9(9):2408–2416, 1993.

[6] J. R. Lu, M. Hromadova, R. K. Thomas, and J. Penfold. Neutron reflection from triethylene glycol monododecyl ether adsorbed at the air-liquid interface: the variation of the hydrocarbon chain distribution with surface concentration. *Langmuir*, 9(9):2417–2425, 1993.

[7] J. R. Lu, Z. X. Li, R. K. Thomas, E. J. Staples, L. Thompson, I. Tucker, and J. Penfold. Neutron reflection from a layer of monododecyl octaethylene glycol adsorbed at the air-liquid interface: the structure of the layer and the effects of temperature. *The Journal of Physical Chemistry*, 98(26):6559–6567, 1994.

[8] J. R. Lu, E. M. Lee, R. K. Thomas, J. Penfold, and S. L. Flitsch. Direct determination by neutron reflection of the structure of triethylene glycol monododecyl ether layers at the air/water interface. *Langmuir*, 9(5):1352–1360, 1993.

[9] Y. Chevalier, Y. Storet, S. Pourchet, and P. Le Perchec. Tensioactive properties of zwitterionic carboxybetaine amphiphiles. *Langmuir*, 7(5):848–853, 1991.

[10] R. G. Laughlin. Fundamentals of the zwitterionic hydrophilic group. *Langmuir*, 7(5):842–847, 1991.

[11] S. Welling-Wester, M. Feijlbrief, D. GAM. Koedijk, and G. W. Welling. Detergent extraction of herpes simplex virus type 1 glycoprotein d by zwitterionic and non-ionic detergents and purification by ion-exchange high-performance liquid chromatography. *Journal of chromatography A*, 816(1):29–37, 1998.

[12] L. D. Rhein, M. Schlossman, A. O Lenick, and P. Somasundaran. Surfactants in personal care products and decorative cosmetics third edition. *SURFACTANT SCIENCE SERIES*, 135, 2007.

[13] R. A. Robinson and R. H. Stokes. *Electrolyte solutions*. Courier Corporation, 2002.

[14] N. Bjerrum. Dissociation constants of polybasic acids and their application to the calculation of molecular dimensions. *Z. phys. Chem*, 106:219–242, 1923.

[15] J. G. Weers, J. F. Rathman, F. U. Axe, C. A. Crichlow, L. D. Foland, D. R. Scheuing, R. J. Wiersema, and A. G. Zielske. Effect of the intramolecular charge separation distance on the solution properties of betaines and sulfobetaines. *Langmuir*, 7(5):854–867, 1991.

[16] R. Wüstneck, J. Kriwanek, M. Herbst, G. Wasow, and K. Haage. The adsorption behaviour of long-chain n-alkyl betaines and their hydrobromides. *Colloids and surfaces*, 66(1):1–9, 1992.

[17] J. R. Lu, Z. X. Li, J. Smallwood, R. K. Thomas, and J. Penfold. Detailed structure of the hydrocarbon chain in a surfactant monolayer at the air/water interface: neutron reflection from hexadecyltrimethylammonium bromide. *The Journal of Physical Chemistry*, 99(20):8233–8243, 1995.

[18] J. R. Lu, R. K. Thomas, and J. Penfold. Surfactant layers at the air/water interface: structure and composition. *Advances in colloid and interface science*, 84(1-3):143–304, 2000.

[19] P. X. Li, Z. X. Li, H.i Shen, R. K. Thomas, J. Penfold, and J. R. Lu. Application of the gibbs equation to the adsorption of nonionic surfactants and polymers at the air–water interface: Comparison with surface excesses determined directly using neutron reflectivity. *Langmuir*, 29(30):9324–9334, 2013.

[20] H. Xu, P. X. Li, K. Ma, R. K. Thomas, J. Penfold, and J. R. Lu. Limitations in the application of the gibbs equation to anionic surfactants at the air/water surface: sodium dodecylsulfate and sodium dodecylmonooxyethylenesulfate above and below the cmc. *Langmuir*, 29(30):9335–9351, 2013.

[21] J. N. Phillips. The energetics of micelle formation. *Transactions of the Faraday Society*, 51:561–569, 1955.

[22] K. Tori and T. Nakagawa. Colloid chemical properties of ampholytic surfactants. 5. temperature and salt effects on critical micelle concentration of long-chain alkyl betaine. *KOLLOID-ZEITSCHRIFT AND ZEITSCHRIFT FUR POLYMERE*, 189(1):50, 1963.

[23] F. Zhao and M. J. Rosen. Relationship of structure to properties of surfactants. 12. synthesis and surface properties of long-chain 2-pyridinium alkanoates. *The Journal of Physical Chemistry*, 88(24):6041–6043, 1984.

[24] R. G. Laughlin and G. H. Brown. Advances in liquid crystals. *Academic Press, New York*, 3:41, 1978.

[25] B. Faucompre and B. Lindman. Self-association of zwitterionic and nonionic surfactants. nmr self-diffusion studies. *Journal of Physical Chemistry*, 91(2):383–389, 1987.

[26] K. W. Herrmann. Micellar properties of some zwitterionic surfactants. *Journal of Colloid and Interface Science*, 22(4):352–359, 1966.

[27] J. D. Hines, P. R. Garrett, G. K. Rennie, R. K. Thomas, and J. Penfold. Structure of an adsorbed layer of n-dodecyl-n, n-dimethylamino acetate at the air/solution interface as determined by neutron reflection. *The Journal of Physical Chemistry B*, 101(36):7121–7126, 1997.

[28] M. Yaseen, J. R. Lu, J. R. P. Webster, and J. Penfold. Adsorption of single chain zwitterionic phosphocholine surfactants: Effects of length of alkyl chain and head group linker. *Biophysical chemistry*, 117(3):263–273, 2005.

[29] P. X. Li, R. K. Thomas, and J. Penfold. Limitations in the use of surface tension and the gibbs equation to determine surface excesses of cationic surfactants. *Langmuir*, 30(23):6739–6747, 2014.

[30] T. L. Crowley, E. M. Lee, E. A. Simister, and R. K. Thomas. The use of contrast variation in the specular reflection of neutrons from interfaces. *Physica B: Condensed Matter*, 173(1):143–156, 1991.

[31] J. Penfold and R. K. Thomas. Solvent distribution in non-ionic surfactant monolayers. *Physical Chemistry Chemical Physics*, 4(12):2648–2652, 2002.

[32] O. Gershevitz and C. N. Sukenik. In situ ftir-atr analysis and titration of carboxylic acid-terminated sams. *Journal of the American Chemical Society*, 126(2):482–483, 2004.

[33] K. Ma, P. X. Li, C. C. Dong, R. K. Thomas, and J. Penfold. Unusual adsorption at the airwater interface of a zwitterionic carboxybetaine with a large charge separation. *Langmuir*, DOI: 10.1021/acs.langmuir.6b00074.

Chapter 8

Concluding Remarks

The optimization of mixtures of surfactants in aqueous solutions is of considerable interest, for both practical and theoretical reasons. There are many examples in the literature showing that the binary mixtures of different surfactants that behave nonidealy in such a way that important properties of the mixtures are completely changed from those of the individual species. In order to take advantage of this synergy, it is necessary to gain a better understanding of the mechanism of mixing behaviour. Through this thesis, neutron reflection (NR) and surface tension (ST) were used to characterize a series of mixtures of two ionic surfactants, one anionic (SDS) and one cationic (DTAB), with two zwitterionic surfactants dodecyl dimethylammonium propanesulfonate (DSB) and dodecyl dimethylammonium acetate (DB) at both air–liquid and solid–liquid interfaces. A series of dodecyl carboxybetaine with different spacers separating quaternary ammonium and carboxylate group was also examined by using NR and ST to yield insight of the structural features of the adsorbed layers.

The adsorption of the mixed systems SDS/DSB and DTAB/DSB at air–liquid

interface were examined using NR and ST. An enhancement of adsorption was observed for mixture SDS/DSB compared to the adsorption of the pure components above the CMC, which indicates a strong synergy in the mixed system. The pseudophase approximation with an expansion of the excess free energy G_E was applied by simultaneously fitting the NR and ST data. It was found that the excess free energy of mixture SDS/DSB is asymmetric for the adsorbed layer. Similar asymmetrical features were found for mixtures SDS/DB and DTAB/DSB but no synergy in the total adsorption was observed for the latter. These are the strongest interacting systems to be examined with mixing that is more complicated than the regular solution model. Thus the data could be successfully fitted is useful, although the problem of how to treat the dissociation of the ionic surfactant remains a significant theoretical problem.

The mixtures at the solid–aqueous interface showed different interfacial behaviour according to the concentration studied. The large variation in total adsorption above the mixed CMC is associated with the arrangement of individual molecules in the inner layer adjacent to the solid substrate. For the mixtures containing anionic SDS, the adsorption behaviours are completely changed from the pure components. Maxima in the adsorption just above the mixed CMC occurred due to the combination of structural effects of the mixture and an possibly ion segregation effect. The presence of cationic DTAB enhanced the adsorption of DSB but suppressed that of DB, which can be attributed to different structural features in the adsorbed layer. The enhanced adsorption of DTAB/DSB was found to reach an approximate plateau as both surfactant and its counterion Br^- were adsorbed. The reduction of adsorption of DTAB/DB is suggested to be a combination of the

close approach of the carboxy group to the surface and a reduction in the pK_a by the negatively charged surface. A new feature identified here is the possibility of an ion segregation effect at the surface. Previously, a sharp surface maximum in the adsorption of SDS on sapphire has been attributed to adsorption of the DS^- ion, not the whole SDS molecule [1]. The composition dependence of the SDS/DSB layer indicates that something occurs here, on silica. Parallel behaviour was identified in the SDS/$C_{12}E_6$ system. Although this must be associated with same segregation, it is difficult to be more definite and , since adsorption at hydrophilic surface is not well understood it should be explored further.

Chapters 4–6 explored the strong interaction of closely spaced zwitterionic surfactant with ionic surfactants. The work in Chapter 7 was originally meant to focus on the effect of different zwitterionic charge spacing on their interaction. However, it became clear in the early experiments that something unusual was occurring in the pure zwitterionic compounds. Thus, the adsorbed layers showed different arrangements according to the increasing length of spacers in headgroup. For the surfactants with $(CH_2)_1$ and $(CH_2)_4$ spacers, it was found that the spacers are well immersed in the water. However, the $(CH_2)_8$ spacer is significantly above the water and the distribution of $(CH_2)_8$ spacer along the surface normal was projected out of the water, contrary to an earlier hypothesis that it forms a loop. It was also observed that the carboxybetaine with longest spacer reaches surface saturation at concentration well below the CMC, which may be associated with the micelle destabilized by the long spacer. This behaviour suggests that studies on mixtures of theses larger spacer surfactants would be more like ionic–ionic mixtures and therefore are particularly interesting.

Bibliography

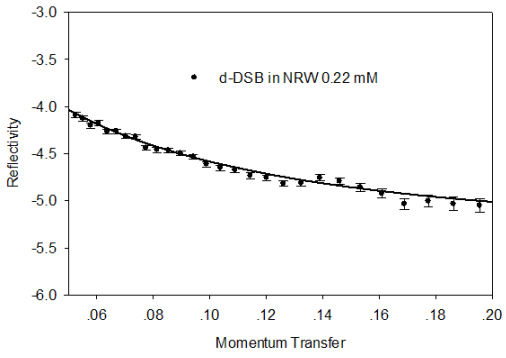
[1] N. N. Li, R. K. Thomas, and A. R. Rennie. Neutron reflectometry of anionic surfactants on sapphire: A strong maximum in the adsorption near the critical micelle concentration. *Journal of Colloid and Interface Science*, 471:81–88, 2016.

Appendices

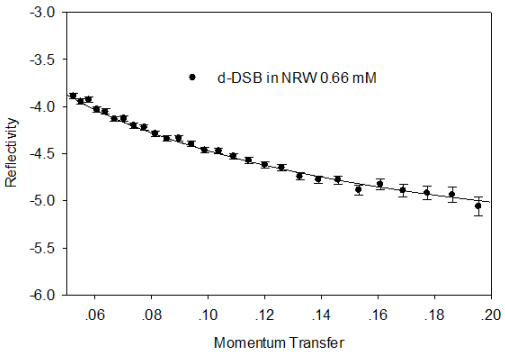
Appendix A

Neutron reflection fitting profiles at air–liquid interface

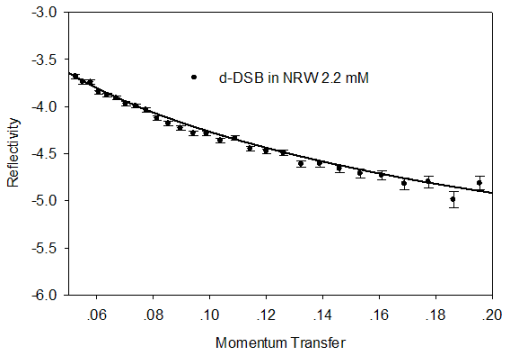
The following Figures from A.1 to A.4 are the corresponding diagrams of neutron fits for deuterated DSB at air–liquid interface. The actual fitting parameters are assembled in Table (4.1), Chapter 4.



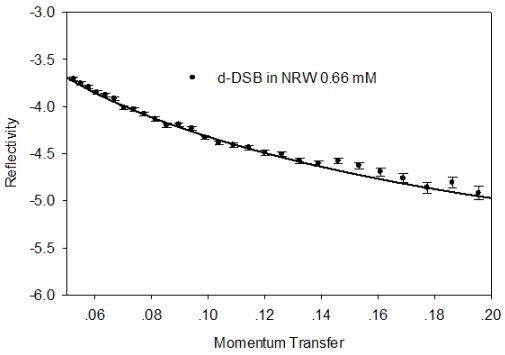
A.1



A.2

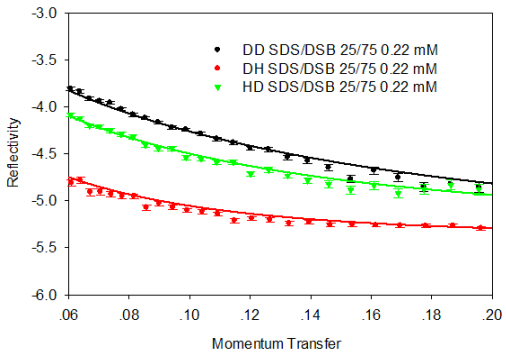


A.3

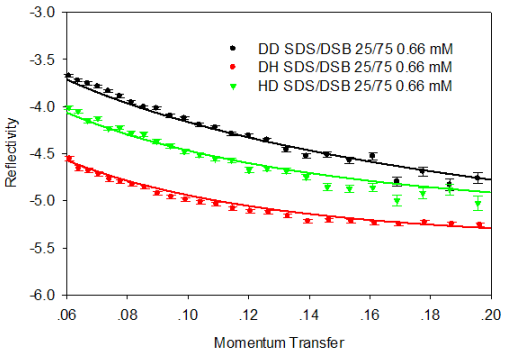


A.4

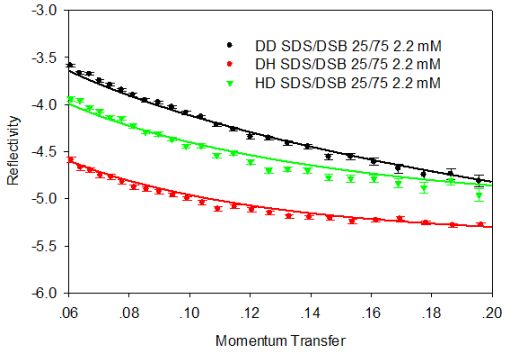
The following Figures A.5 to A.28 are the fitted neutron reflectivity profiles for SDS/DSB and DTAB/DSB mixtures at air–liquid interface. The corresponding fitting parameters are list in Table (4.5), Chapter 4.



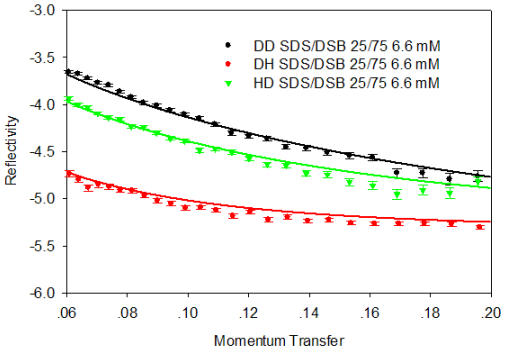
A.5



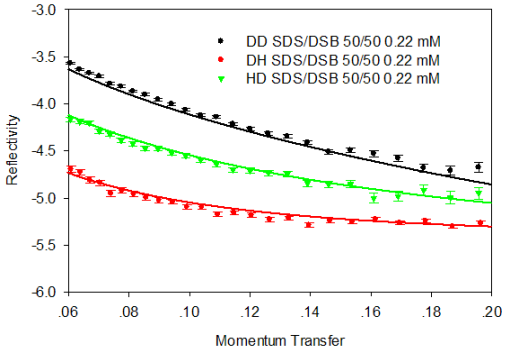
A.6



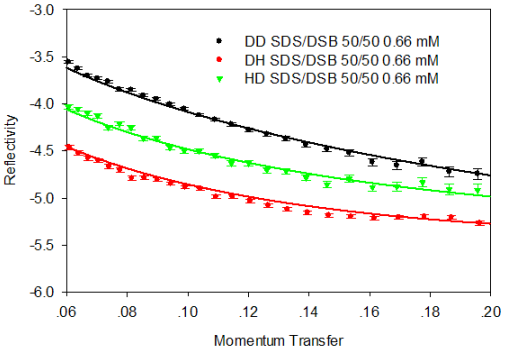
A.7



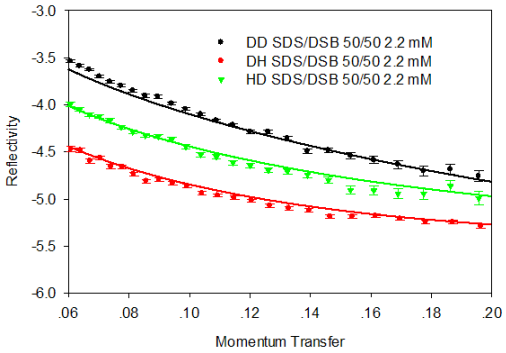
A.8



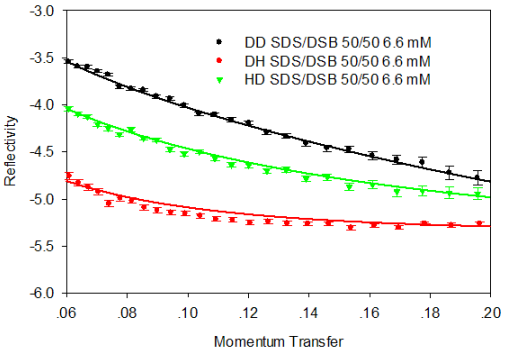
A.9



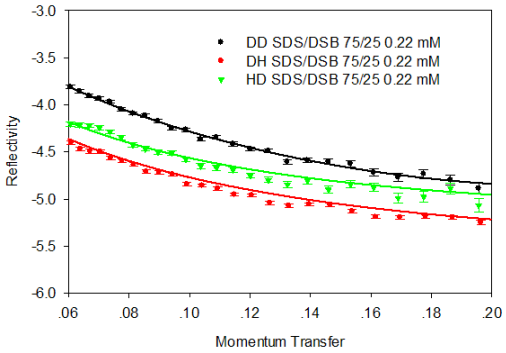
A.10



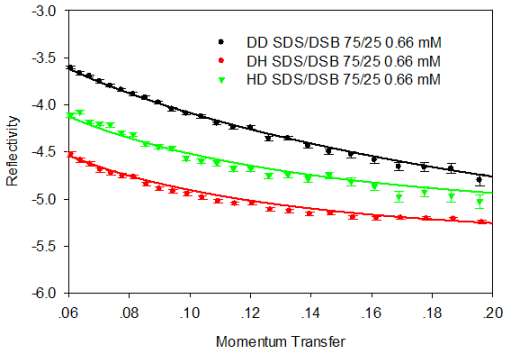
A.11



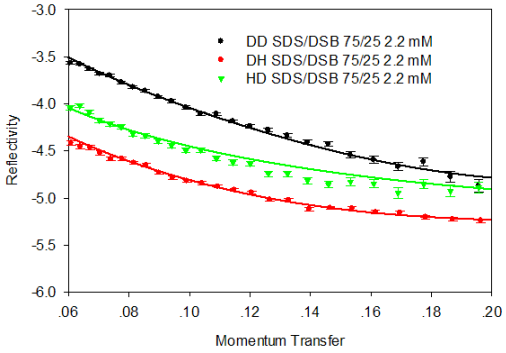
A.12



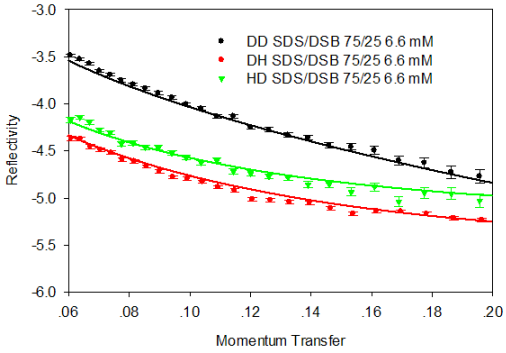
A.13



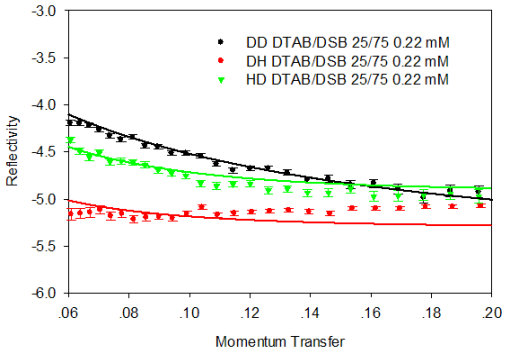
A.14



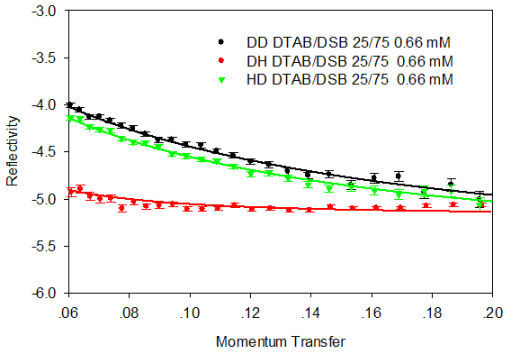
A.15



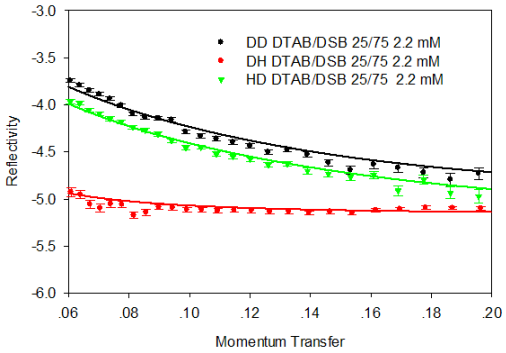
A.16



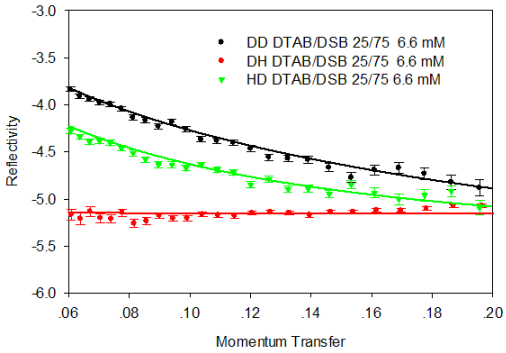
A.17



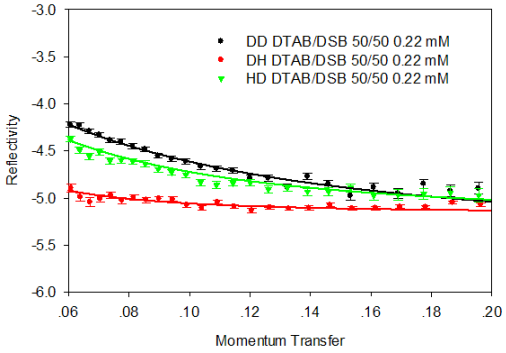
A.18



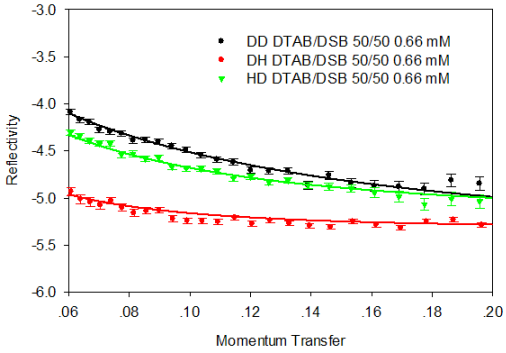
A.19



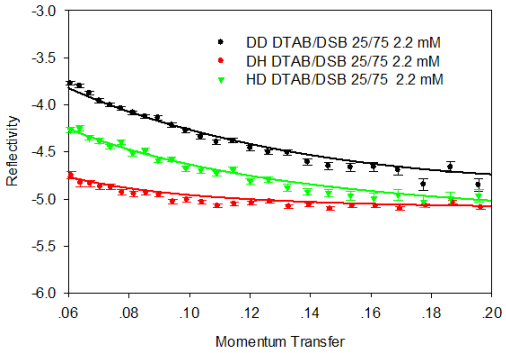
A.20



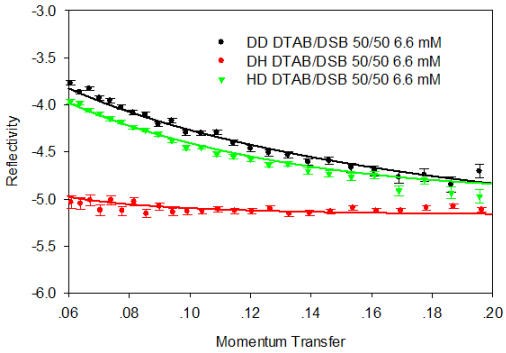
A.21



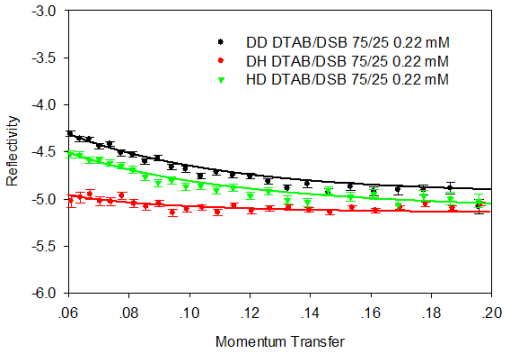
A.22



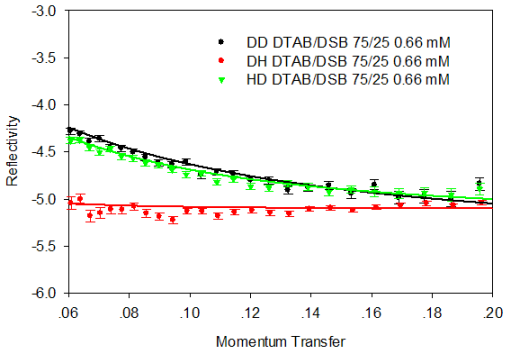
A.23



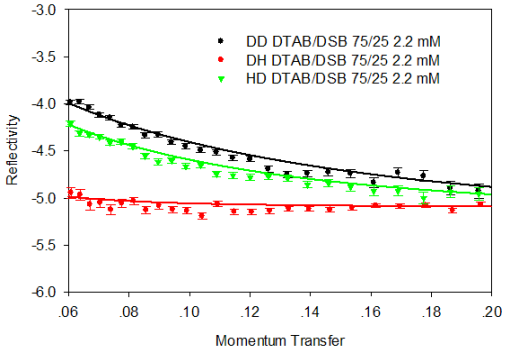
A.24



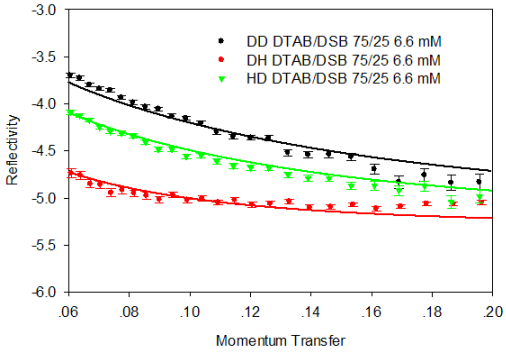
A.25



A.26



A.27

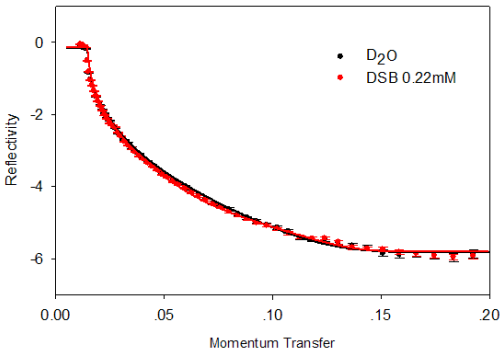


A.28

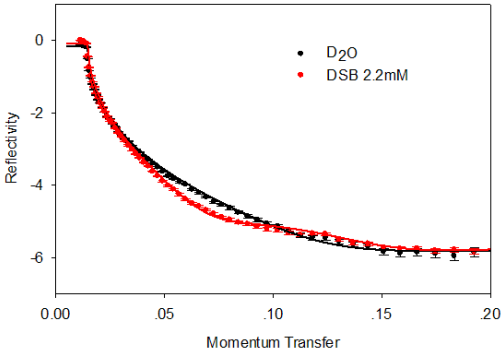
Appendix B

Neutron reflection fitting profiles at solid–aqueous interface

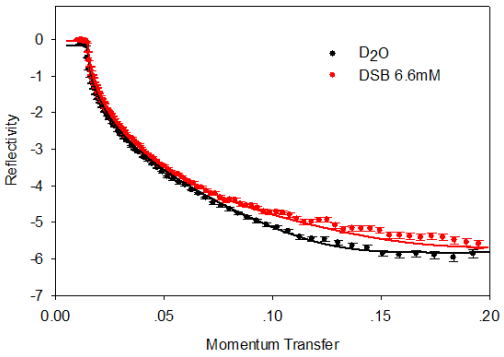
The following diagrams from B.1 to B.7 are the fitted neutron reflection profiles of DSB and DB component at solid–aqueous interface, the corresponding fitting parameters are assembled in Table (5.2), Chapter 5.



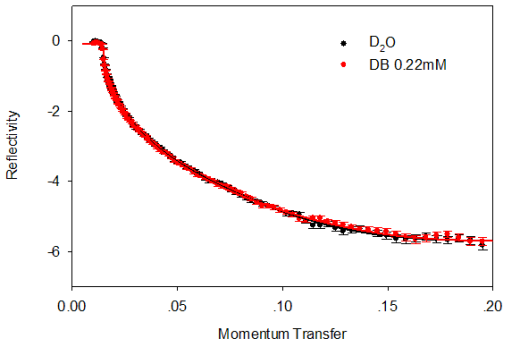
B.1



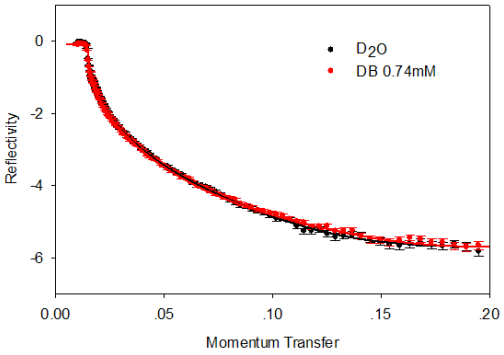
B.2


Reflectivity
Momentum Transfer
D2O
DSB 6.6mM

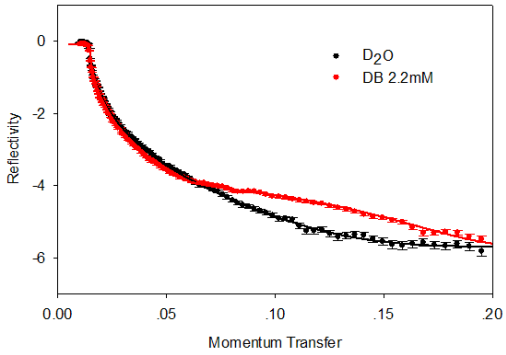
B.3


Reflectivity
Momentum Transfer
D2O
DB 0.22mM

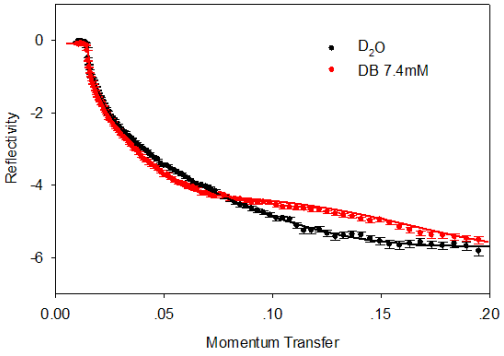
B.4


Reflectivity
Momentum Transfer
D2O
DB 0.74mM

B.5

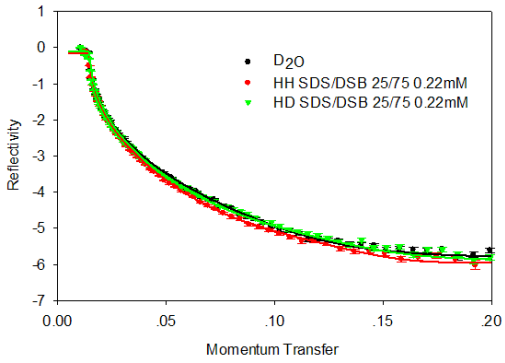

Reflectivity
Momentum Transfer
D2O
DB 2.2mM

B.6

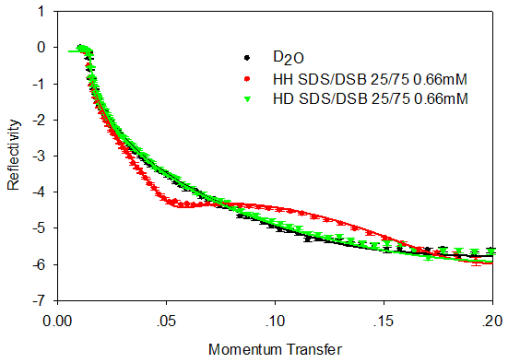

Reflectivity
Momentum Transfer
D2O
DB 7.4mM

B.7

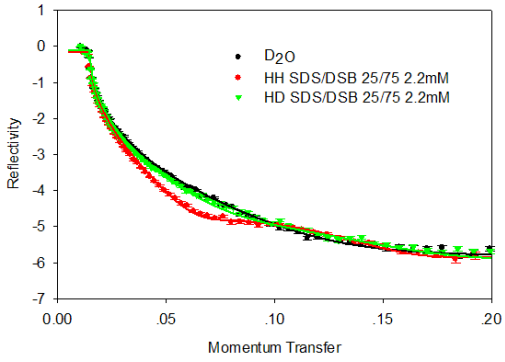
The following Figures B.8 to B.31 are the fitted neutron reflection profiles for SDS/zwitterionic mixtures, the corresponding fitting parameters are listed in Tables (5.3) and (5.4) in Chapter 5 for SDS/DSB and SDS/DB respectively.



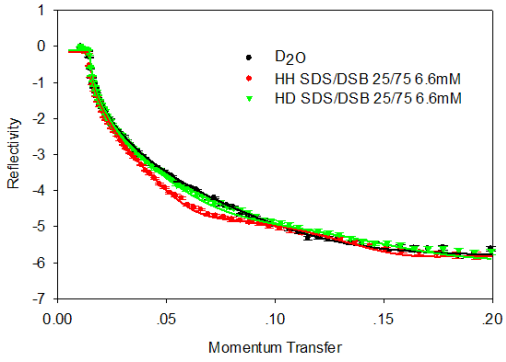
B.8



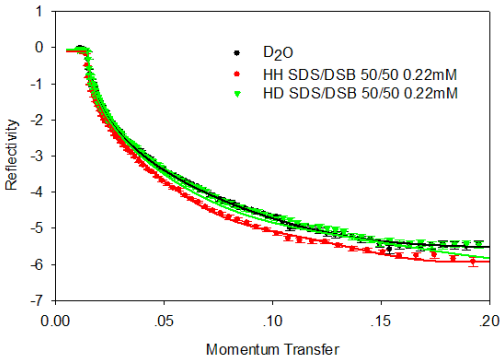
B.9



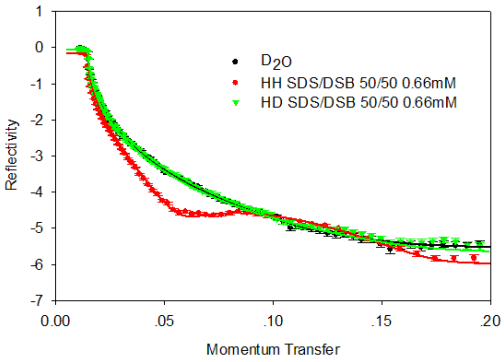
B.10



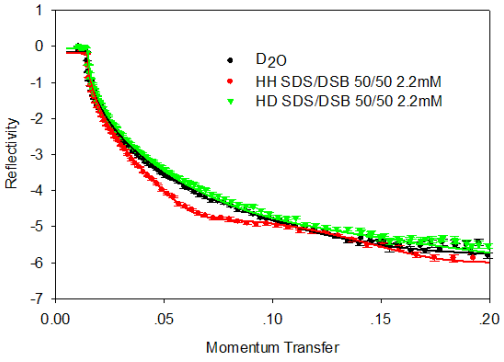
B.11



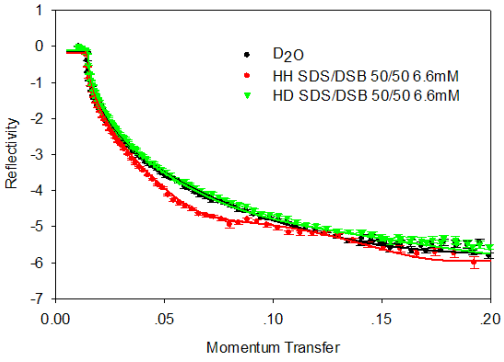
B.12



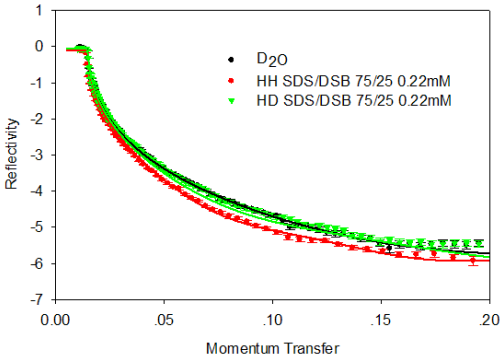
B.13



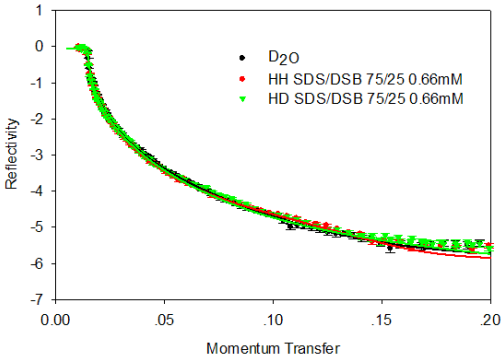
B.14



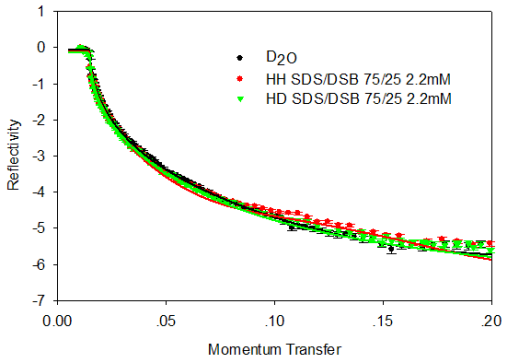
B.15



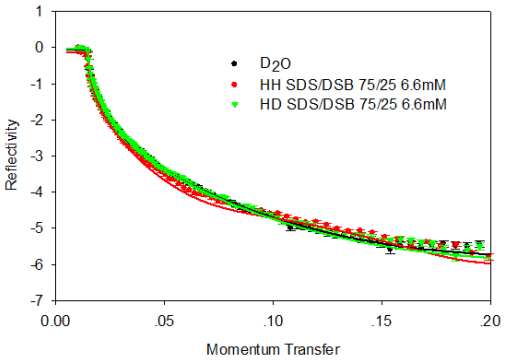
B.16



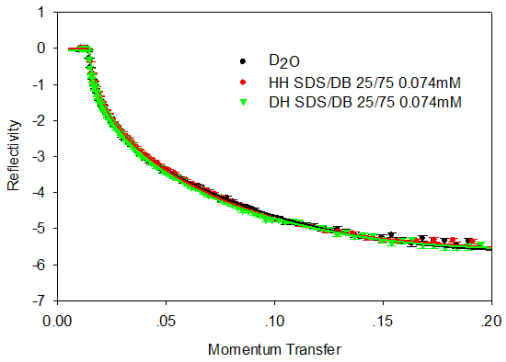
B.17



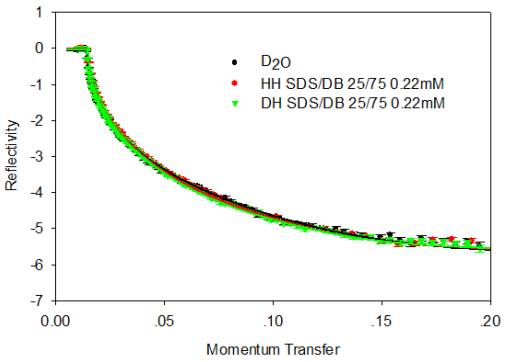
B.18



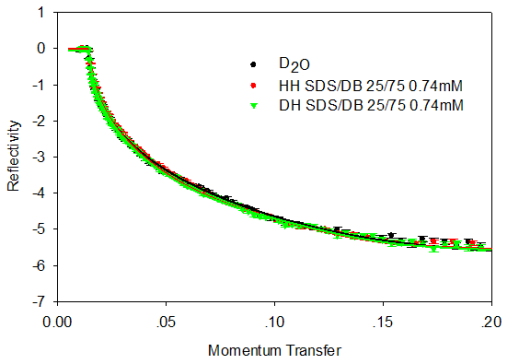
B.19



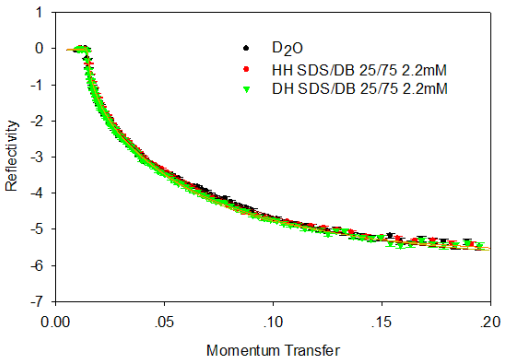
B.20



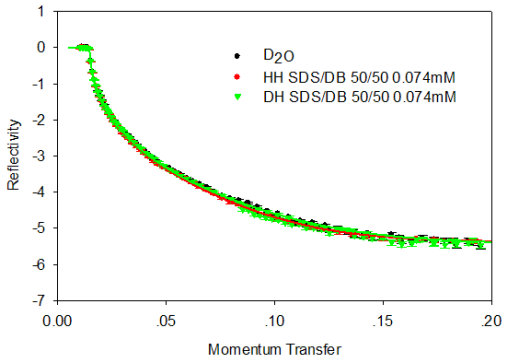
B.21



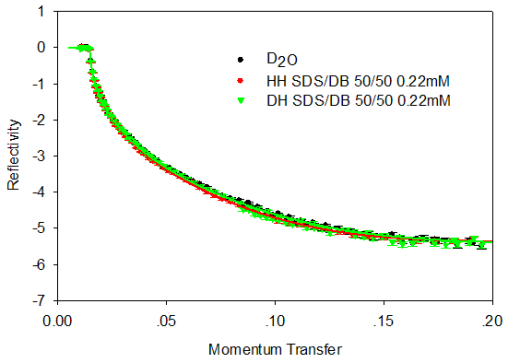
B.22



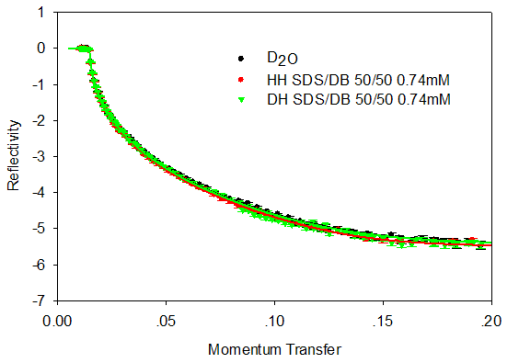
B.23



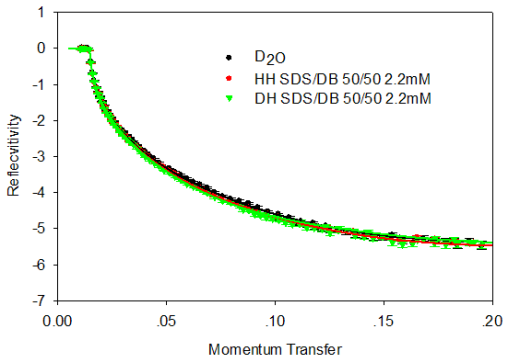
B.24



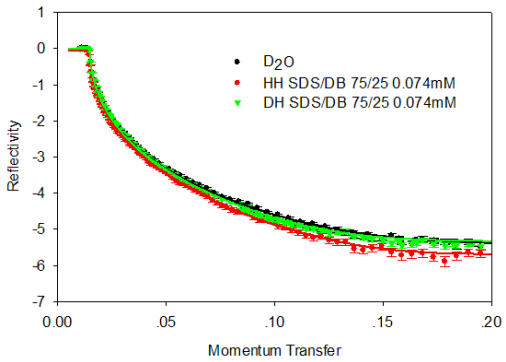
B.25



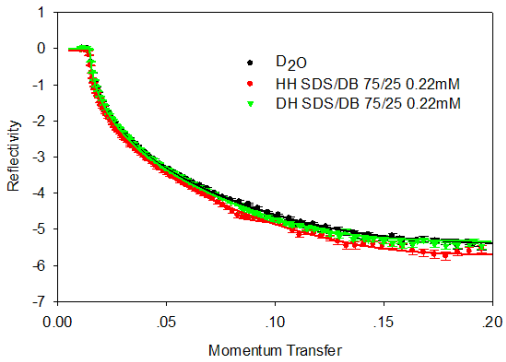
B.26



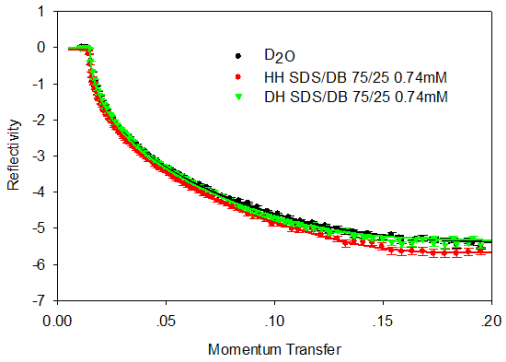
B.27



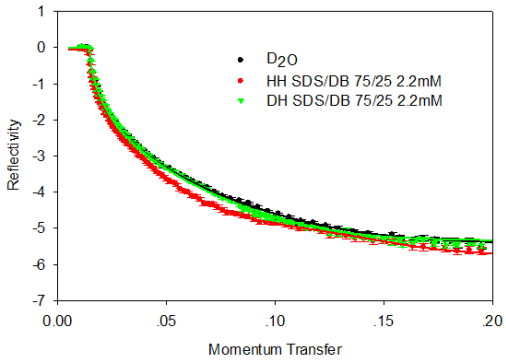
B.28



B.29

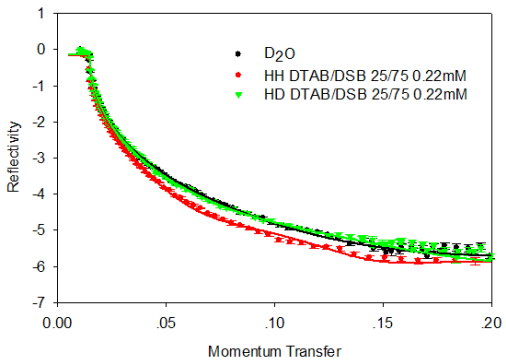


B.30

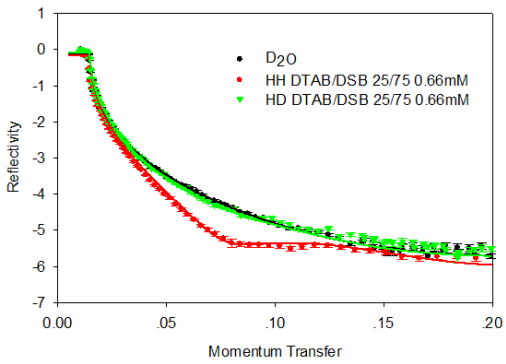


B.31

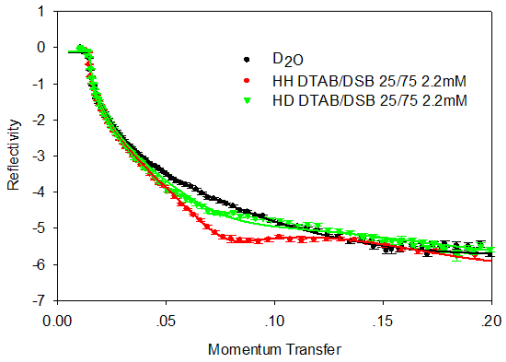
The following Figures B.32 to B.55 are the fitted neutron reflection profiles of DTAB/zwitterionic mixtures, the corresponding fitting parameters are listed in Tables (6.1) and (6.2) in Chapter 6 for DTAB/DSB and DTAB/DB respectively.



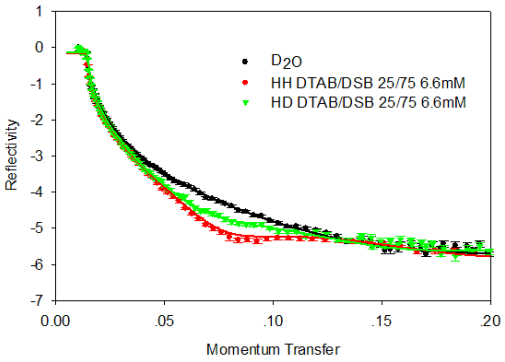
B.32



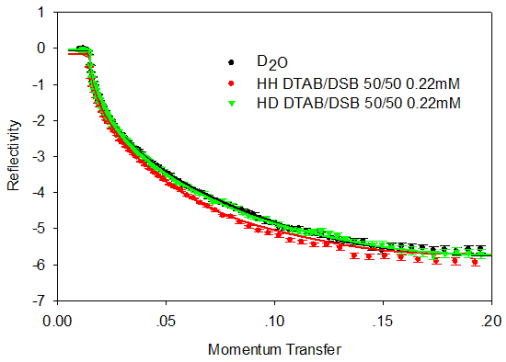
B.33



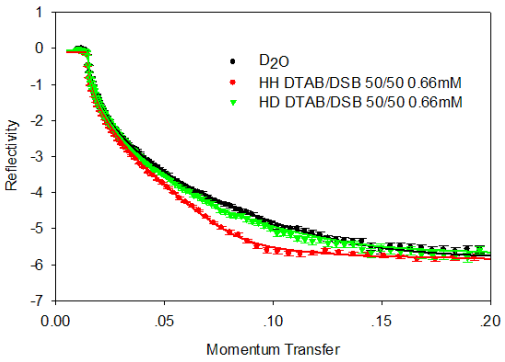
B.34



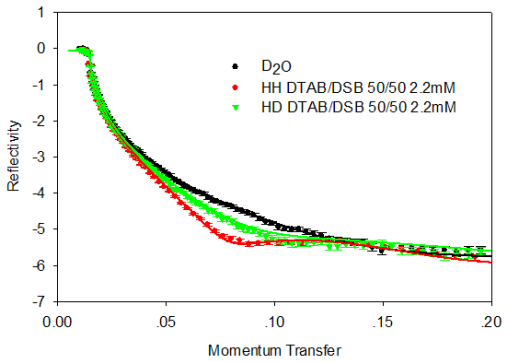
B.35



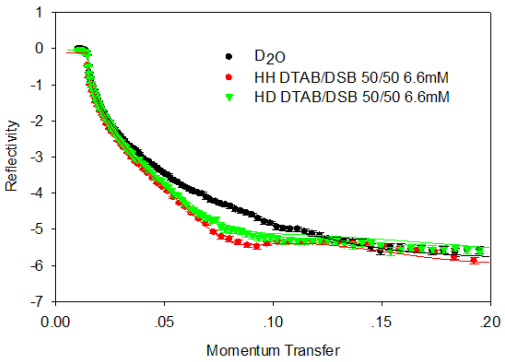
B.36



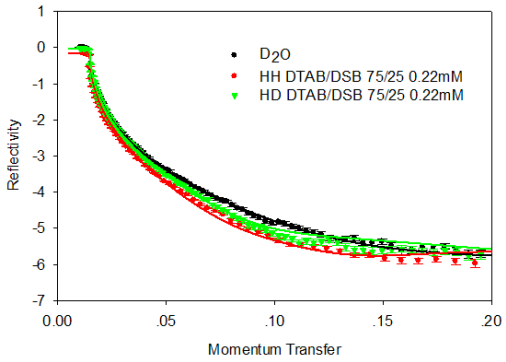
B.37



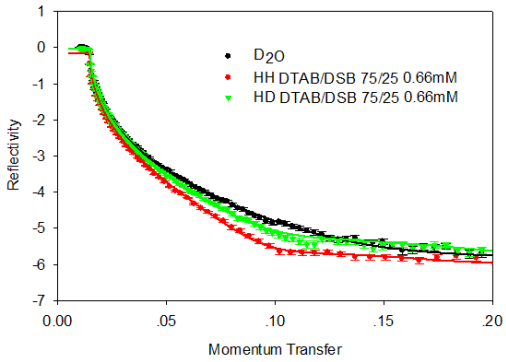
B.38



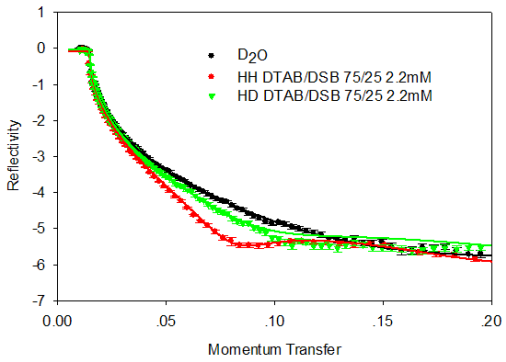
B.39



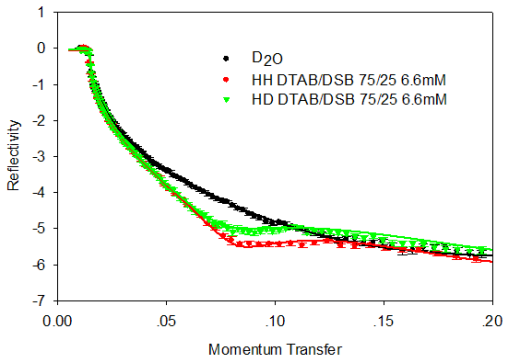
B.40



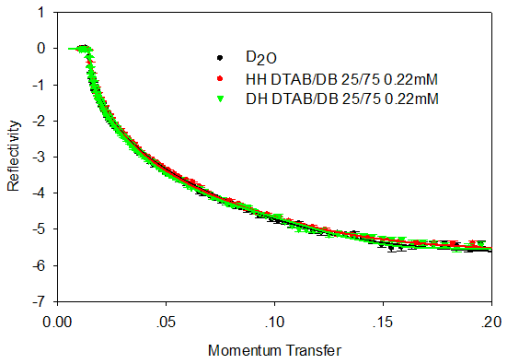
B.41



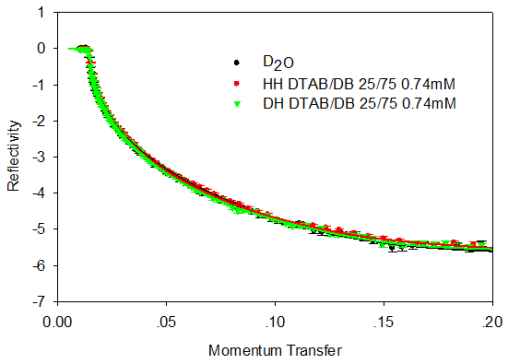
B.42



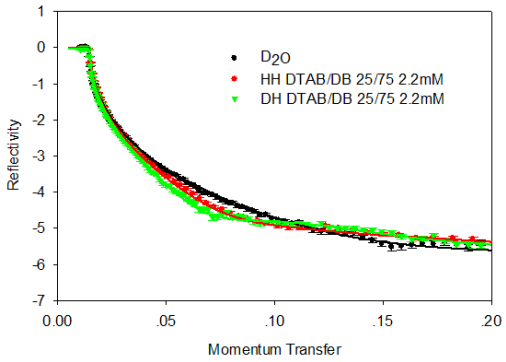
B.43



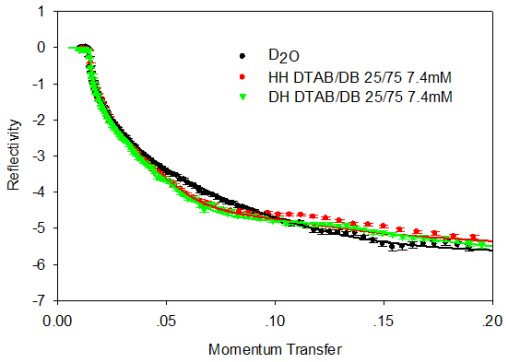
B.44



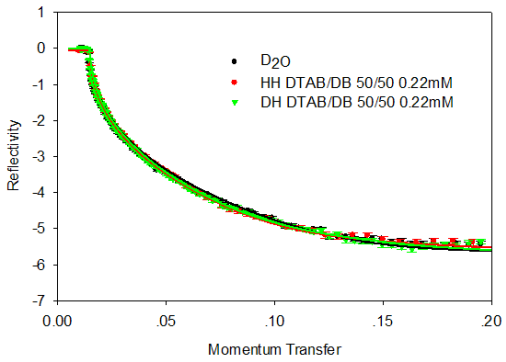
B.45



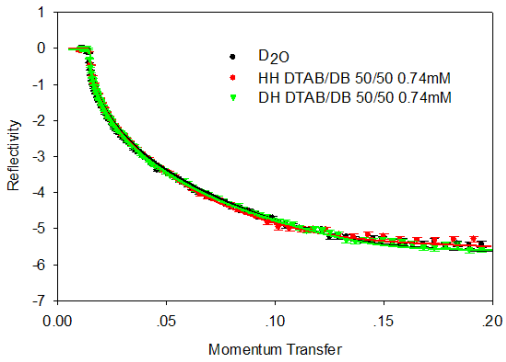
B.46



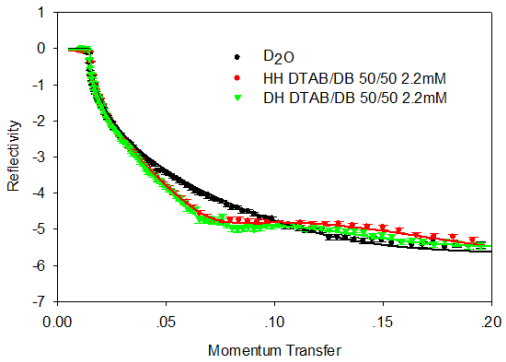
B.47



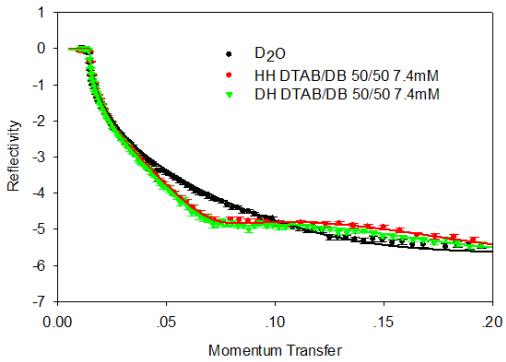
B.48



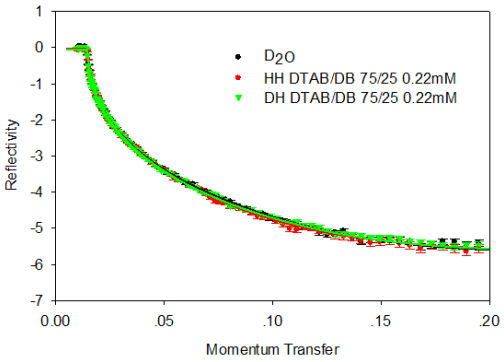
B.49



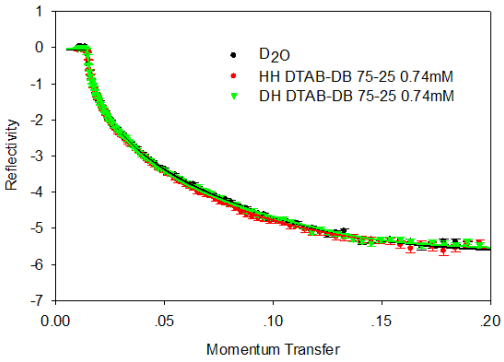
B.50



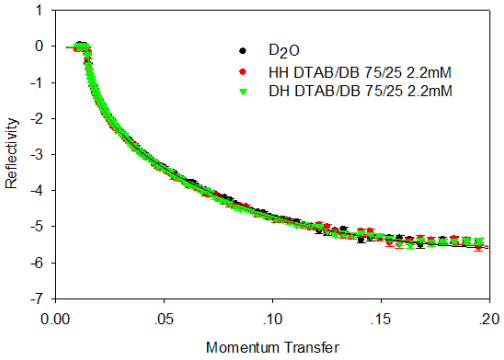
B.51



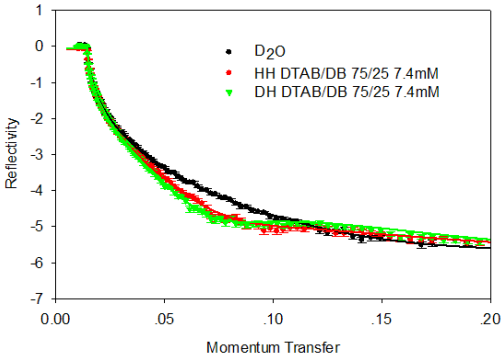
B.52



B.53



B.54



B.55